

(C) 1

C.12

RJM
NOV 5 1992
NOV 25 1992



Evaluation of an Airjet Distortion Generator Used to Produce Steady-State, Total-Pressure Distortion at the Inlet of a General Electric F101-GE-100 Turbofan Engine

J. D. Hubble and R. E. Smith
ARO, Inc.

August 1979

Final Report for Period March 30 — May 31, 1978

TECHNICAL REPORTS
FILE COPY

PROPERTY OF U.S. AIR FORCE
AEDC TECHNICAL LIBRARY

Approved for public release; distribution unlimited.

Property of U. S. Air Force
AEDC LIBRARY
F40600-77-C-0003

ARNOLD ENGINEERING DEVELOPMENT CENTER
ARNOLD AIR FORCE STATION, TENNESSEE
AIR FORCE SYSTEMS COMMAND
UNITED STATES AIR FORCE

NOTICES

When U. S. Government drawings, specifications, or other data are used for any purpose other than a definitely related Government procurement operation, the Government thereby incurs no responsibility nor any obligation whatsoever, and the fact that the Government may have formulated, furnished, or in any way supplied the said drawings, specifications, or other data, is not to be regarded by implication or otherwise, or in any manner licensing the holder or any other person or corporation, or conveying any rights or permission to manufacture, use, or sell any patented invention that may in any way be related thereto.

Qualified users may obtain copies of this report from the Defense Documentation Center.

References to named commercial products in this report are not to be considered in any sense as an indorsement of the product by the United States Air Force or the Government.

This report has been reviewed by the Information Office (OI) and is releasable to the National Technical Information Service (NTIS). At NTIS, it will be available to the general public, including foreign nations.

APPROVAL STATEMENT

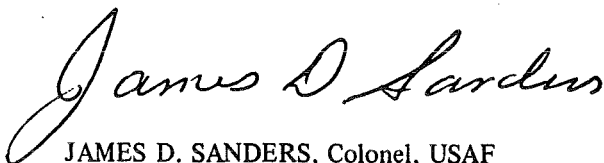
This report has been reviewed and approved.



DANIEL W. CHEATHAM, III, 1st Lt., USAF
Test Director, ETF Division
Directorate of Test Operations

Approved for publication:

FOR THE COMMANDER



JAMES D. SANDERS, Colonel, USAF
Director of Test Operations
Deputy for Operations

UNCLASSIFIED

REPORT DOCUMENTATION PAGE		READ INSTRUCTIONS BEFORE COMPLETING FORM
1. REPORT NUMBER AEDC-TR-78-73	2. GOVT ACCESSION NO.	3. RECIPIENT'S CATALOG NUMBER
4. TITLE (and Subtitle) EVALUATION OF AN AIRJET DISTORTION GENERATOR USED TO PRODUCE STEADY-STATE, TOTAL-PRESSURE DISTORTION AT THE INLET OF A GENERAL ELECTRIC F101-GE-100 TURBOFAN ENGINE		5. TYPE OF REPORT & PERIOD COVERED Final Report - March 30 - May 31, 1978
7. AUTHOR(s) J. D. Hubble and R. E. Smith, ARO, Inc. a Sverdrup Corporation Company		6. PERFORMING ORG. REPORT NUMBER
9. PERFORMING ORGANIZATION NAME AND ADDRESS Arnold Engineering Development Center/DO Air Force Systems Command Arnold Air Force Station, Tennessee 37389		8. CONTRACT OR GRANT NUMBER(s)
11. CONTROLLING OFFICE NAME AND ADDRESS Aeronautical Systems Division/YZEE Wright-Patterson AFB, Ohio 45433		10. PROGRAM ELEMENT, PROJECT, TASK AREA & WORK UNIT NUMBERS Program Element 64215F
		12. REPORT DATE August 1979
14. MONITORING AGENCY NAME & ADDRESS (if different from Controlling Office)		13. NUMBER OF PAGES 89
		15. SECURITY CLASS. (of this report) UNCLASSIFIED
		15a. DECLASSIFICATION DOWNGRADING SCHEDULE N/A
16. DISTRIBUTION STATEMENT (of this Report) Approved for public release; distribution unlimited.		
17. DISTRIBUTION STATEMENT (of the abstract entered in Block 20, if different from Report)		
18. SUPPLEMENTARY NOTES Available in DDC		
19. KEY WORDS (Continue on reverse side if necessary and identify by block number) performance distortion test methods generators steady-state F101-GE-100 pressure (total) turbofan engines		
20. ABSTRACT (Continue on reverse side if necessary and identify by block number) A performance evaluation of an airjet distortion generator (ADG) system used to produce steady-state, total-pressure distortion at the inlet to a turbine engine was conducted. The capability of the system to duplicate screen-generated, classical and composite patterns and to maintain a constant distortion pattern over a range of airflows is presented. The effect of Reynolds number on the system's capability to match patterns is		

UNCLASSIFIED

UNCLASSIFIED

20. ABSTRACT (Continued)

also investigated. A comparison of the effects of inlet distortion produced by screens to that produced by the airjet distortion generator system on the stability characteristics of the General Electric F101-GE-100 turbofan engine is described.

UNCLASSIFIED

PREFACE

The work reported herein was conducted by the Arnold Engineering Development Center (AEDC), Air Force Systems Command (AFSC), under sponsorship of the Aeronautical Systems Division (ASD/YZEE), Wright-Patterson AFB, Ohio. The results of the test were obtained by ARO, Inc., AEDC Division (a Sverdrup Corporation Company), operating contractor for the AEDC, AFSC, Arnold Air Force Station, Tennessee, under ARO Projects No. E41K-09 and E41K-19. The data analysis was completed on August 25, 1978, and the manuscript was submitted for publication on October 23, 1978.

CONTENTS

	<u>Page</u>
1.0 INTRODUCTION	9
2.0 APPARATUS	
2.1 Test Article	10
2.2 Test Equipment	11
2.3 Test Cell and Installation	12
2.4 Instrumentation	13
3.0 PROCEDURE	
3.1 Test Conditions	13
3.2 Airjet Distortion Generator System	14
3.3 Engine Operation	14
3.4 Engine Operation - Stability Testing	14
3.5 Methods of Calculation	14
4.0 RESULTS AND DISCUSSION	
4.1 Inlet Total-Pressure Pattern Fidelity	15
4.2 Engine Stability Response	19
4.3 System Performance Reliability	21
5.0 SUMMARY OF RESULTS	22
REFERENCES	23

ILLUSTRATIONS

Figure

1. Airjet Distortion Generator System	
a. F101 Engine/ADG System Installed in Test Cell	25
b. Primary and Secondary Airflow	26
2. Engine Front Frame Showing Total-Pressure Probes	27
3. Airjet Distortion Generator Air Supply System	28
4. Airjet Assembly	
a. Airjet Distortion Generator System Schematic	29
b. Airjet Assembly Manifold and Air Supply Lines	30
c. Air Injection Assembly Struts	31
d. Airjet Assembly Installed	32
5. Computer Control Logic for Airjet Distortion Generator	
Airflow Distribution System	33
6. F101-GE-100 Engine	34

	<u>Page</u>
7. Inlet Distortion Screens	
a. 50-percent Hub Radial Screen (141)	35
b. 180-deg, 1/rev Screen (106)	36
c. F101 Specification Screen (354.7M)	37
8. Facility Instrumentation Stations	38
9. Engine Fan and Compressor Instrumentation	39
10. Steady-State Distortion Comparison for 180-deg, 1/rev Pattern (2), (Low-Speed Fan Surge)	
a. Engine Inlet Isobar Maps for Screen and ADG System Distortion	40
b. Distortion Indices for Screen and ADG System Distortion	40
c. Individual Normalized Pressures at 40 Spatial Locations	40
11. Steady-State Distortion Comparison for 180-deg, 1/rev Pattern (1), (High-Speed Fan Surge)	
a. Engine Inlet Isobar Maps for Screen and ADG System Distortion	41
b. Distortion Indices for Screen and ADG System Distortion	41
c. Individual Normalized Pressures at 40 Spatial Locations	41
12. Steady-State Distortion Comparison for 180-deg, 1/rev Pattern (23), (Core Surge)	
a. Engine Inlet Isobar Maps for Screen and ADG System Distortion	42
b. Distortion Indices for Screen and ADG System Distortion	42
c. Individual Normalized Pressures at 40 Spatial Locations	42
13. Steady-State Distortion Comparison for 50-percent Hub Radial Pattern (4), (Low-Speed Fan Surge)	
a. Engine Inlet Isobar Maps for Screen and ADG System Distortion	43
b. Distortion Indices for Screen and ADG System Distortion	43
c. Individual Normalized Pressures at 40 Spatial Locations	43
14. Steady-State Distortion Comparison for 50-percent Hub Radial Pattern (3), (High-Speed Fan Surge)	
a. Engine Inlet Isobar Maps for Screen and ADG System Distortion	44
b. Distortion Indices for Screen and ADG System Distortion	44
c. Individual Normalized Pressures at 40 Spatial Locations	44
15. Steady-State Distortion Comparison for 50-percent Hub Radial Pattern (25), (Core Surge)	
a. Engine Inlet Isobar Maps for Screen and ADG System Distortion	45
b. Distortion Indices for Screen and ADG System Distortion	45
c. Individual Normalized Pressures at 40 Spatial Locations	45

16. Steady-State Distortion Comparison for F101 Specification Pattern (26), (High-Speed Fan Surge)	
a. Engine Inlet Isobar Maps for Screen and ADG System Distortion	46
b. Distortion Indices for Screen and ADG System Distortion	46
c. Individual Normalized Pressures at 40 Spatial Locations	46
17. Steady-State Distortion Comparison for F101 Specification Pattern (27), (Core Surge)	
a. Engine Inlet Isobar Maps for Screen and ADG System Distortion	47
b. Distortion Indices for Screen and ADG System Distortion	47
c. Individual Normalized Pressures at 40 Spatial Locations	47
18. Steady-State and Dynamic Distortion for a Clean Inlet	
a. Engine Inlet Isobar Map for a Clean Inlet	48
b. Engine Inlet RMS Distribution Map for a Clean Inlet	48
c. Distortion Indices for a Clean Inlet	48
19. Dynamic Distortion Comparison for 50-percent Hub Radial Pattern (4), (Low-Speed Fan Surge)	
a. Engine Inlet RMS Distribution Maps for Screen and ADG System Distortion	49
b. Distortion Indices for Screen and ADG System Distortion	49
c. Power Spectral Density Characteristics for Screen and ADG System Distortion	49
20. Dynamic Distortion Comparison for 50-percent Hub Radial Pattern (3), (High-Speed Fan Surge)	
a. Engine Inlet RMS Distribution Maps for Screen and ADG System Distortion	50
b. Distortion Indices for Screen and ADG System Distortion	50
c. Power Spectral Density Characteristics for Screen and ADG System Distortion	50
21. Dynamic Distortion Comparison for 50-percent Hub Radial Pattern (25), (Core Surge)	
a. Engine Inlet RMS Distribution Maps for Screen and ADG System Distortion	51
b. Distortion Indices for Screen and ADG System Distortion	51
c. Power Spectral Density Characteristics for Screen and ADG System Distortion	51

	<u>Page</u>
22. Dynamic Distortion Comparison for F101 Specification Pattern (26), (High-Speed Fan Surge)	
a. Engine Inlet RMS Distribution Maps for Screen and ADG System Distortion	52
b. Distortion Indices for Screen and ADG System Distortion	52
c. Power Spectral Density Characteristics for Screen and ADG System Distortion	52
23. Dynamic Distortion Comparison for F101 Specification Pattern (27), (Core Surge)	
a. Engine Inlet RMS Distribution Maps for Screen and ADG System Distortion	53
b. Distortion Indices for Screen and ADG System Distortion	53
c. Power Spectral Density Characteristics for Screen and ADG System Distortion	53
24. Steady-State Distortion Comparison with Screen Generated Patterns for Other Engine/Rig Tests	
a. 180-deg, 1/rev Pattern (1), 100-percent Fan Speed Surge	54
b. 180-deg, 1/rev Pattern (2), 90-percent Fan Speed Surge	54
c. 180-deg, 1/rev Pattern (23), Core Surge	54
d. 180-deg, 1/rev Modified Pattern (35), 90-percent Fan Speed Surge	55
e. Tip Radial Pattern (5), 90-percent Fan Speed Surge	55
f. Tip Radial Pattern (6), 75-percent Fan Speed Surge	55
g. Tip Radial Pattern (7), 100-percent Fan Speed Surge	56
h. Composite Pattern (14), Sea-Level-Static with Crosswind	56
i. Composite Pattern (15), PWT Full-Scale, Sea-Level-Static	56
j. Composite Pattern (16), PWT Full-Scale, Sea-Level-Static	57
k. Composite Pattern (30), 100-percent Fan Speed Surge	57
l. Composite Pattern (31), Core Surge	57
m. Composite Pattern (32), 100-percent Fan Speed Surge	58
n. Composite Pattern (33), Core Surge	58
o. Composite Pattern (11), Simulated Supersonic	58
p. Composite Pattern (9), Simulated Subsonic	59
q. Composite Pattern (34), Modified Simulated Subsonic	59
25. Reynolds Number Effect on Patterns	
a. F101 Specification Pattern (26) at 100-percent Fan Speed Surge	60
b. F101 Specification Pattern (27) at Core Surge	61
26. General Electric Distortion Sensitivity Curves for the F101 Fan	62

Page

27. Pattern Stability during Airflow Change	
a. 180-deg, 1/rev Pattern (Screen 106)	63
b. 50-percent Hub Radial Pattern (Screen 141)	64
28. Pattern Repeatability	65
29. Engine Performance Deterioration	66

TABLES

1. Posttest Estimates of Data Uncertainties	
a. Parameter Measurement Uncertainty for Steady-State Data	67
b. Parameter Measurement Uncertainty for Time-Averaged Transient Data	69
c. Parameter Measurement Uncertainty for Transient Data	71
d. Calculated Parameter Uncertainty for Steady-State Data	71
e. Calculated Parameter Uncertainty for Time-Averaged Transient Data	72
2. Test Summary	73
3. Chronological Test Summary	79
4. Pattern Matches during Baseline Testing	82
5. Pattern Matches (Other Than Baseline)	83
6. Engine Stability Comparison for Baseline Tests	84
7. Engine Stability Comparison (Other Than Baseline)	85
8. Surge Pressure Ratio Comparison after Correction to Desired Distortion Level	86

APPENDIX

A. METHODS OF CALCULATION	87
-------------------------------------	----

1.0 INTRODUCTION

The recent increase of emphasis on the effects of inlet total-pressure distortion on turbine engine stability and performance has resulted in a major effort at ground test facilities to improve the duplication of the inlet total-pressure profiles encountered during operation of engines over the aircraft flight envelope. An engine will encounter a variety of distortion patterns over a wide range of engine airflow rates. To adequately define the engine stability characteristics, testing with a large number of unique distortion patterns is required. The most widely accepted approach for producing the distortion patterns has been the use of complex assemblies of various porosity screens. The inherent inflexibility of the screen configuration (single design operating point) and the extensive development effort required for each screen dictated the need for a more flexible method of producing total-pressure distortion. In response to this need, an effort to provide an alternate method has been in progress at the Arnold Engineering Development Center (AEDC) during recent years (Ref. 1).

The airjet distortion generator (ADG) system provides a method for producing steady-state, total-pressure spatial distortion at the inlet of turbine engines. Selected engine inlet total-pressure patterns can be produced by controlling the airflow through a system of counterflow jets located in the engine inlet ducting. The digital computer control system, which controls the airflow rate through each jet, makes the airjet system an efficient tool for setting a wide range of inlet distortion patterns in a timely manner.

The development of the ADG at the AEDC started with a segmented prototype generator, followed by a parametric functional and structural investigation using an engine cold-pipe simulator in conjunction with an ADG. The next program (Ref. 1) at AEDC investigated the total ADG system capability when being used with a typical present-day turbofan engine in a normal turbine engine test environment. The primary objective of this test project was to verify that an ADG system can replace varying porosity screen overlays for inlet pressure distortion testing of turbojet and turbofan engines. The scope of this investigation not only included the assessment of the fidelity with which the ADG could produce a desired parametric total-pressure pattern, but also provided (1) a direct comparison of F101-GE-100 turbofan engine surge characteristics with distortion patterns generated by both screens and the ADG, (2) engine surge characteristics with selected composite patterns simulated with the ADG and compared to historical screen data, and (3) a documentation of the effect of Reynolds number on the surge characteristics with inlet distortion patterns set by the ADG.

2.0 APPARATUS

2.1 TEST ARTICLE

2.1.1 General Description

The ADG (Fig. 1) consists of three basic systems, a high-pressure air control and temperature-conditioning module, airjet rake spool assembly, and the distortion pattern digital computer control system. The pressure sensor probes for the computer inputs for pattern control were located in the front frame of the F101-GE-100 engine (Fig. 2), and ADG hardware from a previous AEDC investigation (Ref. 1) was used where possible. A detailed description of the ADG system is presented in Ref. 1; only a general description with details of major modifications is presented in this report.

2.1.2 High-Pressure Air Control and Temperature-Conditioning Module

The high-pressure air module (Fig. 3) supplied secondary air to the airjet supply manifold at the desired pressure level and temperature to match the primary inlet air temperature when expanded to the inlet pressure level. A bypass system (Fig. 3) allows the secondary air system to be temperature conditioned before introducing the flow into the primary engine inlet stream. This bypass system is manually closed as flow is demanded for the airjets by the computer, but the remaining secondary airflow system operations were automatic. Both the high- and low-temperature-conditioning systems were successfully utilized. The only modifications from the Ref. 1 system were the inlet control valve and bypass plumbing, excluding piping changes for the Propulsion Development Test Cell (J-2) (Test Cell J-2) adaptation.

2.1.3 Airjet Rake Spool Assembly

The airjet assembly (Fig. 4) consists of the supply manifold, 56 flow control valves, 24 aerodynamically designed airjet struts mounted in a spool assembly which contains the 56 air injection ports, and the associated piping. The control valves, opening or closing, can be either manually or computer operated. Valve selection can be independent in all modes, off, or manually opening, or manually closing. Valve operation is accomplished by preset selection of any or all of three variable timers, which can be set to operate valves for time durations of from 0.1 sec to 15 sec. The average timing to fully open the ball-type metering valves is 9 sec, with initial opening occurring at 2.55 sec.

2.1.4 Distortion Pattern Computer Control System

The 56 air control valves are individually controlled by a digital computer. Engine inlet pressure level is determined from total-pressure measurements at the engine face. The pressure levels measured at the engine inlet are transposed to equivalent locations (comparable flow area for each pressure valve) at the plane of the jets and normalized by the face average pressure. The transposed local pressure ratios are interpolated to the locations of the 56 jets. Circumferential interpolation is linear, whereas radial interpolation is from a second-order Lagrangian curve fit. The computer compares the actual pressure level at each spatial location to the desired level and commands the airjet valves to either open or close as required to establish the desired pressure levels.

The command to each individual airjet valve is determined by the digital computer program logic as shown in Fig. 5. Basic logic functions determine the overall pattern root mean square error (RMSE) and the individual error (EI) at each spatial location. Valve direction is determined by comparing the measured pressure level with the desired pressure level at each spatial location; if the measured pressure level is higher than desired, the valve is directed to open; if measured pressure is lower than desired, the valve is directed to close. The selection of control valves to be repositioned is determined by comparing the error in local pressure level with the overall pattern error. Those valves controlling secondary airflow to areas with local pressure errors greater than the overall pattern error are directed to move and all remaining valves are unchanged. The amount of valve movement is the same for all valves and is determined by comparing the overall pattern error with preselected ranges. The range of overall pattern error dictates the particular valve travel time. Valve travel times are selected such that valve travel becomes smaller as overall pattern error is reduced.

2.2 TEST EQUIPMENT

2.2.1 Turbofan Engine

The engine used for this test was an F101-GE-100 engine (Fig. 6). The engine is an augmented, mixed flow, turbofan engine with aerodynamically coupled low- and high-pressure sections and a variable area exhaust nozzle. The low-pressure section consists of a two-stage fan driven by a two-stage, low-pressure turbine. Variable inlet guide vane flaps are used on the fan. The high-pressure section is composed of a nine-stage compressor, an annular combustor, and a single-stage, high-pressure, air-cooled turbine. The compressor utilizes variable geometry inlet guide vanes and stator vanes for the first three stages. The secondary nozzle was not installed for this test, and the primary nozzle had extended flaps to reduce the normal minimum area such that fan stalls could be obtained by manual nozzle closure.

The initial testing was conducted using one engine (S/N 470006/10), whereas later testing utilized another engine (S/N 470006/11). The second engine sustained compressor damage, but was rebuilt by replacement of damaged compressor blades. Testing was completed with this rebuilt engine.

2.2.2 Inlet Distortion Screens

Three distortion screen patterns were used during the test program for baseline direct comparison for ADG performance. The three screen patterns used (Fig. 7) simulated a classical 1/rev square wave, a hub radial, and a combination pattern of both tip radial and 1/rev distributions. The desired total-pressure patterns which were duplicated by the ADG were defined from measured inlet pressure values with the screens installed. The 1/rev square wave screen testing was conducted using engine S/N 470006/10. All other testing was conducted using engine S/N 470006/11.

2.3 TEST CELL AND INSTALLATION

The AEDC Test Cell J-2 (Ref. 2) is a water-cooled test cell which has a 20-ft diameter by 69-ft-long test section. The engine is mounted in a General Electric-supplied frame rigidly attached to the floating portion of the overhead water-cooled thrust stand. The engine is isolated from the engine inlet ducting, which is also mounted from the thrust stand, by a flexible seal. The floating thrust stand is isolated from the test cell ducting by a labyrinth seal. The ADG system was used in conjunction with the normal engine test installation.

The initial testing was with distortion screens, and the airjet strut assembly was not installed. The screen location is just downstream of the airjet strut location (Fig. 4a), and the screen support grid remained installed during all testing.

The ADG high-pressure air control and temperature-conditioning module is located outside the Test Cell J-2. High-pressure air is supplied at pressures up to 4,000 psi through filter stations with 150-, 100-, and 40- μ filters. A 4-in. line supplied the air from the module to the airjet spool assembly.

The engine is supplied conditioned air from the facility rotating compressors and associated machinery. The engine exhaust flow is removed from the test cell through an 8-ft-diam diffuser and the facility rotating exhaust compressor systems.

A facility system using gaseous nitrogen was provided to supply a false compressor discharge (FP3) pressure signal to the main fuel control system of the engine during compressor surge investigations rather than the engine compressor discharge pressure signal. Operation of the system was remotely selected and controlled to vary the fuel flow acceleration schedule during surge demonstrations according to preselected FP3 levels.

2.4 INSTRUMENTATION

Instrumentation was provided to measure steady-state aerodynamic pressures and temperatures; dynamic pressures; fuel system pressures, temperatures, and flow rates; rotational speeds; exhaust nozzle area; engine accelerations; and engine control system signals. Aerodynamic pressure and temperature measurements were made at the test cell locations shown in Fig. 8 and at the engine stations shown in Fig. 9.

Posttest estimates of measurement uncertainties for the critical parameters are presented in Table 1. Plane 1 and plane 14/25 (Fig. 9) pressure transducers were used for the ADG control and dynamic measurements. Bonded strain-gage-type transducers were used for ADG control feedback signals and for all transient data acquisition. These systems had a 4-Hz minimum response and were calibrated by resistance shunt pressure equivalent substitution. The Kulite® close-coupled transducers were mounted within the engine probes, and data were filtered at one-half of the fan and compressor rotational frequencies, plane 1 at 125 Hz, and plane 25 at 250 Hz. The Kulite pressure transducers were pretest calibrated by applying a known pressure across all transducers in both the increasing and decreasing pressure mode. This was accomplished by a pneumatic system plumbed to each transducer that allowed a known pressure to be applied to either or both sides of the sensor to obtain a zero pressure level signal. Because of the tendency of the transducers to shift with temperature and time, each transducer was electrically nulled and a single-step calibration applied within 30 min before obtaining dynamic data. These data were acquired through an analog distortion analyzer (ADA) and RMS-to-DC converter for online display. These outputs, plus the Kulite pressure signals, were recorded on FM multiplex tape systems for offline analysis.

3.0 PROCEDURE

3.1 TEST CONDITIONS

Conditioned air was supplied to the engine inlet at the total pressure and temperature required to simulate the desired test matrix condition. Testing was not conducted at the simulated altitudes normally associated with the specific patterns being simulated. Inlet pressures were reduced to minimize engine deterioration during the induced engine surges, and the inlet temperature was reduced to allow adequate turbine temperature margin to obtain fan stalls without causing fan speed reduction.

3.2 AIRJET DISTORTION GENERATOR SYSTEM

The ADG secondary airflow was conditioned to match the engine inlet air supply by first bypassing the airjet rake spool assembly. The secondary air automatic control system was then set to maintain the inlet temperature match and the preselected airjet rake manifold pressure. The manifold pressure was nominally set at 550 psia, but was reduced to approximately 300 psia at the lower inlet pressure (2 to 4 psia) conditions. When all support systems were set and stabilized, the distortion pattern computer control system was activated; as the airjet distribution system valves were opened, the secondary bypass valve was closed.

3.3 ENGINE OPERATION

Engine starts were accomplished by windmilling the engine with facility airflow and a 5-psia nominal pressure differential across the engine, and then advancing the throttle to the idle position (18 deg). After stabilizing at idle, the specific test condition was set and the throttle was advanced to the desired power setting.

3.4 ENGINE OPERATION - STABILITY TESTING

Engine stability was evaluated with clean inlet, inlet pressure distortion screens and distortion patterns set with the ADG. The engine was started as previously described and stabilized for a period of 15 min at a specific corrected airflow for each pattern using the airflow limiting system (ALS). The engine was intentionally stalled for determination of the surge margin of both fan and high-pressure compressor.

Whenever engine stalls occurred, the power lever was immediately reduced to the idle position (18 deg). If the stall persisted, the engine was shut down.

Fan stalls were induced along constant speed lines by exhaust nozzle closure. Incremental nozzle closure was accomplished by a remote control to the AFT control $\Delta P/P$ (fan duct Mach number) adjustment.

Compressor stalls were induced by "fuel stepping" the compressor. The fuel steps were accomplished by switching with a dual ALS from a low to a high engine rpm in a 500-rpm step and raising the fuel schedule by the use of the false FP3 system.

3.5 METHODS OF CALCULATION

The methods used to calculate the data parameters are presented in Appendix A. Uncertainties for calculated parameters are presented in Table 1.

4.0 RESULTS AND DISCUSSION

A performance evaluation of an ADG system was conducted to verify that an ADG system can replace varying porosity screen overlays for inlet pressure distortion testing of turbojet and turbofan engines.

The scope of this investigation not only included the assessment of the fidelity with which the ADG could produce a desired parametric total-pressure pattern, but also provided (1) a direct comparison of F101-GE-100 turbofan engine surge characteristics with distortion patterns generated by both screens and the ADG, (2) engine surge characteristics with selected composite patterns simulated with the ADG and compared to historical screen data, and (3) a documentation of the effect of Reynolds number on the surge characteristics with inlet distortion patterns set by the ADG.

First, the test results relative to the primary objective are presented, and second, additional test results are presented concerning the operation and performance of the ADG system (Tables 2 and 3).

4.1 INLET TOTAL-PRESSURE PATTERN FIDELITY

The ADG system is designed to produce steady-state, total-pressure spatial distortion of the airflow at the inlet of a turbine engine. The fidelity of the inlet distortion patterns produced by the ADG system was evaluated for 10 classical and 12 composite inlet distortion patterns. Six classical and two composite distortion patterns were produced and measured using distortion screens installed in the engine inlet ducting. Distortion pattern measurements were available from other sources for the remaining inlet distortion patterns. The ADG system was then used to reproduce the inlet pressure pattern measurements.

4.1.1 Comparison with Screen-Generated Patterns for Engine S/N 470006/11

Screen-generated inlet distortion patterns were produced for six classical patterns 180-deg, 1/rev and 50-percent hub radial patterns at fan speeds from 90 to 100 percent and two composite patterns (F101 specification patterns). Each screen-generated pattern was then reproduced by the ADG system. A summary of results is shown in Table 4.

Steady-state, total-pressure distortion pattern quality can be described by the pattern characteristic appearance and distortion level DIST1 (Appendix A). Pattern characteristics, as presented by isobar maps at the engine inlet, are presented in Figs. 10 through 17. An isobar map of a clean engine inlet is presented in Fig. 18a. For each pattern, the ADG system produced similar areas of high and low total pressure and maintained similar area contours to those produced by the distortion screens. The distortion level of the classical patterns produced by the ADG system agreed with the screen-produced distortion

level within 1.5 percent DIST1. For the composite patterns, agreement was within 6 percent DIST1.

An evaluation of the circumferential and radial distortion can be made with the use of the parameters IDC and IDR (Appendix A). For the three classical 50-percent hub radial patterns, IDR values for patterns produced by the ADG system were slightly lower in magnitude in both the hub and tip regions than the IDR values for the screen-produced patterns (maximum $\Delta IDR = 0.01$). For the three 180-deg, 1/rev patterns IDR values were slightly higher in magnitude in both the hub and tip regions for ADG "system-produced" patterns than the IDR values for "screen-produced" patterns (maximum $\Delta IDR = 0.02$). In the composite patterns the ADG system again gave lower IDR values in the hub region, but IDR values in the tip region were slightly higher than those from the screen-produced patterns (maximum $\Delta IDR = 0.02$). For the three 50-percent hub radial patterns, IDC values in the hub region for both ADG system and screen-produced patterns agreed; but in the tip region, the ADG system patterns were somewhat higher (maximum $\Delta IDC = 0.04$). For the 180-deg, 1/rev low-speed fan surge pattern, IDC values agreed in the tip region but were low ($\Delta IDC = 0.02$) in the hub region for the ADG system pattern. Both the 180-deg, 1/rev high-speed fan surge and core surge patterns resulted in slightly lower IDC values in the hub and tip region (maximum $\Delta IDC = 0.02$). In both composite patterns, the ADG system gave slightly lower IDC values in the hub region and slightly higher values in the tip region (maximum $\Delta IDC = 0.02$). IDR and IDC values as functions of ring number are given in Figs. 10 through 18.

Although pattern characteristics and distortion level are good indications of pattern quality, the specific definition of each inlet pattern should be made on the basis of a comparison of individual pressure levels at the specific spatial locations. Individual pressure values for each pattern are compared in Figs. 10 through 17. The overall agreement between the measured and desired local pressure levels can be quantified by the RMSE (Appendix A). For the five patterns, the RMSE ranged from 1.1 to 2.5 percent. This is less error than that nominally obtained with screens using current design techniques (Ref. 1). The largest RMSE generally occurred at the highest distortion levels. Individual RMSE values are given in Figs. 10 through 18. In general, the steady-state agreement between the ADG system patterns and screen patterns was good, with excellent agreement on the six classical patterns.

A survey of time variant total-pressure was made for three classical and two composite pressure patterns produced by both the ADG system and by inlet distortion screens. To get a quantitative comparison of the turbulence levels produced by the ADG system and an inlet distortion screen, RMS values were calculated for each spatial location.

Characteristics of the time variant total pressure can be seen in total-pressure RMS distribution maps. Figures 19 through 23 present maps of normalized total-pressure RMS and PRMS/PF (face-averaged normalized RMS) for the three classical and two composite patterns produced by both distortion methods. A map of normalized total-pressure RMS for a clean engine inlet is presented in Fig. 18c. In general, inlet total-pressure distortion patterns produced by distortion screens showed approximately one-half as high levels of PRMS (0.4 to 0.6 percent) as the same distortion patterns produced by the ADG system (1.1 to 1.3 percent). In the screen-produced patterns, the highest levels of total-pressure RMS were consistently observed to be near the outer wall region similar to the RMS distribution for the clean inlet. However, for the values of PRMS from distortion screen-produced patterns these "highest" levels are still quite low (0.7 to 0.8 percent). For distortion patterns produced by the ADG system the highest levels of total-pressure RMS fall in the regions of steepest total-pressure gradient, remaining lower in the flat areas of both high and low total pressure.

An evaluation of the dynamic circumferential and radial distortion can be made by again using the parameters IDC and IDR. For the 50-percent hub radial patterns, instantaneous values of IDC and IDR are presented at the time of maximum IDR. For the composite patterns, instantaneous values for IDC and IDR are presented at the time of maximum IDC. Dynamic values for IDC and IDR as functions of ring number are presented in Figs. 19 through 23 along with the steady-state IDC and IDR for the same patterns. Dynamics had little effect on the radial gradient (maximum $\Delta IDR = 0.01$), but had slightly larger effect on the circumferential gradient (maximum $\Delta IDC = 0.05$).

To evaluate the frequency and energy of the time variant total pressure, a comparison of the power spectral density (PSD) functions (Appendix A) for each pattern is presented (Figs. 19 through 23). In general, the functions for the ADG system patterns are slightly higher and flatter than the PSD functions for the screen patterns. The higher levels indicate more turbulent energy in the ADG system pattern, whereas, the flatness indicates a distribution closer to that of white noise, as would be expected from the jet mixing.

4.1.2 Comparison with Previous Engine/Rig Test Results

Inlet total-pressure pattern measurements were available from other engine/rig tests for an additional seven classical and ten composite patterns. Each pattern was reproduced by the ADG system, and the results are summarized in Table 5.

Pattern characteristics and distortion levels are shown in Fig. 24a through q in the form of isobar maps and corresponding DIST1 values for each pattern. Similar areas of high and low pressure were produced by the ADG system as were shown in the screen-produced patterns. In all but the most highly distorted patterns, similar pressure contours were maintained.

Duplications of four 180-deg, 1/rev square wave patterns with distortion levels varying from 16.3 to 32.2 percent total distortion and varying pressure gradient severity were attempted with the ADG system. RMSE values ranged from 1.5 to 6.3 percent with smaller values for patterns with less severe gradients (Fig. 24a through d) (lower values of IDC). Distortion level disagreement ranged from 0.0 to 10.2 percent DIST1 with best agreement for patterns with lower total distortion levels.

Three classical tip radial patterns were attempted with total distortion levels ranging from 16.2 to 23.2 percent and varying gradient severity. RMSE values ranged from 1.8 to 4.3 percent as gradient severity increased from a pattern maximum IDR value of 0.081 to 0.105 (Fig. 24e through g). Distortion level agreement ranged from 1.4 to 8.9 percent DIST1 with the worst case occurring at the highest total distortion level.

Ten composite inlet total-pressure distortion patterns were attempted with total distortion levels ranging from 13.5 to 24.7 percent and varying combinations of radial and circumferential distortion. RMSE values ranged from 2.2 to 5.1 percent while distortion level agreement ranged from 0.3 to 7.9 percent, again with the worst agreement occurring at the highest total distortion level (Fig. 24h through q).

Overall, the ADG system could closely match patterns at high corrected airflow rates but could not match patterns with severe gradients at lower corrected airflows, indicating that with lowered velocity in the primary flow the counterflowing jets were not as effective in reducing total pressure. For a tip radial pattern with 100-percent fan speed, a radial gradient of 16.2 percent was achieved whereas only 10.9-percent radial gradient was achieved at 75-percent fan speed (Fig. 24f and g). This indicates that the Test Cell J-2 ADG installation is too limited in both radial and circumferential distortion to match the most severe patterns.

4.1.3 Effect of Reynolds Number on Patterns

To determine the effect of changes in Reynolds number on inlet total-pressure pattern fidelity, two composite patterns (F101 specification pattern at high-speed fan surge and F101 specification pattern at core surge) were matched by the ADG system at inlet pressures of 8, 4, and 2 psia, corresponding to Reynolds number indices of 0.6, 0.3, and 0.15, respectively. For both patterns attempted, results were consistent at each Reynolds number index. Values for RMSE varied only 0.2 percent for the fan surge and 0.4 percent for the core surge. This is within the repeatability of the ADG system (Section 4.3.2). DIST1 values varied 1.6 to 2.3 percent for the fan and core surge patterns, respectively. Individual values for RMSE and DIST1 are presented along with isobar maps at each Reynolds number in Fig. 25. Radial distortion as shown by IDR remained essentially unchanged under each condition for both patterns. However, values for IDC indicate the

circumferential distortion in the tip region increased slightly for both patterns as Reynolds number was decreased. IDC and IDR values for these two patterns are presented as functions of ring number in Fig. 25.

For both the fan surge and core surge patterns the magnitude of the time variant inlet total pressure increased with decreasing Reynolds number. PRMS increased from 1.2 to 1.4 to 2.1, corresponding to Reynolds number indices (RNI) of 0.6, 0.3, and 0.15 for the core surge pattern, whereas PRMS values for the fan surge were 1.4, 1.4, and 2.4. However, these variations in PRMS are within the repeatability of the data system at the pressure level required to achieve a Reynolds number index of 0.15.

4.2 ENGINE STABILITY RESPONSE

The currently acceptable method of producing steady-state total-pressure distortion for turbine engine stability testing uses the technique of installing various porosity screens in the engine inlet. In order for the ADG system to be an acceptable alternate method, it is necessary to define any differences in engine stability with distortion produced by the two methods. During this test, engine stability was determined for ten classical and three composite distortion patterns produced by the ADG system. In addition, engine stability was determined for three of the classical and two of the composite distortion patterns produced by inlet screens. This procedure provided a direct comparison of engine operation with the same pattern produced by the two methods.

4.2.1 Comparison of Engine's Response to Screen-Generated Patterns for Engine S/N 470006/11

Engine stability was determined for three classical patterns and two composite patterns with each pattern being produced by both inlet distortion screens and the ADG system, providing a direct comparison for engine operation under each method of inlet pressure distortion. Results are summarized in Table 6.

Fan surges occurred with the 50-percent hub radial pattern and the engine operating at 90-percent and 100-percent fan speed and loaded as described in Section 3.3. The fan normal operating level with ADG system distortion was 1.4 percent higher than the normal operating level with inlet screen-produced distortion at the low-speed condition. At the higher fan speed, the fan normal operating level with ADG system distortion was 2.6 percent higher than the normal operating level with screen distortion. The ADG system distortion produced higher surge pressure ratios than were produced by screen distortion with values of 1.0 percent and 2.3 percent at low-speed fan stall and high-speed fan stall (Table 6).

A core surge occurred with the 50-percent hub radial pattern and the engine loaded as previously described. The core surge pressure ratio was 1.4 percent lower with ADG system distortion than the surge pressure ratio with screen distortion (Table 6).

The engine fan and core were both surged with the composite F101 specification pattern. Fan normal operating level was 3.5 percent higher with ADG system distortion than with screen distortion. Surge pressure ratios for both engine components were less than one percent higher (0.4 percent for the fan and 0.6 percent for the core) with ADG system distortion than with screen distortion (Table 6).

In general, engine response agreement was good. Engine response to screen- and ADG system-produced distortion agreed within an average of one percent.

4.2.2 Comparison of Engine's Response to Screen-Generated Patterns for Other Engine/Rig Test

Engine stability was determined for three 180-deg, 1/rev distortion patterns, one modified 180-deg, 1/rev distortion pattern, two 50-percent tip radial patterns, and one F101 specification pattern. Comparisons were made with stability responses from previous engine/rig tests. Results are shown in Table 7.

High- and low-speed fan surges occurred with the ADG system producing the 180-deg, 1/rev distortion pattern. Surge pressure ratio for the high-speed surge was 1.6 percent low with ADG-produced distortion, whereas the low-speed surge pressure ratio was 2.6 percent higher than the corresponding screen value. A core surge also occurred, giving a 0.9 percent lower surge pressure ratio under ADG system distortion. Using the modified 180-deg, 1/rev distortion pattern, a fan surge was obtained with the ADG system producing a 6.3 percent higher surge pressure ratio than resulted with screen distortion.

High- and low-speed fan surges were again obtained with ADG system-produced 50-percent tip radial distortion. Surge pressure ratio for the high-speed surge was 2.3 percent lower with ADG system distortion, whereas the low-speed surge pressure ratio was 15.9 percent higher than the corresponding screen value. Finally, a fan surge was obtained with the F101 specification pattern. The surge pressure ratio with ADG system distortion was 13.8 percent higher than the corresponding screen value.

The results discussed above indicate that when the patterns are matched within a 3-percent RMSE that there is little difference in the engine's stability response (-2.3 to 2.6 percent in surge pressure ratio). However, for the patterns not well matched (RMSE = 4.3 to 6.3 percent), large disagreements in the engine's stability response occurred which, as explained in Section 4.2.3, appears to be solely the result of the mis-set steady-state distortion pattern.

4.2.3 Evaluation of Engine Response Differences

In some cases, surge pressure ratio with ADG system-generated inlet distortion was significantly different from surge pressure ratios with screen distortion. However, the patterns with worse surge pressure ratio agreements also had high RMSE values, indicating that the engine was not actually responding to identical patterns. Distortion sensitivity curves (Fig. 26) have been generated by General Electric for the F101 giving surge pressure ratio loss as a function of average IDC for 180-deg, 1/rev patterns and maximum IDR for tip radial and hub radial patterns. By using these curves to correct mismatches in the distortion parameters, a better evaluation can be made of any effects the ADG system itself had on surge pressure ratio. Seven patterns were corrected by both steady-state and dynamic values of IDC and IDR; results are shown in Table 8. In general, surge pressure ratio disagreement was reduced to less than four percent. When considering engine-to-engine and facility-to-facility tolerances, the four-percent disagreement implies that there are no discernible differences in the engine's stability response between a screen-produced and an ADG-produced flow field.

4.3 SYSTEM PERFORMANCE RELIABILITY

4.3.1 Stability of ADG System Patterns

The high degree of flexibility associated with the ADG system was demonstrated for two classical patterns (180-deg, 1/rev square wave pattern and 50-percent hub radial pattern). The capability of the ADG system to produce a constant distortion pattern over a range of corrected engine airflows from 308 to 286 lbm/sec for the 50-percent hub radial pattern and a range of 298 to 271 for the 180-deg, 1/rev square wave pattern is demonstrated by the isobar maps of the patterns presented in Fig. 27. At each airflow level, the pattern characteristics were reproduced with the distortion level (DIST1) maintained in both cases to within one-percent absolute distortion. Both patterns showed almost no change in radial or circumferential distortion, as shown by their respective IDC and IDR values (Fig. 27). This allows patterns to be set with the engine on its normal operating line, and held while the engine is surged.

4.3.2 Repeatability of ADG System Patterns

To further demonstrate the repeatability of the ADG system patterns, a single classical pattern (180-deg, 1/rev square wave) was attempted by the ADG system at three different times throughout the project. Isobar maps again demonstrate the capability of the ADG system to produce a constant inlet distortion pattern (Fig. 24). Distortion levels varied by only 0.5 percent, whereas RMSE was maintained to within a 0.4-percent spread. Maximum values of IDC and IDR also showed little change.

For the ADG system to be a viable replacement for inlet distortion screens in engine testing it must not only reproduce inlet total-pressure profiles as accurately as screens, it must also demonstrate a high degree of operational reliability. The operational reliability of the ADG system was excellent; no major operational problems were experienced throughout the test program. One limiting factor in the ADG system operation is the quantity of high-pressure air used. Minimizing the time required to set a distortion pattern allows more time for inlet distortion engine operation. Pattern set times were consistently under two minutes, averaging approximately one and one-half minutes.

4.3.3 Engine Performance Deterioration

Engine S/N 470006/11 received a performance calibration at sea-level-static (SLS) conditions after a brief engine break-in cycle of four-hours duration. Shortly before completion of this test series, a final SLS performance calibration was obtained as shown in Fig. 25. For an engine operating time of 50 hours at AEDC, specific fuel consumption increased 1.1 percent assessed at a net thrust of 12,000 lbf. During this 50 hours of operation, the engine was subjected to 16 fan and 10 core stalls at inlet pressures ranging from 2 to 8 psia and inlet temperatures of 470 to 684°R.

5.0 SUMMARY OF RESULTS

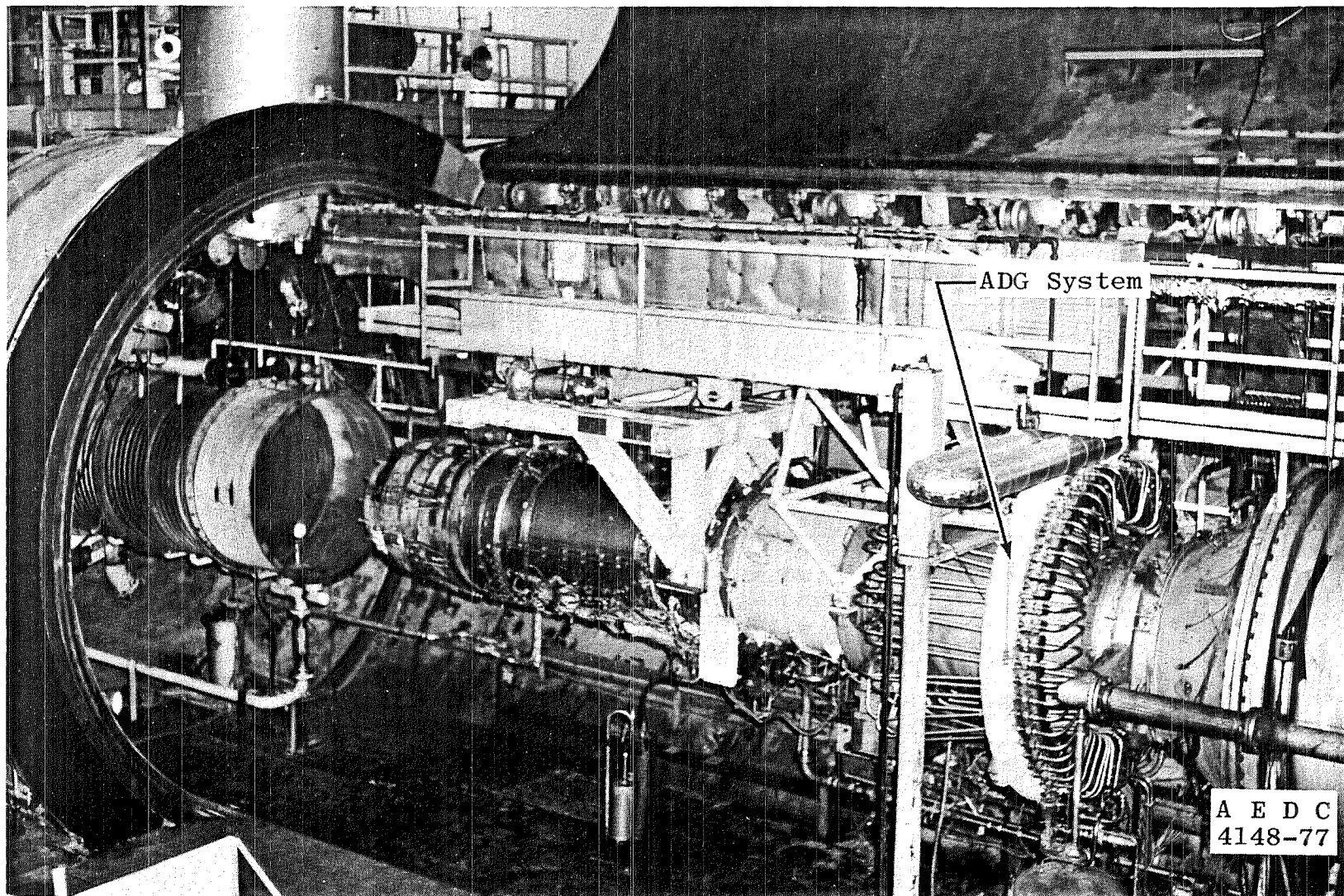
A performance evaluation of an airjet distortion generator system was conducted with ten classical and twelve composite total-pressure distortion patterns. Engine stability response was determined and compared for inlet total-pressure distortion produced by inlet screens and the ADG system. Significant results of this evaluation are summarized as follows:

1. The root mean square error of the steady-state, inlet total-pressure pattern match produced by the ADG system ranged from 1.1 to 2.5 percent for the baseline patterns. This is less error than normally obtained for screens using current design techniques.
2. The root mean square error of the steady-state inlet total-pressure pattern match produced by the ADG system ranged from 1.5 to 6.3 percent for patterns duplicating screen-generated patterns from other engine/rig tests, indicating that the present Test Cell J-2 ADG installation is too limited in both radial and circumferential distortion to match the most severe patterns.
3. Local inlet turbulence levels (PRMS/PF) measured with screen distortion were less than one percent. Local turbulence levels measured with ADG system distortion was less than two percent.

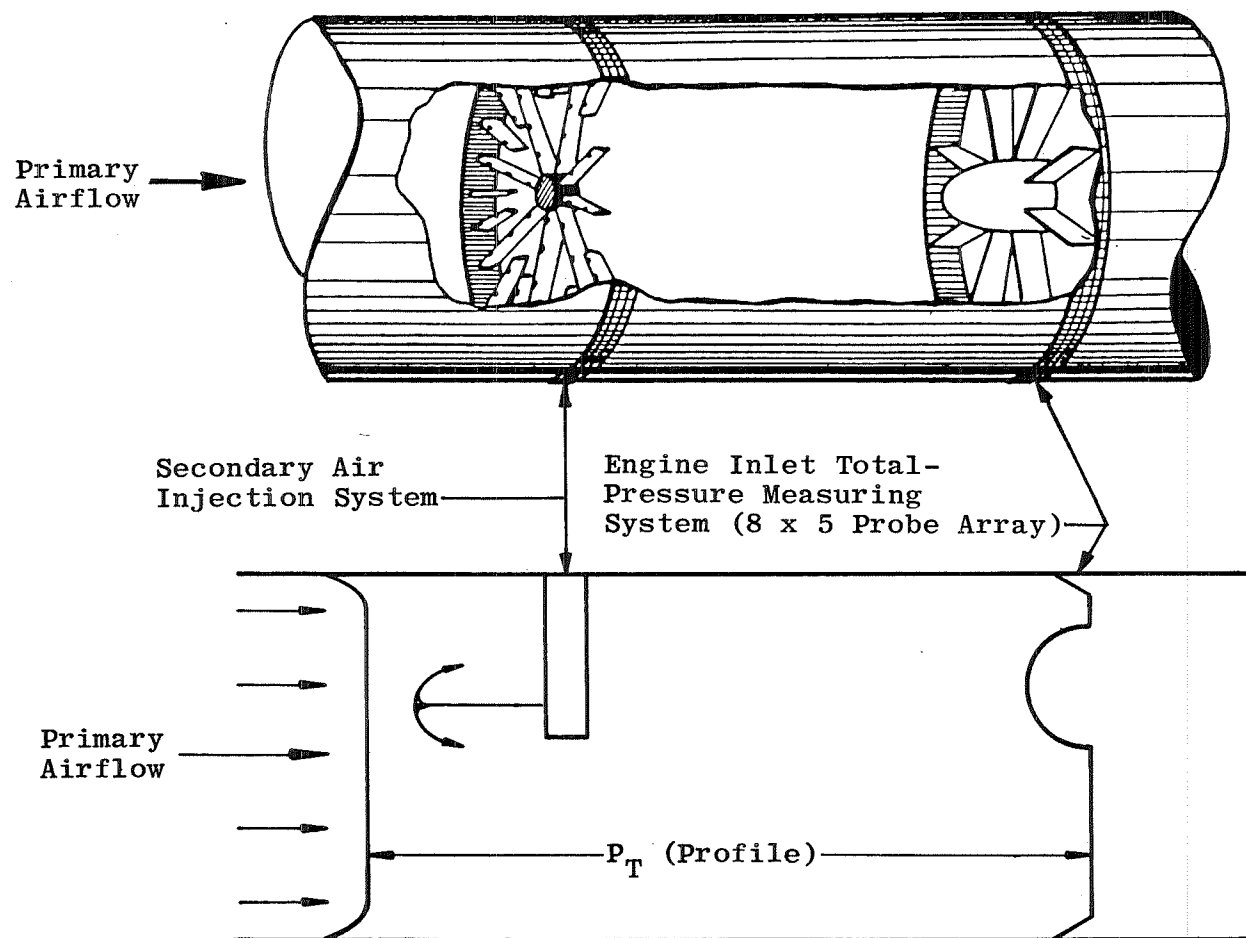
4. Reynolds number changes had little effect on the ability of the ADG system to match a desired pattern. RMSE varied no more than 0.4 percent and DIST1 varied no more than 1.6 percent, both within the repeatability of the ADG system.
5. When screen patterns and ADG system patterns matched within 3 percent RMSE, there was little difference in engine stability response (2.6 to -2.3 percent). Larger deviations in engine stability response for patterns with larger match errors can be accounted for by distortion correction.
6. The stability of the ADG system patterns was excellent. Changes in airflow of up to nine percent caused less than one-percent change in distortion.
7. The repeatability of the ADG system patterns was good. Patterns repeated at various times during the project repeated within ± 2 -percent overall error.
8. The ADG system produced a specified inlet distortion pattern within two minutes after command. The pattern set time demonstrates the increased flexibility of the ADG system as compared with distortion screens.

REFERENCES

1. Overall, B. W. "Evaluation of an Airjet Distortion Generator Used to Produce Steady-State, Total-Pressure Distortion at the Inlet of Turbine Engines." AEDC-TR-76-141 (ADA033883), December 1976.
2. Test Facilities Handbook (Tenth Edition). "Engine Test Facility, Vol. 2." Arnold Engineering Development Center, May 1974.
3. U. S. Standard Atmosphere, 1976. U. S. Government Printing Office, Washington, D.C., December 1976.
4. "Tables of Thermal Properties of Gases." U. S. Department of Commerce, National Bureau of Standards, Circular 564, U. S. Government Printing Office, November 1, 1955.
5. Gordon, S. and McBride, B. J. "Computer Program for Calculation of Complex Chemical Equilibrium Compositions, Rocket Performance, Incident and Reflected Shocks, and Chapman-Jouquet Detonations," NASA SP-273, 1971.
6. Sengers, J. M., Levelt, H., Klein, Max, and Gallagher, John S. "Pressure-Volume-Temperature Relationships of Gases Virial Coefficients." AEDC-TR-71-39 (AD719749), March 1971.



a. F101 engine/ADG system installed in test cell
Figure 1. Airjet distortion generator system.



b. Primary and secondary airflow
Figure 1. Concluded.

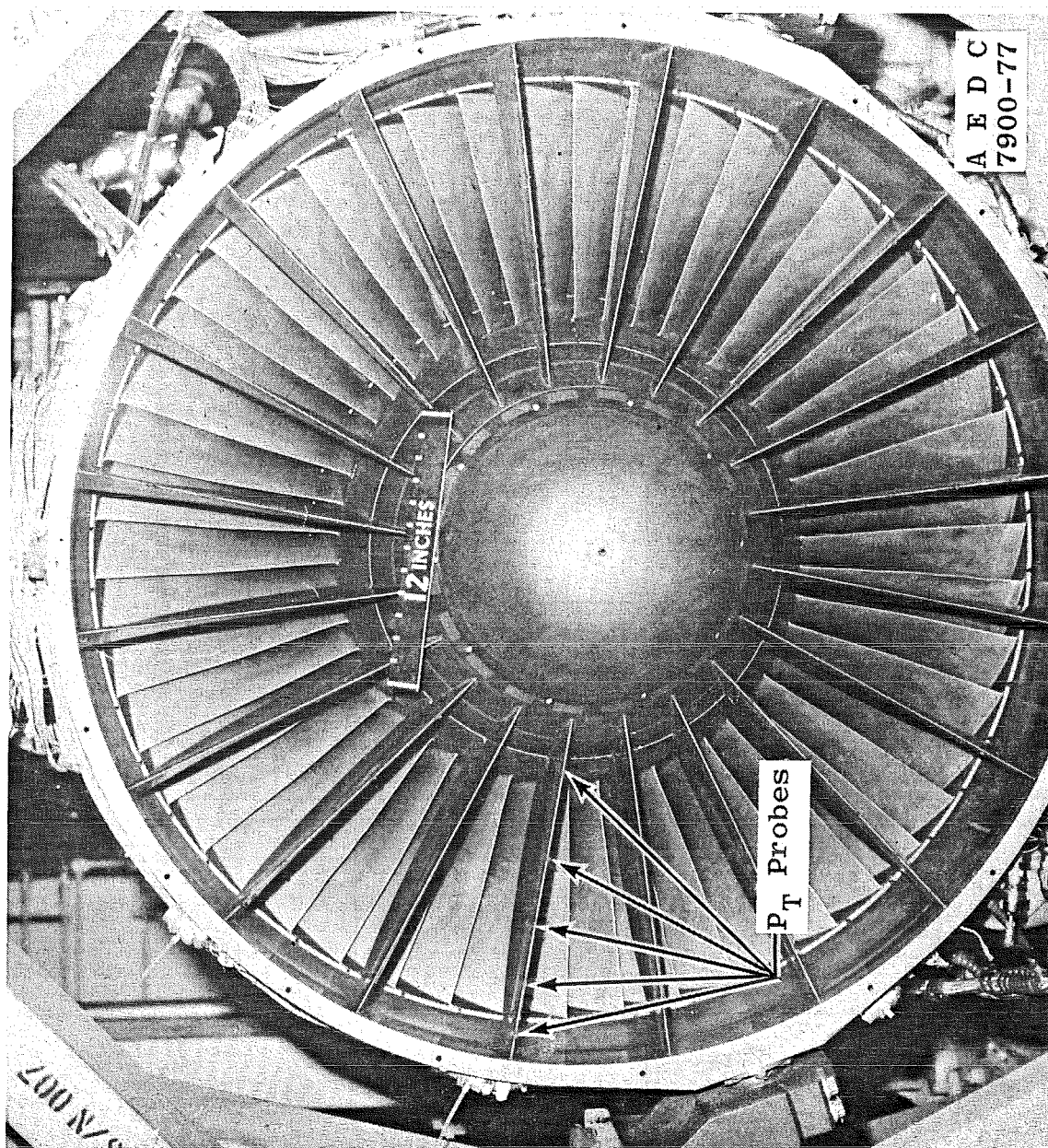


Figure 2. Engine front frame showing total-pressure probes.

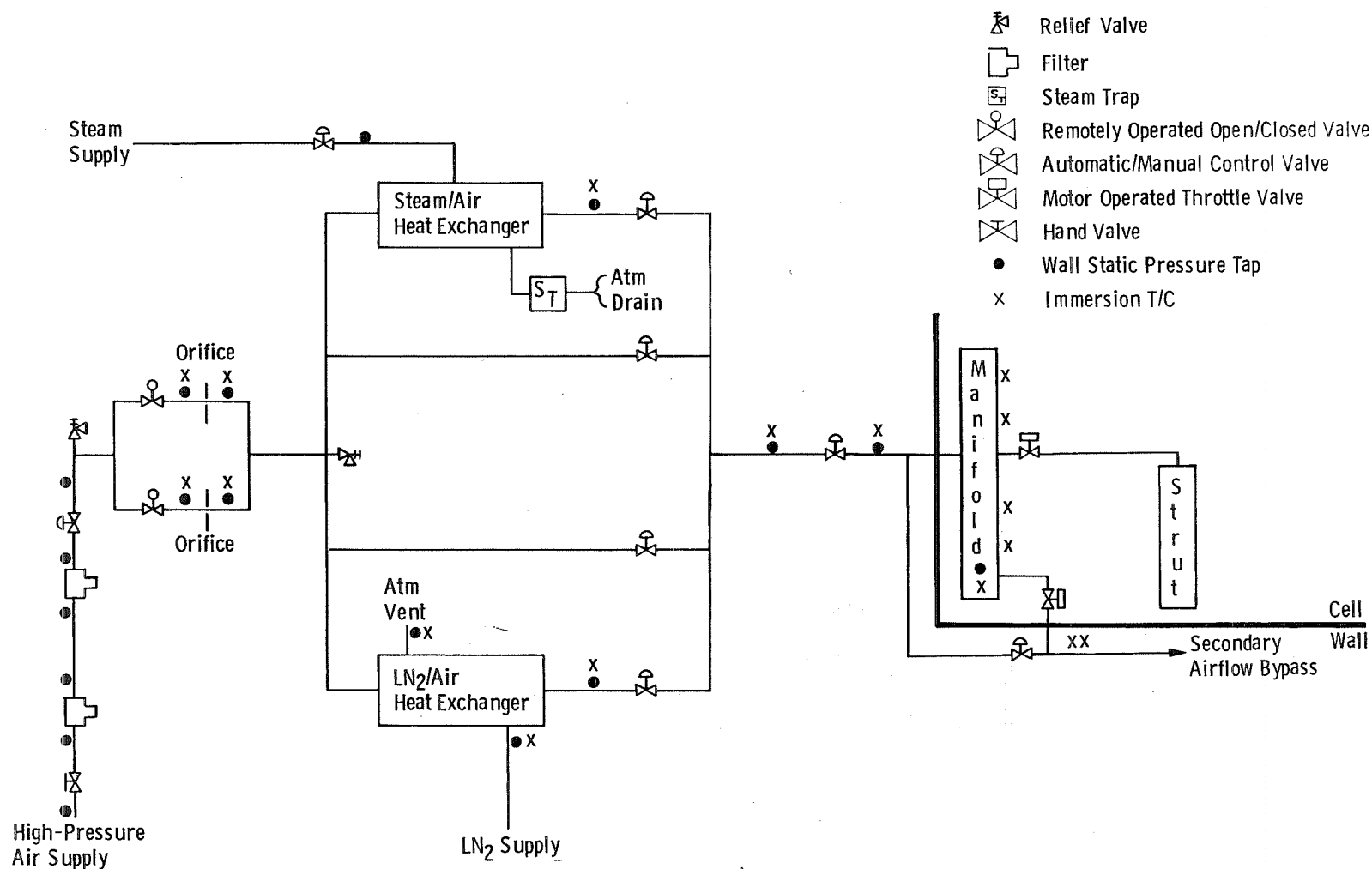
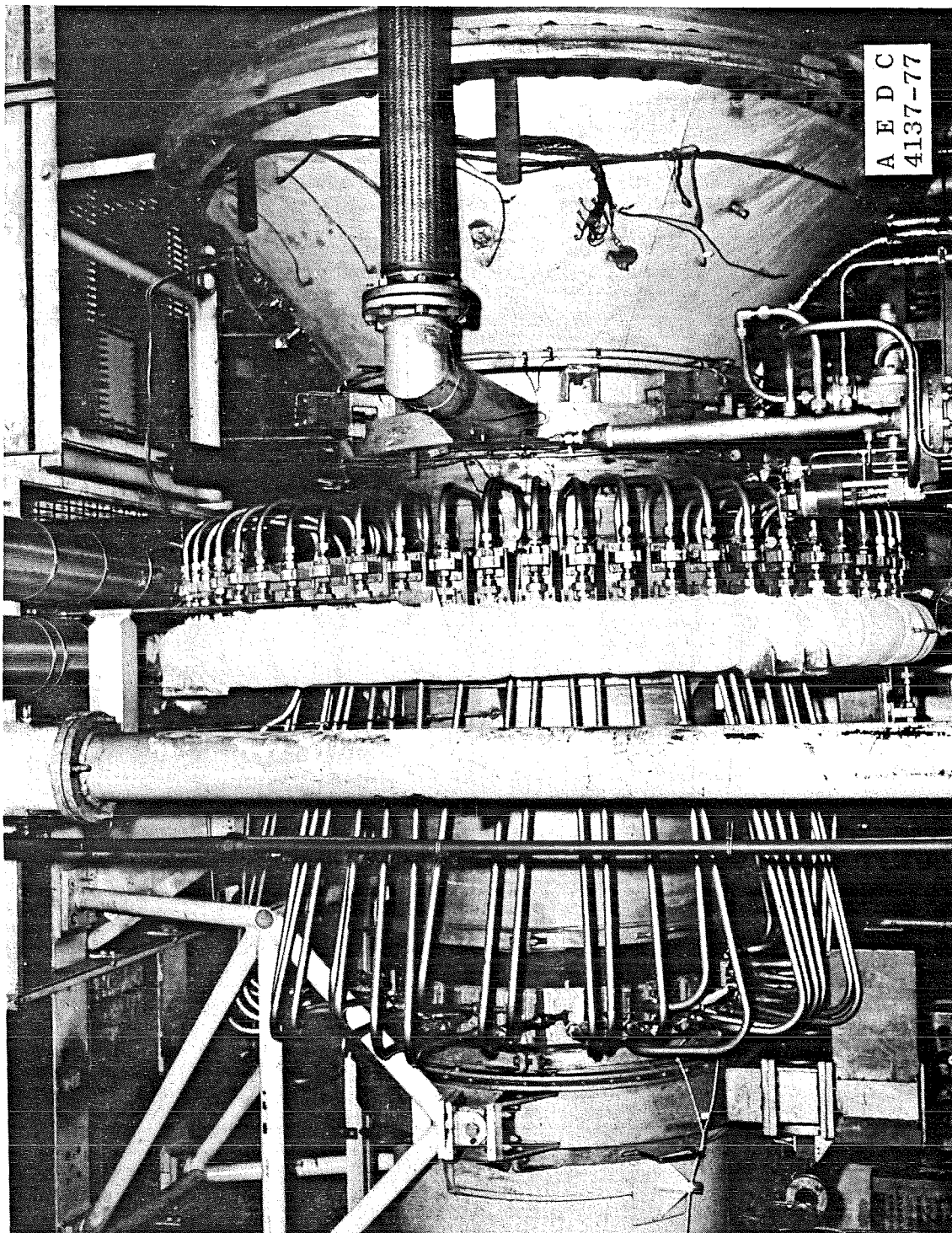
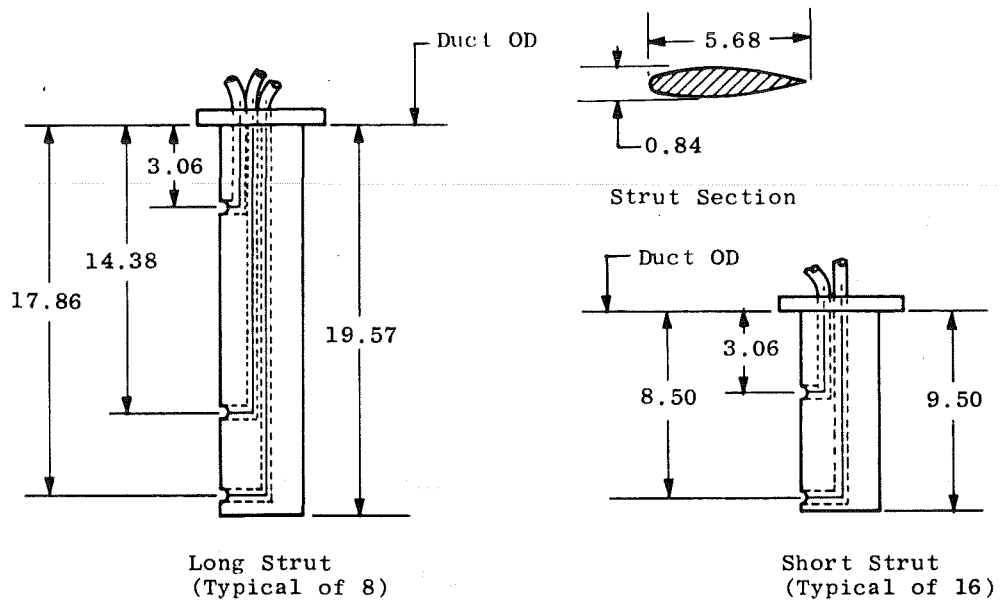


Figure 3. Airjet distortion generator air supply system.

AEDC-TR-78-73



b. Airjet assembly manifold and air supply lines
Figure 4. Continued.

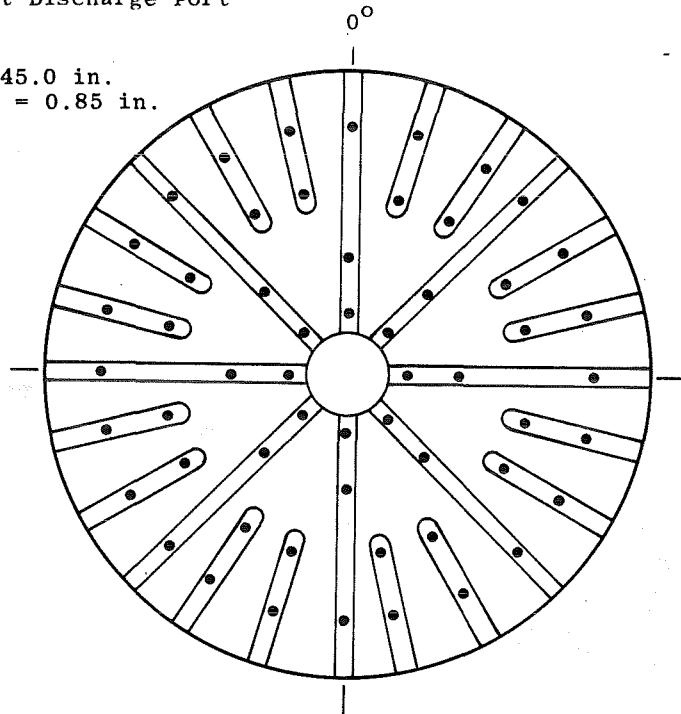


Strut Details

All Dimensions in Inches

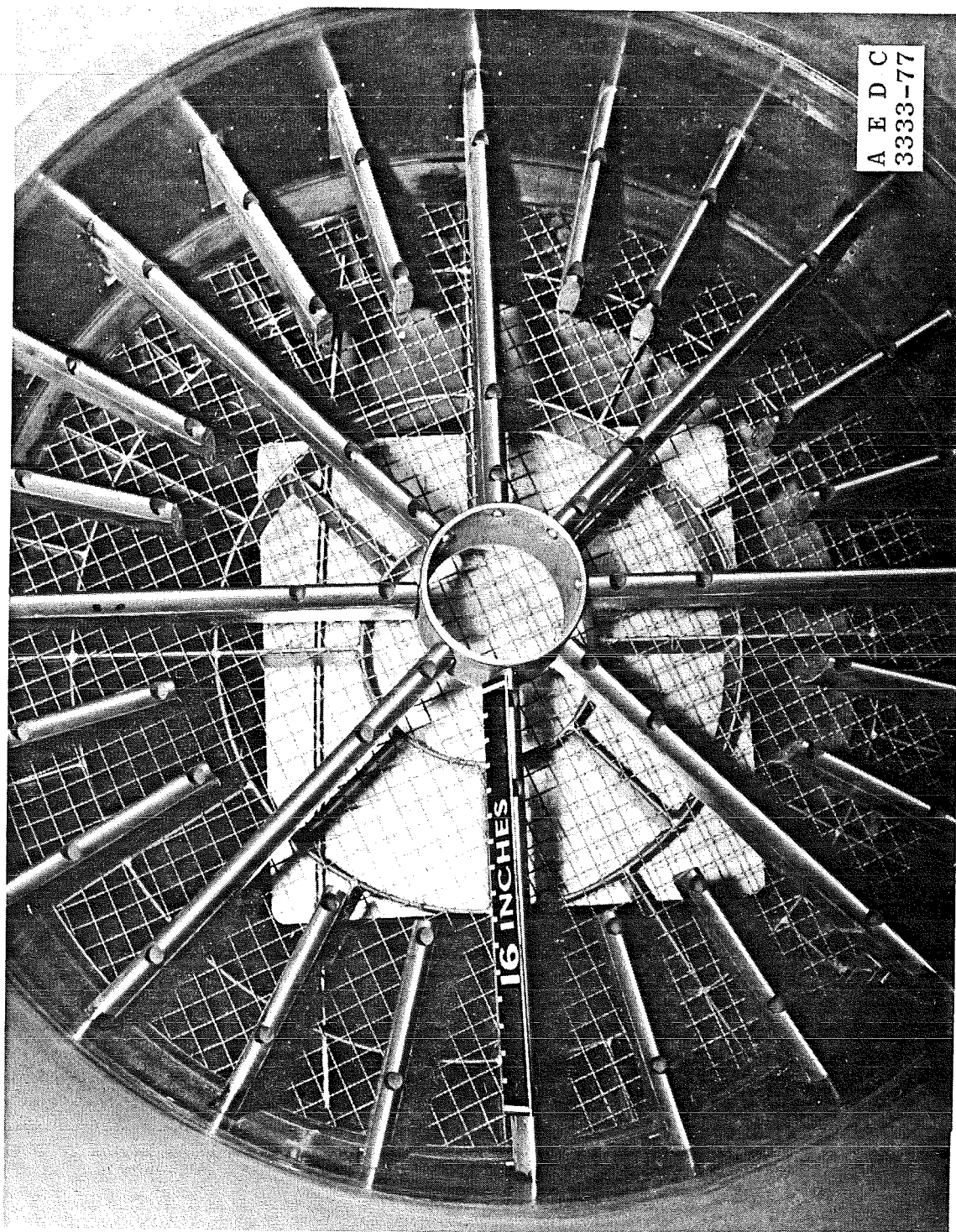
● Strut Discharge Port

Duct Diameter = 45.0 in.
Orifice Diameter = 0.85 in.



Secondary Air Strut/Injection
Orifice Orientation
(View Looking Downstream)

c. Air injection assembly struts
Figure 4. Continued.



d. Airjet assembly installed
Figure 4. Concluded.

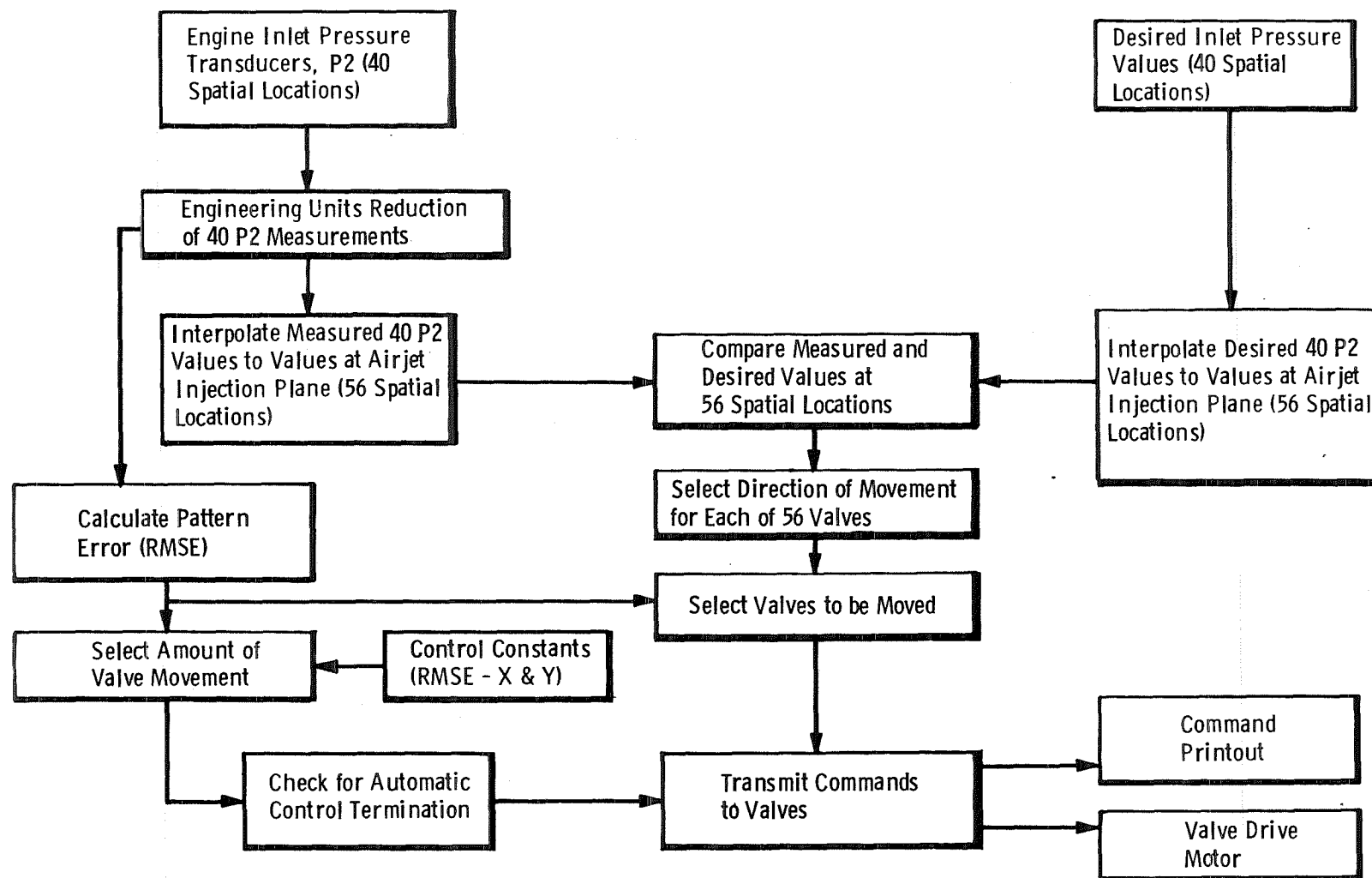


Figure 5. Computer control logic for airjet distortion generator airflow distribution system.

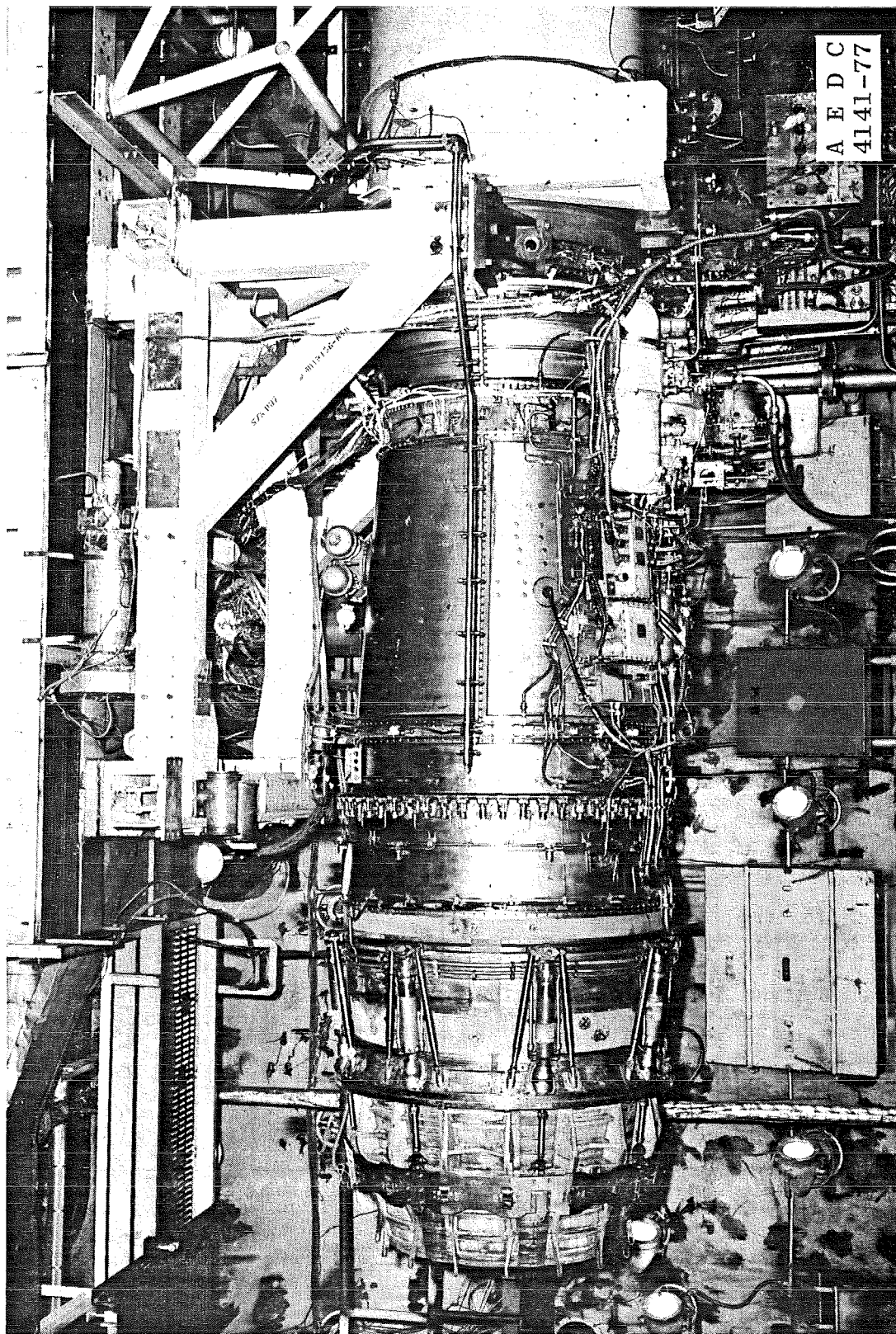
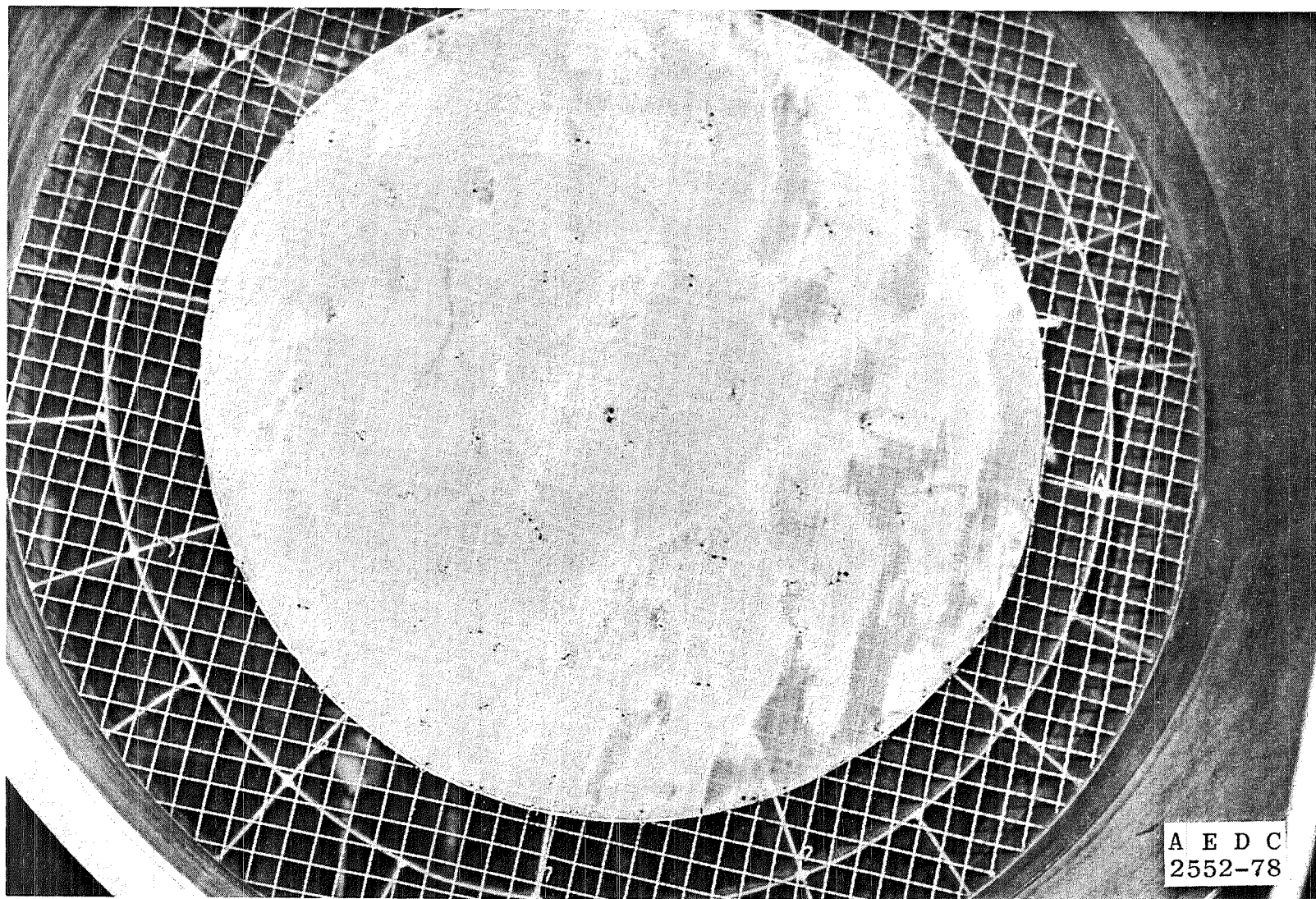
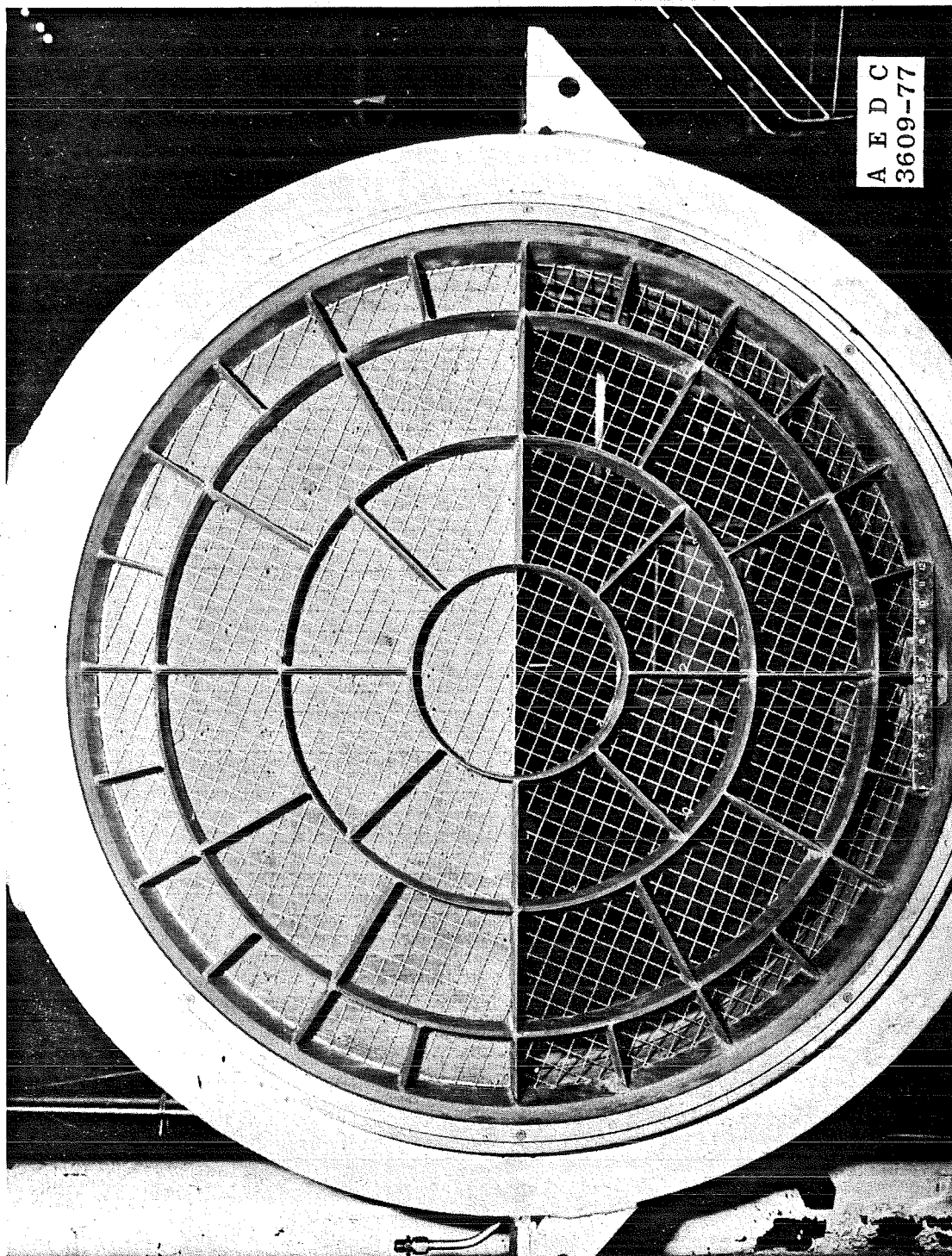


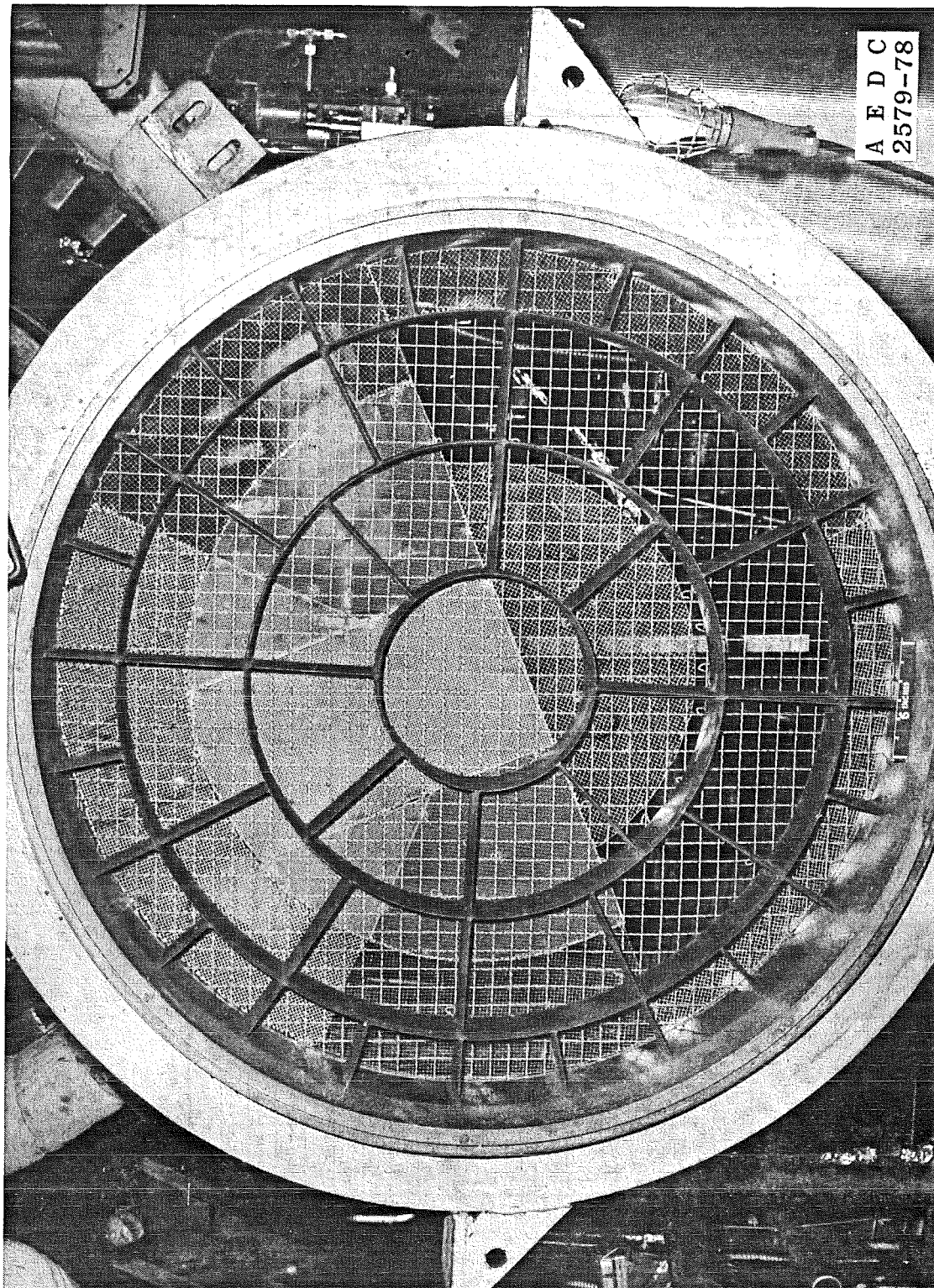
Figure 6. F101-GE-100 engine.



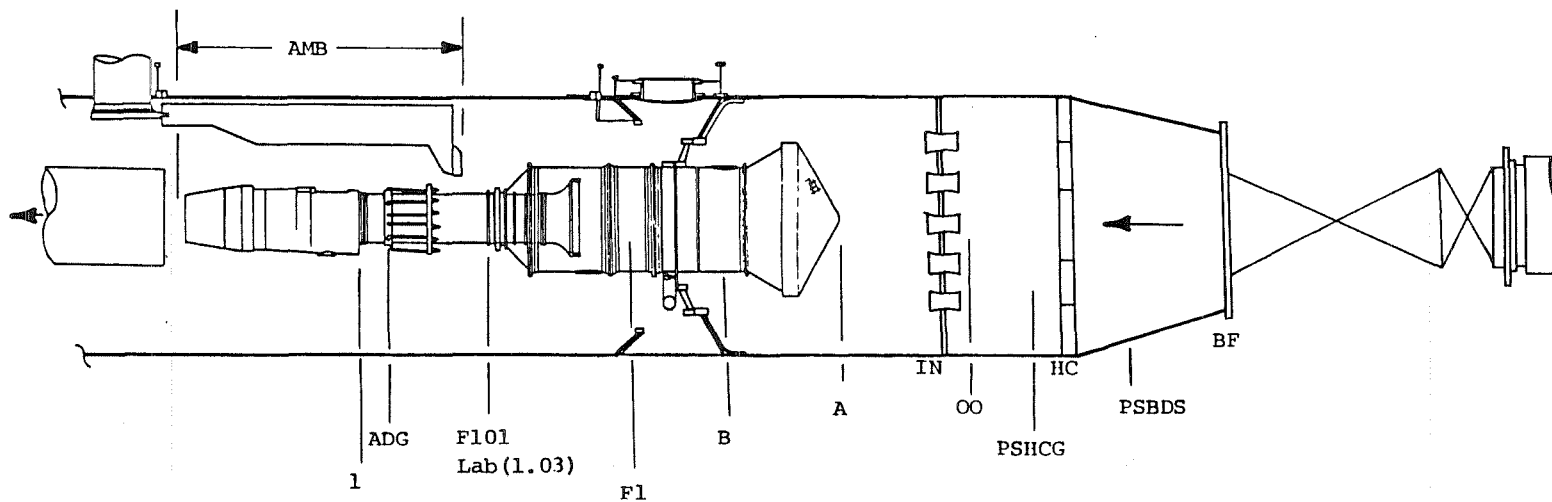
a. 50-percent hub radial screen (141)
Figure 7. Inlet distortion screens.



b. 180-deg, 1/rev screen (106)
Figure 7. Continued.



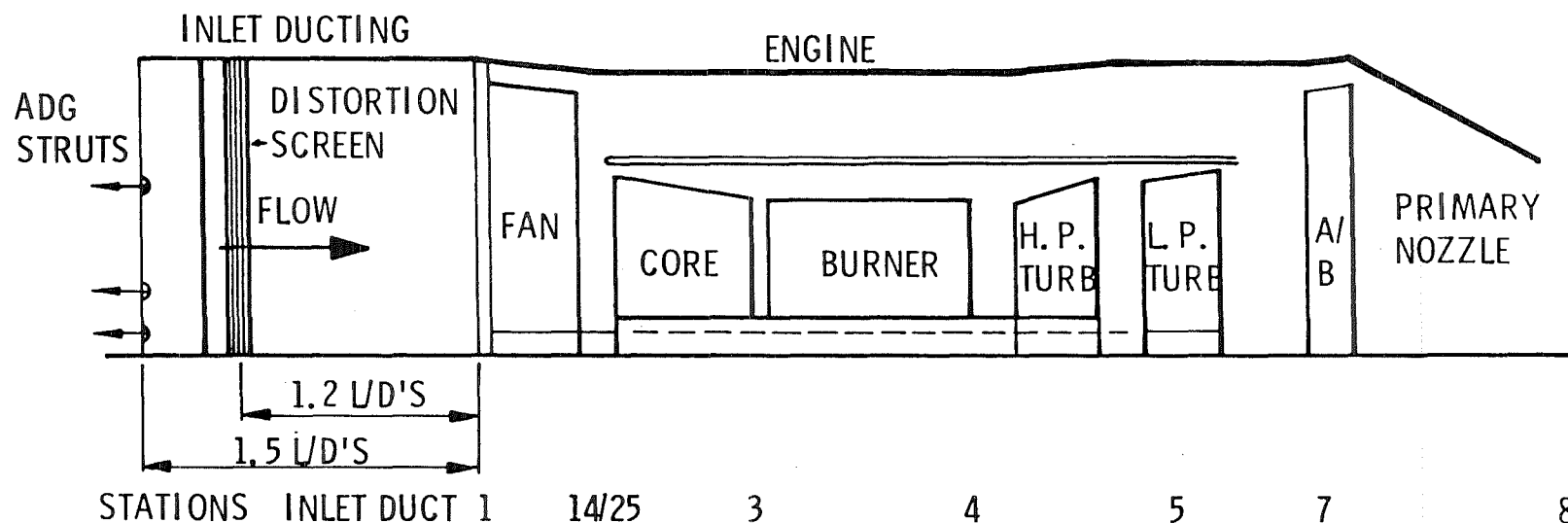
c. F101 specification screen (354.7M)
Figure 7. Concluded.



STATION IDENTIFICATION		TOTAL PRESS	STATIC PRESS	TOTAL TEMP	SKIN TEMP	STRAIN GAGES
BF	VALVE BAFFLES					
HC	HONEYCOMB					
OO	VENTURI INLET	13		33		
IN	VENTURI THROAT		11		11	
A	CONICAL SCREEN INLET					
B	CYLINDRICAL SCREEN INLET				2	
1G	8' DUCT GRID					
F1	8' DUCT RAKES	20	4	20	2	
F101	BELLMOUTH		16		2	
LAB	LAB SEAL		13		2	
ADG	AIRJET DISTORTION GENERATOR	1	1	3		6
1	ENGINE INLET DUCTING	40*/40/40	4			
AMB	CELL AMBIENT		9	8		

*Kulites

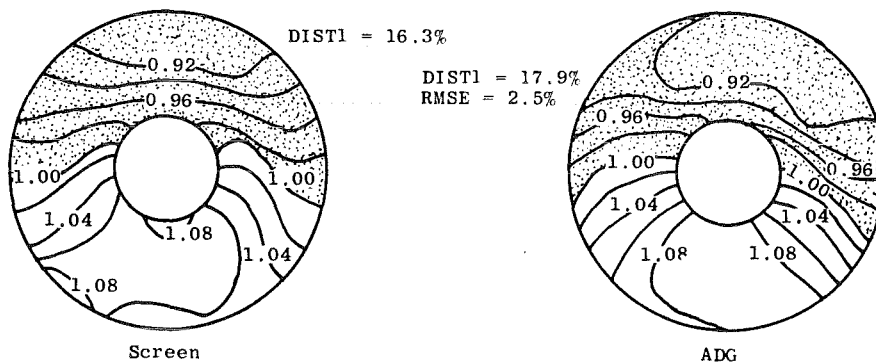
Figure 8. Facility instrumentation stations.



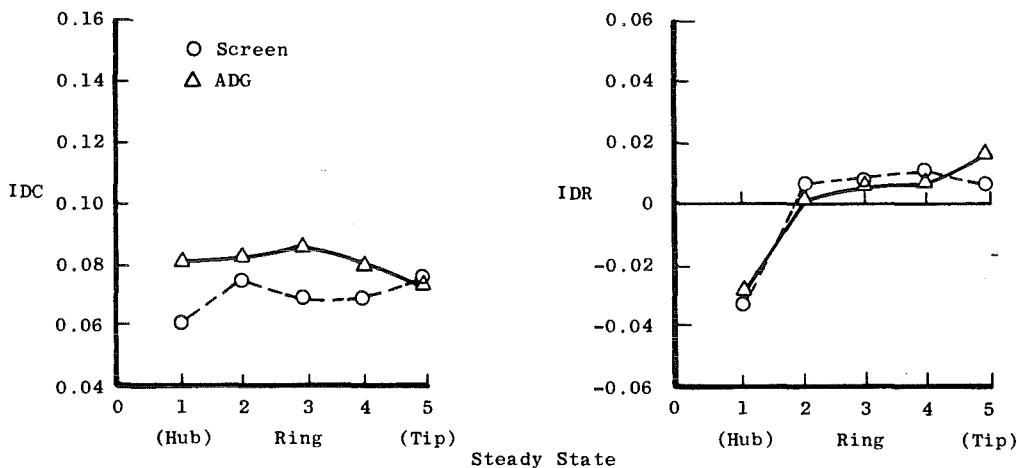
STATION 1	40	S. S. PRESSURES (SCANNER VALVE)
	40	TRANSIENT PRESSURES (CLOSE-COUPLE TRANSDUCERS)
	40	DYNAMIC PRESSURES (KULITES AND ZOC SYSTEMS)
	<u>120</u>	TOTAL @ STATION 1
STATION 14/25	84	S. S. PRESSURES
	64	TRANSIENT PRESSURES
	40	DYNAMIC PRESSURES
	80	TOTAL TEMPERATURES
	<u>268</u>	@ STATION 14/25

Figure 9. Engine fan and compressor instrumentation.

View Looking Upstream



a. Engine inlet isobar maps for screen and ADG system distortion



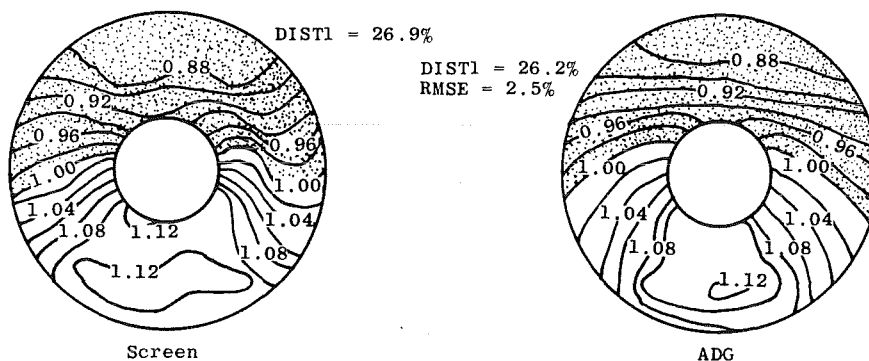
b. Distortion indices for screen and ADG system distortion

Rake Angle	Ring Number (Hub to Tip)									
	1		2		3		4		5	
	Screen	ADG	Screen	ADG	Screen	ADG	Screen	ADG	Screen	ADG
45	0.986	0.984	0.904	0.916	0.907	0.909	0.910	0.918	0.900	0.912
81	1.083	1.033	0.992	0.998	0.943	0.970	0.958	0.952	0.984	0.934
135	1.099	1.082	1.098	1.077	1.101	1.085	1.089	1.089	1.087	1.093
189	1.109	1.087	1.085	1.095	1.099	1.087	1.091	1.089	1.088	1.066
225	1.093	1.090	1.084	1.064	1.101	1.066	1.085	1.070	1.086	1.062
279	1.021	1.007	0.949	0.978	0.954	0.972	0.948	0.954	0.963	0.930
315	0.969	0.982	0.902	0.916	0.911	0.909	0.900	0.913	0.903	0.928
351	0.945	0.949	0.897	0.916	0.911	0.923	0.904	0.923	0.907	0.913

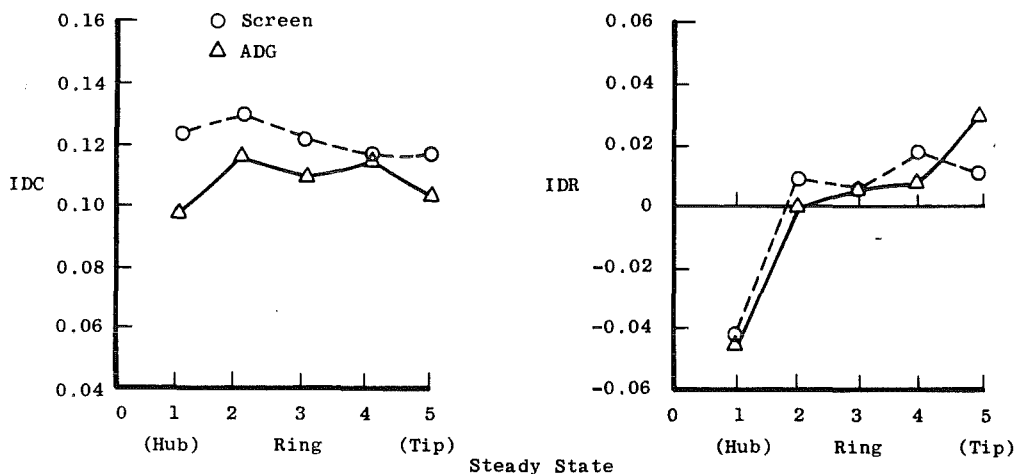
c. Individual normalized pressures at 40 spatial locations

Figure 10. Steady-state distortion comparison for 180-deg, 1/rev pattern (2), (low-speed fan surge).

View Looking Upstream



a. Engine inlet isobar maps for screen and ADG system distortion

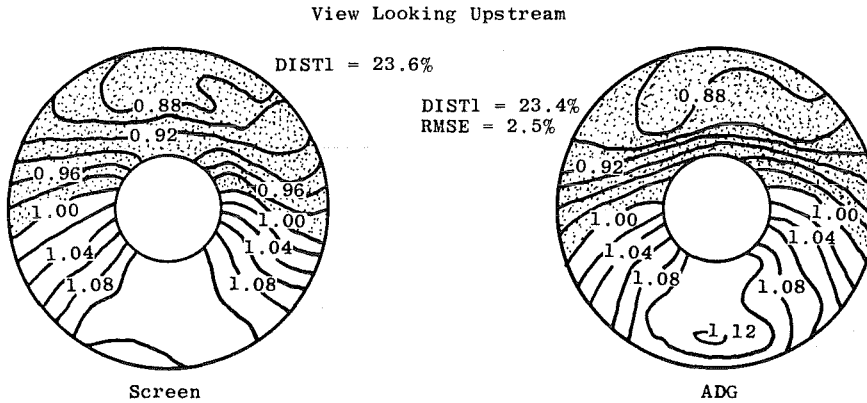


b. Distortion indices for screen and ADG system distortion

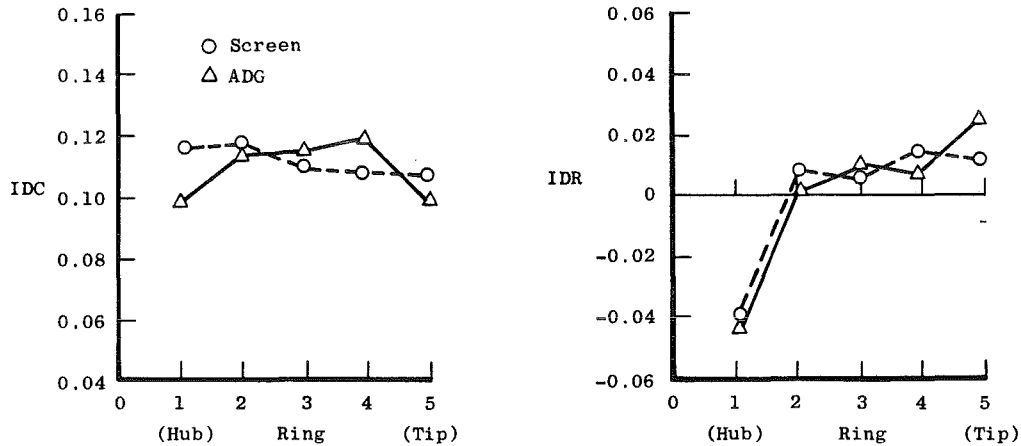
Rake Angle	Ring Number (Hub to Tip)									
	1		2		3		4		5	
	Screen	ADG	Screen	ADG	Screen	ADG	Screen	ADG	Screen	ADG
45	0.990	0.988	0.883	0.906	0.883	0.906	0.883	0.895	0.870	0.873
81	1.099	1.062	0.984	1.004	0.932	0.985	0.942	0.960	0.973	0.933
135	1.113	1.110	1.111	1.089	1.128	1.090	1.110	1.113	1.119	1.093
189	1.115	1.109	1.115	1.115	1.126	1.114	1.120	1.122	0.973	1.075
225	1.116	1.109	1.093	1.070	1.122	1.078	1.094	1.104	1.111	1.062
279	1.022	1.031	0.963	0.990	0.972	0.961	0.926	0.933	0.933	0.926
315	0.935	0.987	0.860	0.907	0.873	0.883	0.865	0.879	0.879	0.887
351	0.918	0.949	0.864	0.885	0.875	0.882	0.869	0.877	0.872	0.865

c. Individual normalized pressures at 40 spatial locations

Figure 11. Steady-state distortion comparison for 180-deg, 1/rev pattern (1), (high-speed fan surge).



a. Engine inlet isobar maps for screen and ADG system distortion

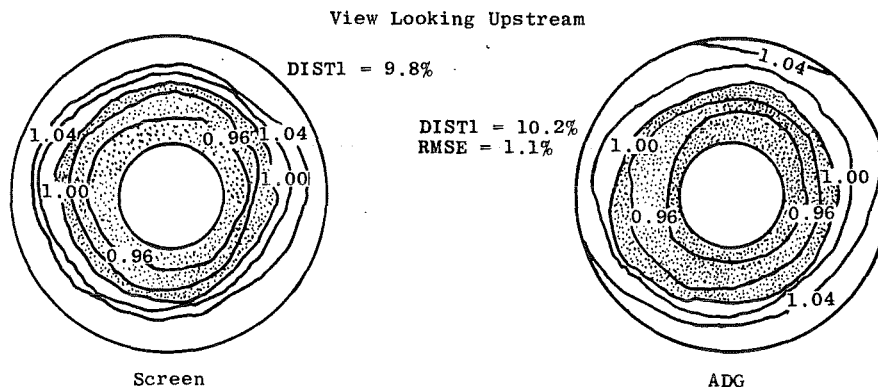


b. Distortion indices for screen and ADG system distortion

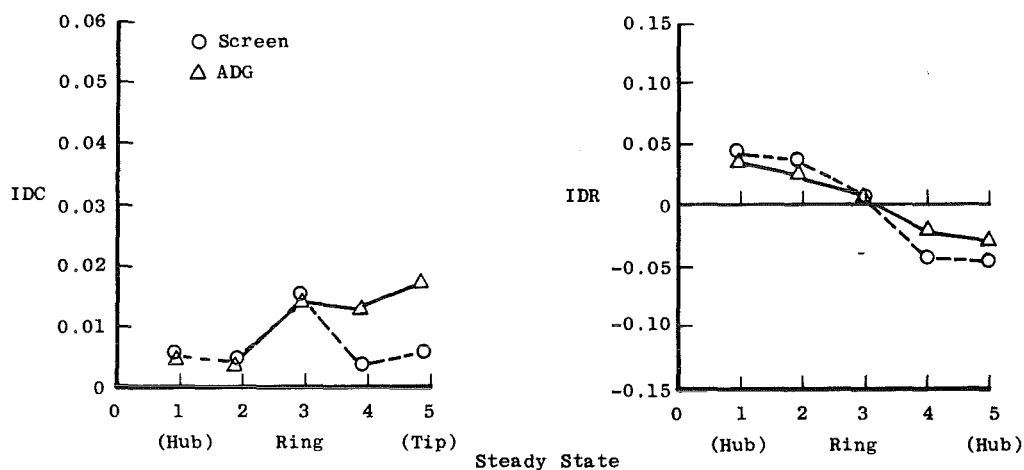
Rake Angle	Ring Number (Hub to Tip)									
	1		2		3		4		5	
	Screen	ADG	Screen	ADG	Screen	ADG	Screen	ADG	Screen	ADG
45	0.984	1.001	0.887	0.898	0.888	0.882	0.900	0.897	0.880	0.880
81	1.095	1.063	0.992	1.010	0.943	0.978	0.950	0.974	0.971	0.944
135	1.100	1.105	1.106	1.085	1.116	1.097	1.101	1.103	1.105	1.073
189	1.105	1.111	1.104	1.106	1.112	1.110	1.105	1.125	1.091	1.098
225	1.108	1.115	1.083	1.082	1.109	1.085	1.083	1.097	1.098	1.079
279	1.021	1.012	0.967	0.989	0.976	0.958	0.938	0.946	0.944	0.921
315	0.951	0.975	0.876	0.888	0.888	0.873	0.876	0.873	0.892	0.891
351	0.923	0.946	0.874	0.882	0.886	0.890	0.881	0.886	0.882	0.875

c. Individual normalized pressures at 40 spatial locations

Figure 12. Steady-state distortion comparison for 180-deg, 1/rev pattern (23), (core surge).



a. Engine inlet isobar maps for screen and ADG system distortion

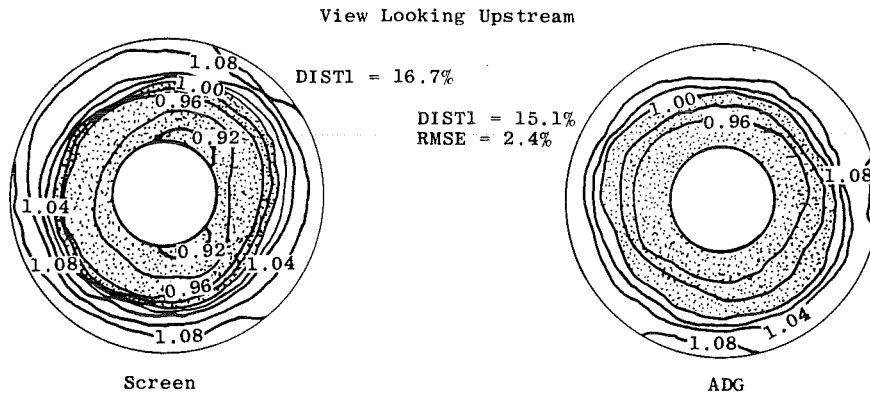


b. Distortion indices for screen and ADG system distortion

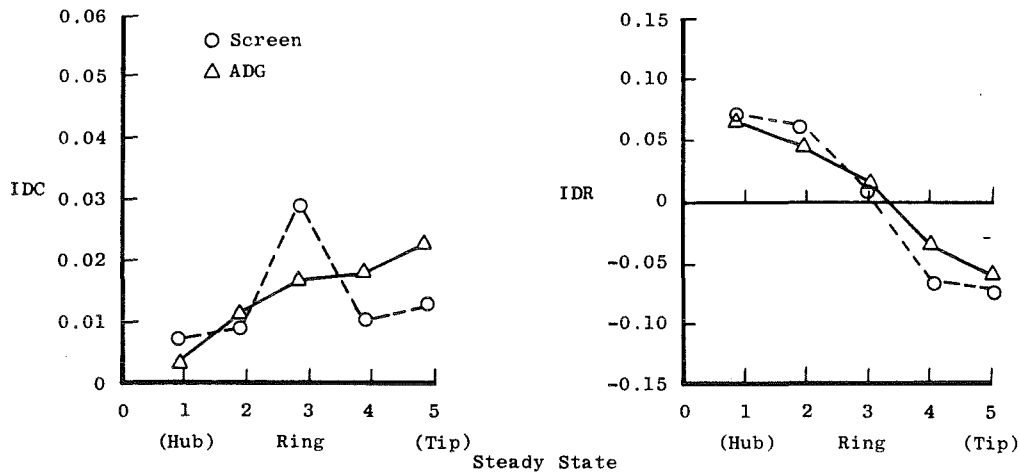
Rake Angle	Ring Number (Hub to Tip)									
	1		2		3		4		5	
	Screen	ADG	Screen	ADG	Screen	ADG	Screen	ADG	Screen	ADG
45	0.958	0.964	0.960	0.980	0.991	1.000	1.039	1.020	1.044	1.033
81	0.965	0.967	0.972	0.981	1.019	1.011	1.039	1.042	1.038	1.042
135	0.954	0.958	0.962	0.975	0.992	0.995	1.041	1.030	1.047	1.051
189	0.954	0.962	0.960	0.976	1.004	1.000	1.052	1.037	1.048	1.044
225	0.963	0.965	0.961	0.974	0.991	0.996	1.039	1.030	1.045	1.043
279	0.958	0.968	0.961	0.973	0.984	0.988	1.043	1.018	1.043	1.022
315	0.963	0.965	0.958	0.972	0.979	0.982	1.038	1.013	1.038	1.025
351	0.956	0.960	0.969	0.976	0.995	0.993	1.037	1.018	1.041	1.041

c. Individual normalized pressures at 40 spatial locations

Figure 13. Steady-state distortion comparison for 50-percent hub radial pattern (4), (low-speed fan surge).



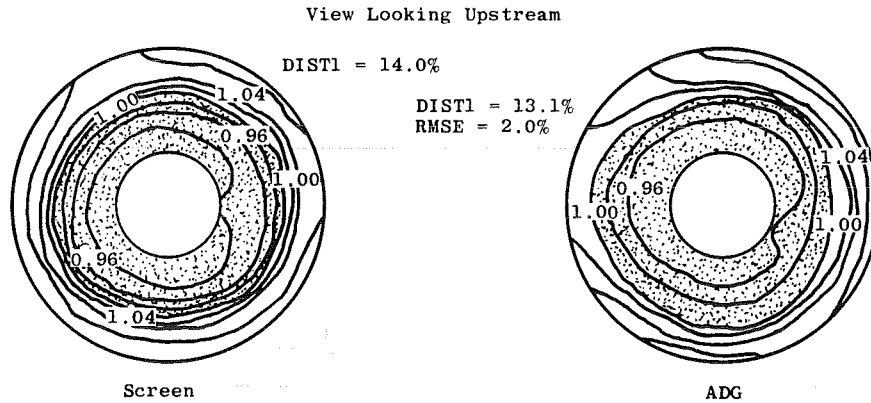
a. Engine inlet isobar maps for screen and ADG system distortion



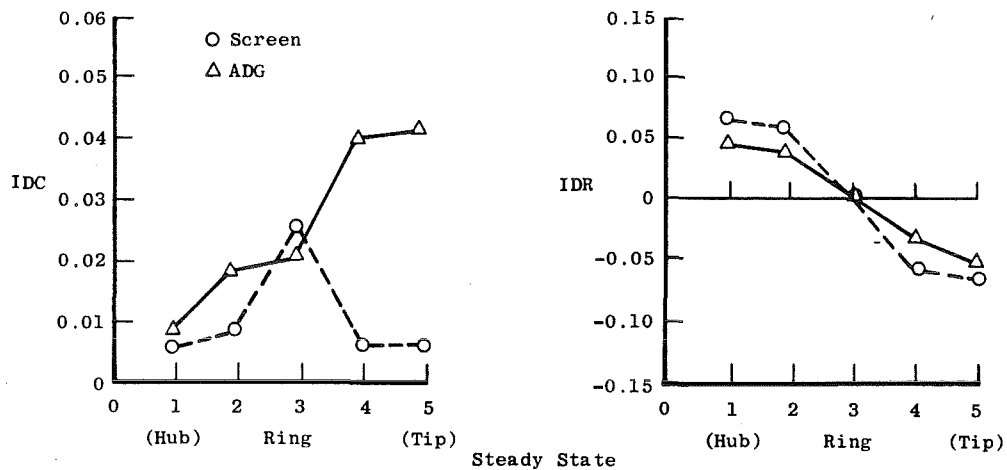
b. Distortion indices for screen and ADG system distortion

Rake Angle	Ring Number (Hub to Tip)									
	1		2		3		4		5	
	Screen	ADG	Screen	ADG	Screen	ADG	Screen	ADG	Screen	ADG
45	0.926	0.941	0.933	0.975	0.999	1.018	1.064	1.053	1.082	1.068
81	0.936	0.940	0.950	0.947	1.020	0.996	1.068	1.064	1.063	1.081
135	0.924	0.936	0.932	0.968	0.981	0.989	1.070	1.028	1.079	1.057
189	0.921	0.937	0.931	0.960	1.014	0.983	1.090	1.044	1.079	1.087
225	0.934	0.938	0.934	0.974	0.990	1.011	1.071	1.052	1.078	1.070
279	0.929	0.940	0.931	0.953	0.973	0.995	1.078	1.029	1.078	1.041
315	0.936	0.945	0.926	0.959	0.961	0.984	1.061	1.022	1.071	1.045
351	0.922	0.941	0.946	0.950	0.986	0.976	1.070	1.027	1.069	1.076

c. Individual normalized pressures at 40 spatial locations
Figure 14. Steady-state distortion comparison for 50-percent hub radial pattern (3), (high-speed fan surge).



a. Engine inlet isobar maps for screen and ADG system distortion

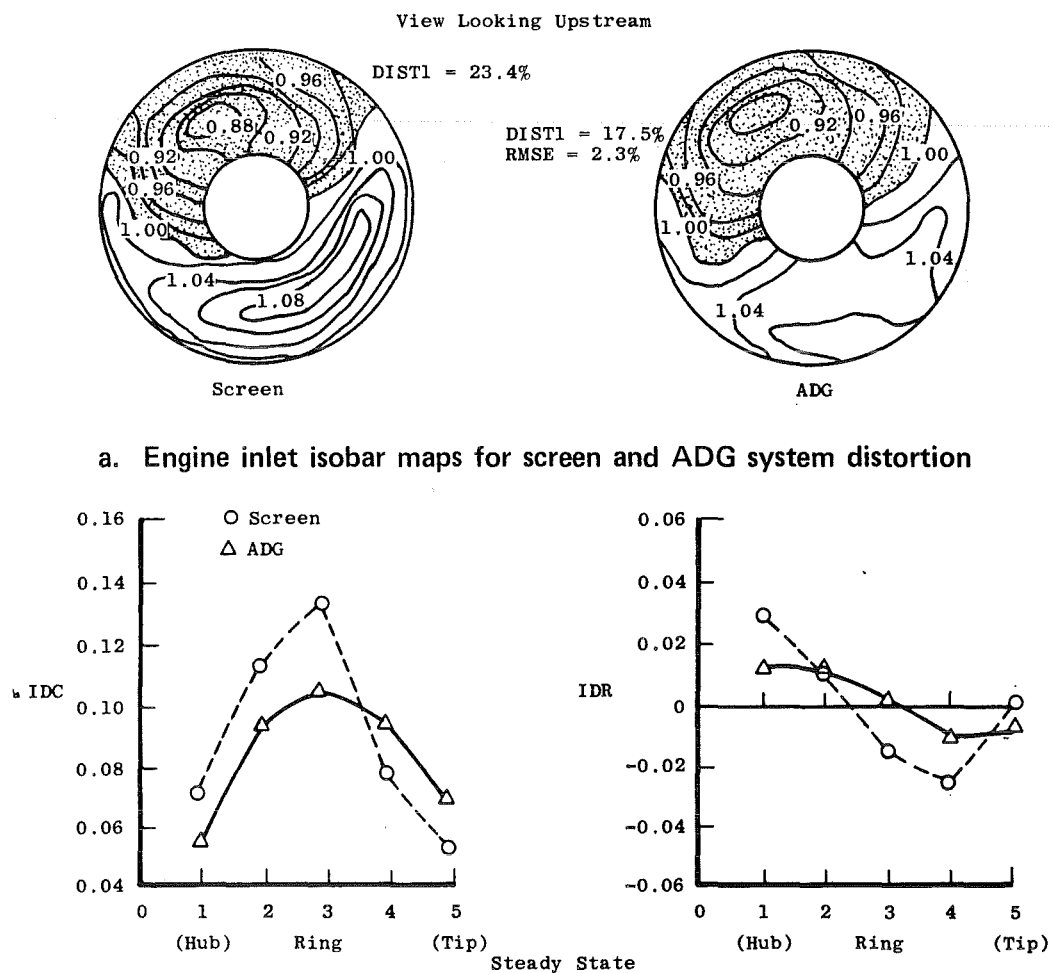


b. Distortion indices for screen and ADG system distortion

Rake Angle	Ring Number (Hub to Tip)									
	1		2		3		4		5	
	Screen	ADG	Screen	ADG	Screen	ADG	Screen	ADG	Screen	ADG
45	0.939	1.058	0.943	0.975	1.000	1.011	1.049	1.058	1.064	1.071
81	0.948	0.948	0.957	0.975	1.028	1.015	1.053	1.063	1.052	1.062
135	0.934	0.968	0.946	0.965	0.994	0.994	1.057	1.035	1.064	1.052
189	0.934	0.946	0.942	0.964	1.011	1.011	1.074	1.062	1.066	1.076
225	0.947	0.943	0.944	0.954	0.995	0.995	1.054	1.042	1.063	1.051
279	0.937	0.950	0.943	0.946	0.981	0.984	1.057	0.997	1.061	1.010
315	0.946	0.957	0.938	0.964	0.973	0.978	1.050	1.001	1.054	1.016
351	0.937	0.947	0.957	0.960	0.998	0.990	1.053	1.040	1.055	1.061

c. Individual normalized pressures at 40 spatial locations

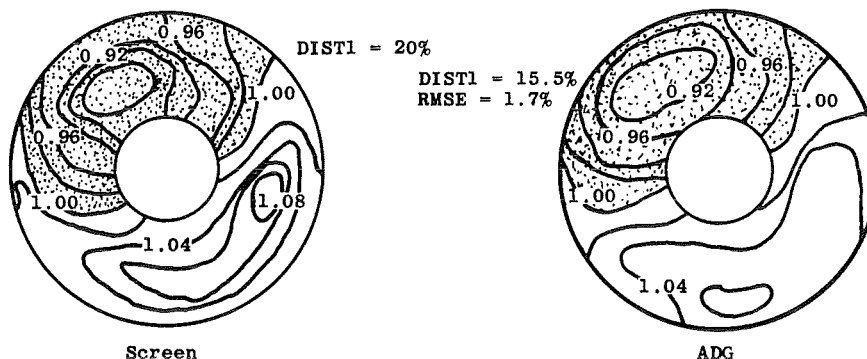
Figure 15. Steady-state distortion comparison for 50-percent hub radial pattern (25), (core surge).



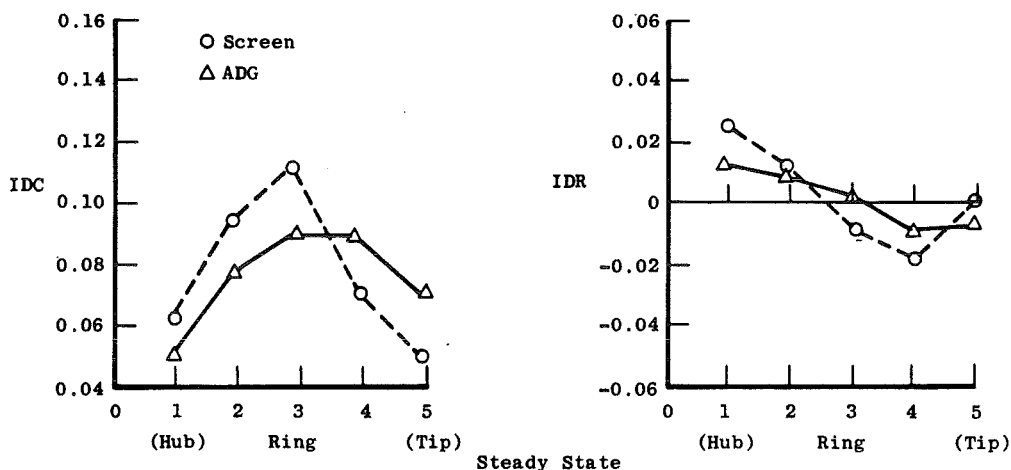
Wake Angle	Ring Number (Hub to Tip)									
	1		2		3		4		5	
	Screen	ADG	Screen	ADG	Screen	ADG	Screen	ADG	Screen	ADG
45	0.938	0.958	0.945	0.960	0.974	0.978	1.022	0.997	1.016	1.002
81	1.024	1.006	1.054	1.035	1.113	1.038	1.081	1.044	1.014	1.033
135	1.026	1.053	1.048	1.042	1.086	1.056	1.045	1.052	1.021	1.052
189	1.027	1.033	1.074	1.060	1.091	1.064	1.057	1.070	1.019	1.070
225	0.992	1.027	1.041	1.036	1.081	1.045	1.039	1.058	1.005	1.029
279	0.993	0.946	0.962	0.945	0.963	0.960	1.033	1.006	1.011	1.005
315	0.901	0.935	0.880	0.897	0.884	0.903	0.953	0.937	0.948	0.957
351	0.905	0.934	0.883	0.899	0.888	0.895	0.949	0.924	0.944	0.946

c. Individual normalized pressures at 40 spatial locations
Figure 16. Steady-state distortion comparison for F101 specification pattern (26), (high-speed fan surge).

View Looking Upstream



a. Engine inlet isobar maps for screen and ADG system distortion



b. Distortion indices for screen and ADG system distortion

Rake Angle	Ring Number (Hub to Tip)									
	1		2		3		4		5	
	Screen	ADG	Screen	ADG	Screen	ADG	Screen	ADG	Screen	ADG
45	0.947	0.964	0.955	0.965	0.974	0.975	1.020	0.990	1.012	0.995
81	1.019	0.996	1.051	1.027	1.096	1.036	1.066	1.039	1.014	1.031
135	1.024	1.032	1.042	1.046	1.073	1.046	1.040	1.049	1.018	1.056
189	1.023	1.033	1.063	1.055	1.076	1.059	1.050	1.057	1.018	1.038
225	0.998	1.032	1.035	1.038	1.069	1.046	1.031	1.053	1.004	1.028
279	0.943	0.958	0.965	0.963	0.968	1.095	1.027	1.002	1.010	1.001
315	0.912	0.947	0.897	0.915	0.901	0.917	0.961	0.943	0.955	0.959
351	0.914	0.944	0.900	0.918	0.901	0.912	0.957	0.929	0.951	0.945

c. Individual normalized pressures at 40 spatial locations

Figure 17. Steady-state distortion comparison for F101 specification pattern (27), (core surge).

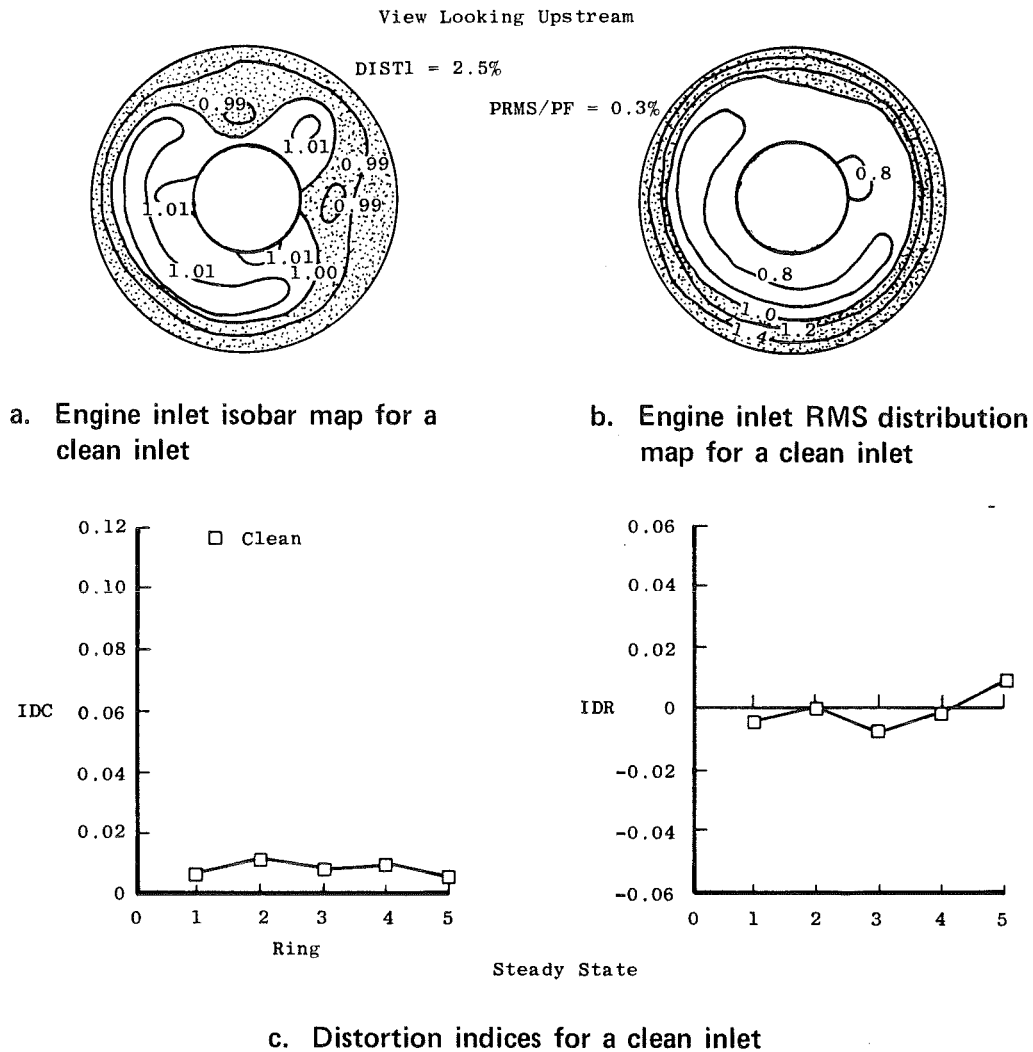
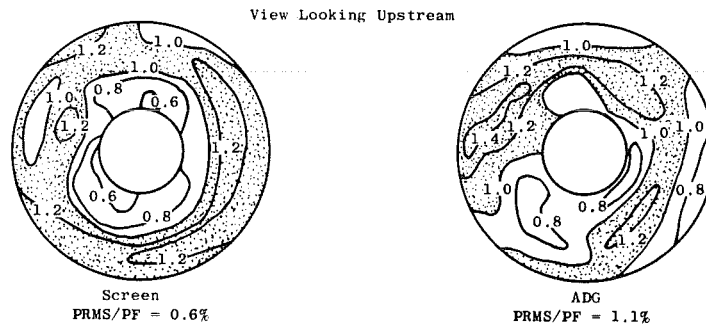
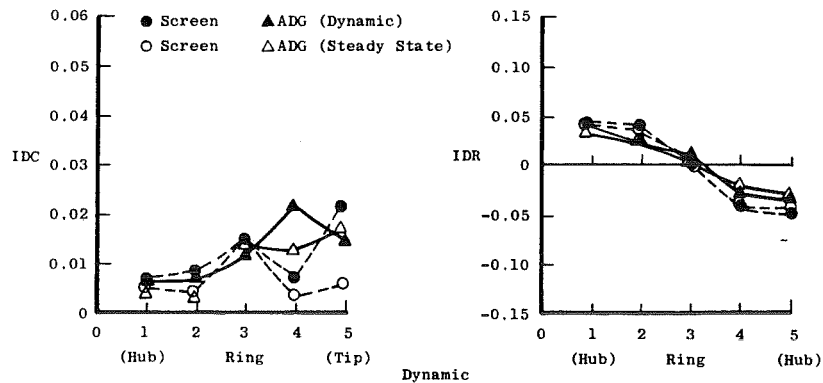


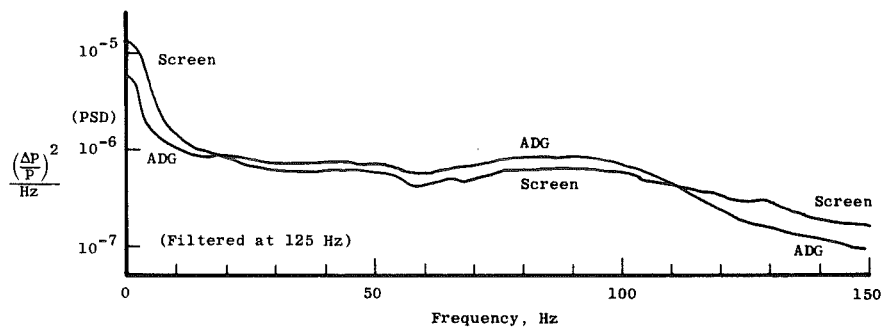
Figure 18. Steady-state and dynamic distortion for a clean inlet.



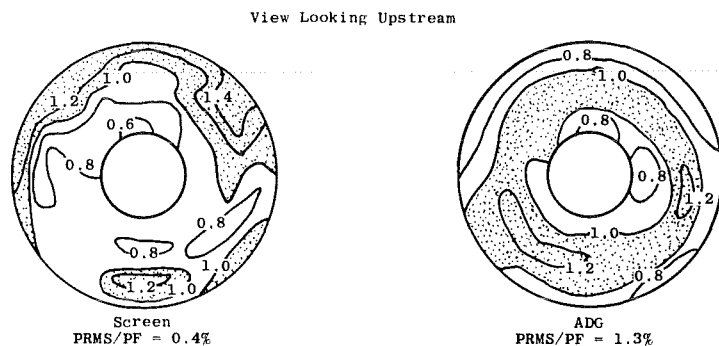
a. Engine inlet RMS distribution maps for screen and ADG system distortion



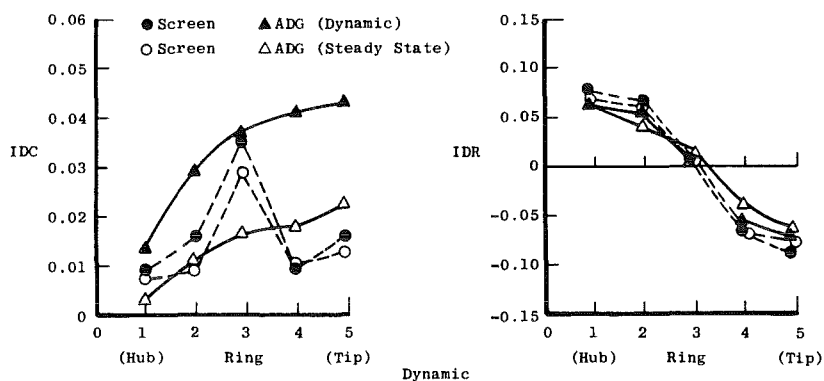
b. Distortion indices for screen and ADG system distortion



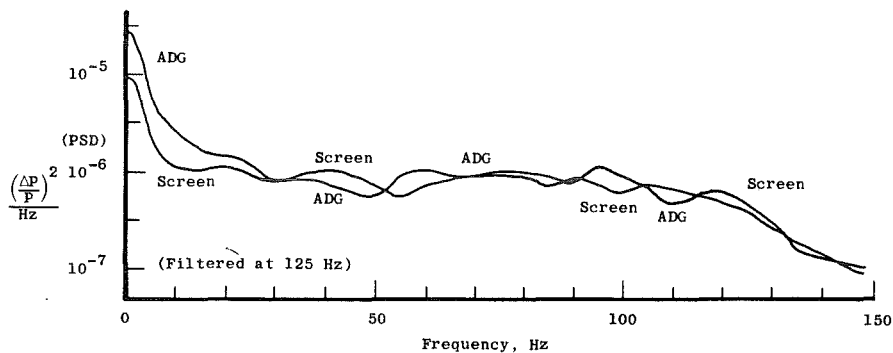
c. Power spectral density characteristics for screen and ADG system distortion
Figure 19. Dynamic distortion comparison for 50-percent hub radial pattern (4), (low-speed fan surge).



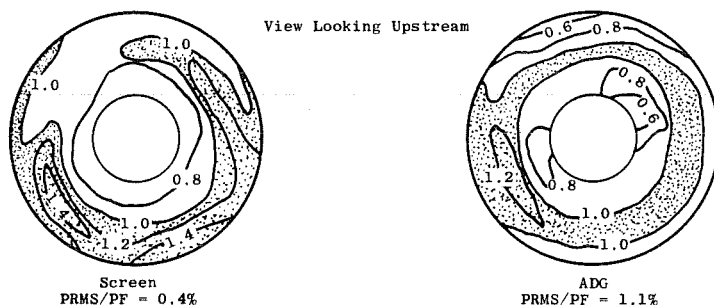
a. Engine inlet RMS distribution maps for screen and ADG system distortion



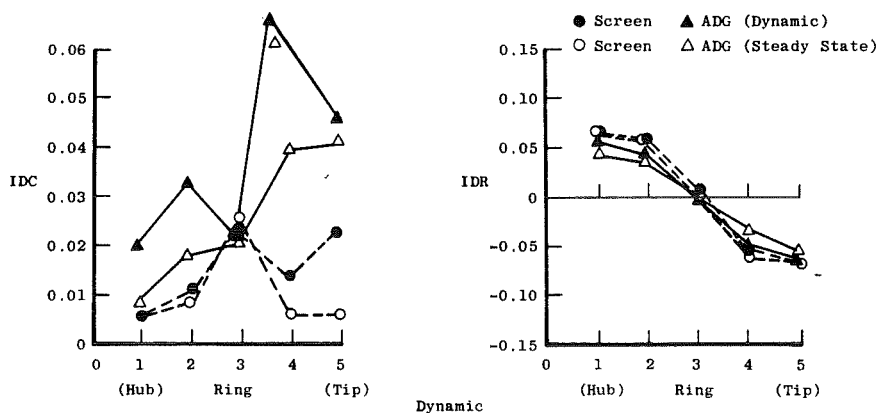
b. Distortion indices for screen and ADG system distortion



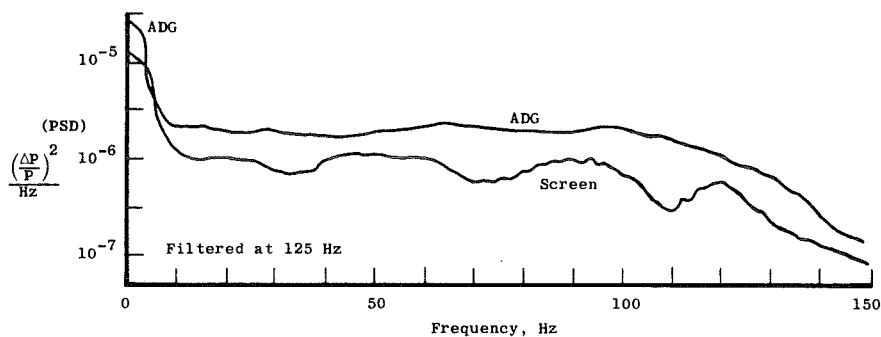
c. Power spectral density characteristics for screen and ADG system distortion
Figure 20. Dynamic distortion comparison for 50-percent hub radial pattern (3), (high-speed fan surge).



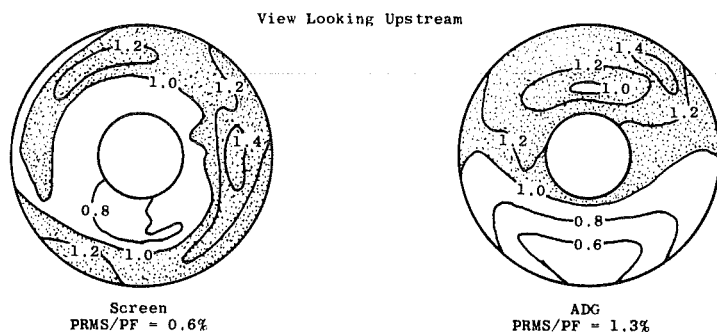
a. Engine inlet RMS distribution maps for screen and ADG system distortion



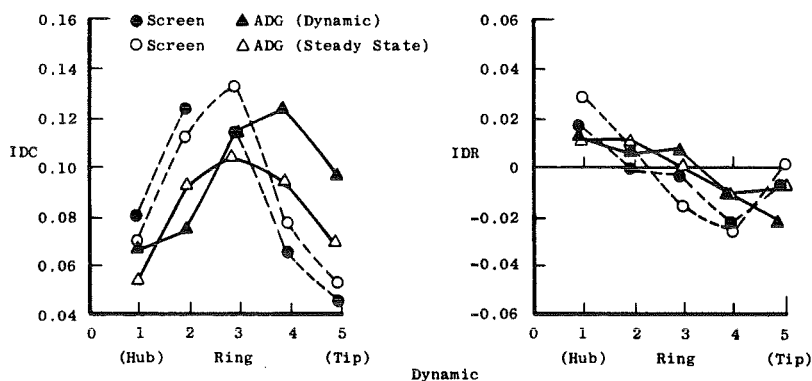
b. Distortion indices for screen and ADG system distortion



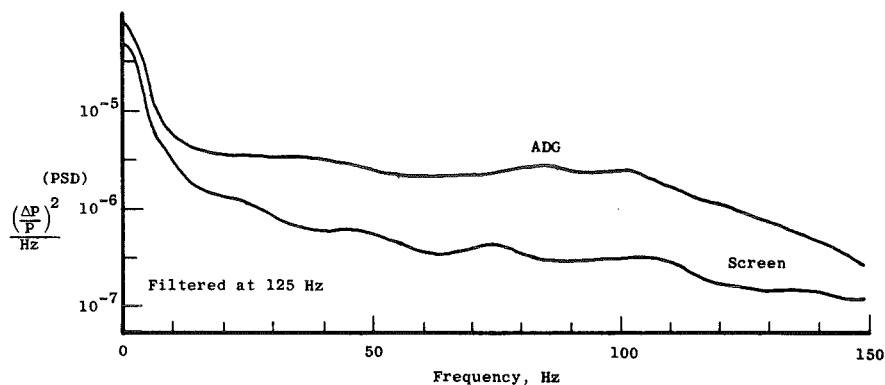
c. Power spectral density characteristics for screen and ADG system distortion
Figure 21. Dynamic distortion comparison for 50-percent hub radial pattern (25), (core surge).



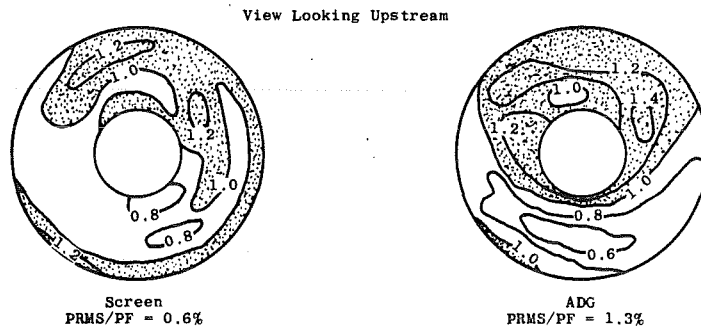
a. Engine inlet RMS distribution maps for screen and ADG system distortion



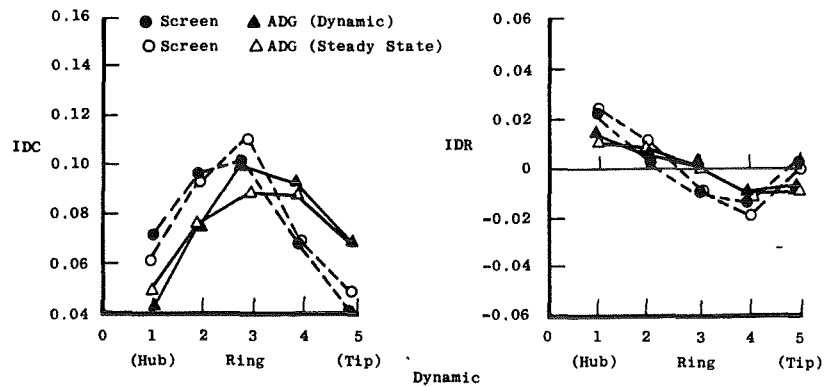
b. Distortion indices for screen and ADG system distortion



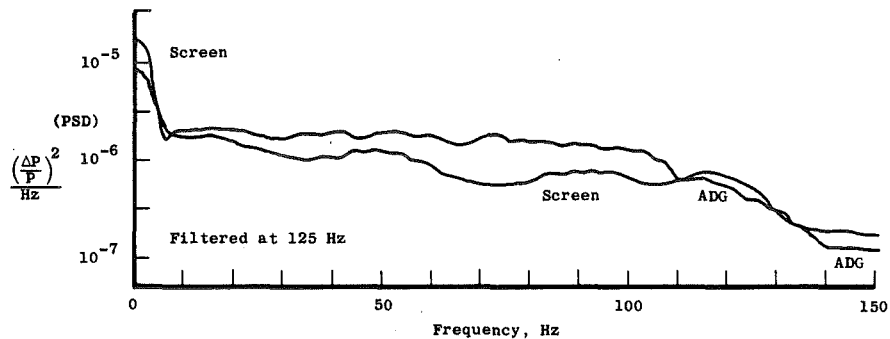
c. Power spectral density characteristics for screen and ADG system distortion
Figure 22. Dynamic distortion comparison for F101 specification pattern (26),
(high-speed fan surge).



a. Engine inlet RMS distribution maps for screen and ADG system distortion

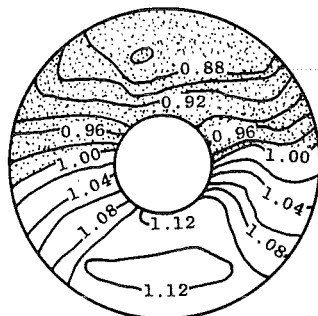


b. Distortion indices for screen and ADG system distortion



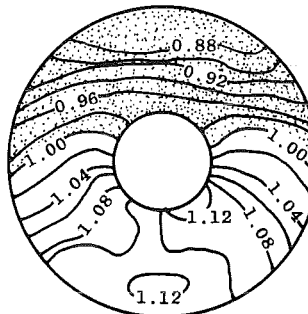
c. Power spectral density characteristics for screen and ADG system distortion
Figure 23. Dynamic distortion comparison for F101 specification Pattern (27), (core surge).

View Looking Upstream



Screen

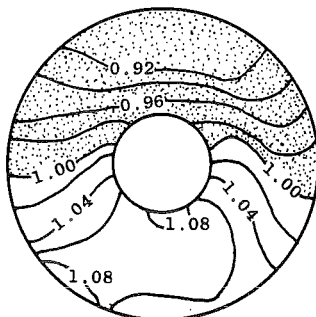
DIST1 = 26.9
IDCM = 0.128(H)
IDRM = 0.013(T)



ADG

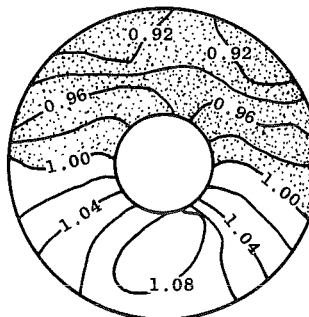
RMSE = 2.7
DIST1 = 26.9
IDCM = 0.110(T)
IDRM = 0.023(T)
IDCMD = 0.14(T)
IDRMD = 0.018(T)

a. 180-deg, 1/rev pattern (1), 100-percent fan speed surge



Screen

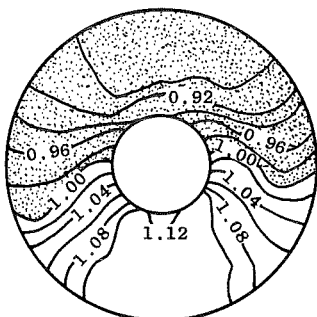
DIST1 = 16.3
IDCM = 0.074(T)
IDRM = 0.007(T)



ADG

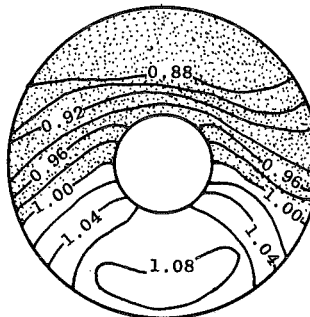
RMSE = 1.5
DIST1 = 16.8
IDCM = 0.074(T)
IDRM = 0.015(T)
IDCMD = 0.088(T)
IDRMD = 0.013(T)

b. 180-deg, 1/rev pattern (2), 90-percent fan speed surge



Screen

DIST1 = 23.6
IDCM = 0.109(T)
IDRM = 0.010(T)



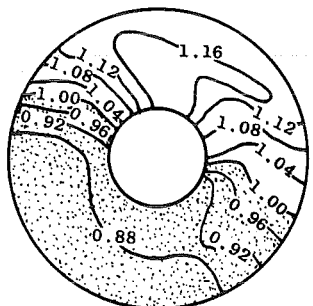
ADG

RMSE = 2.1
DIST1 = 22.8
IDCM = 0.136(H)
IDRM = 0.041(T)
IDCMD = 0.128(T)
IDRMD = 0.025(T)

c. 180-deg, 1/rev pattern (23), core surge

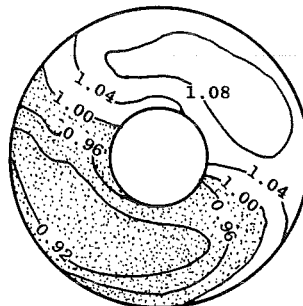
Figure 24. Steady-state distortion comparison with screen generated patterns for other engine/rig tests.

View Looking Upstream



Screen

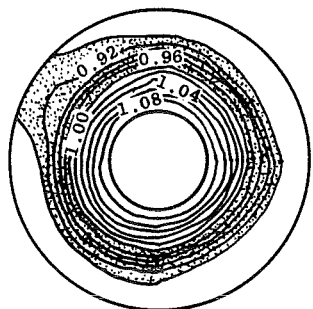
DIST1 = 32.3
IDCM = 0.138 (T)
IDRM = 0.013 (H)



ADG

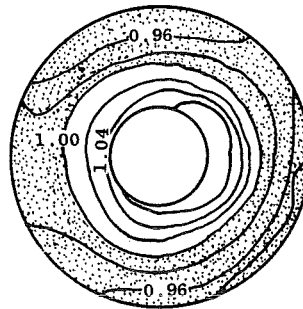
RMSE = 6.3
DIST1 = 22.1
IDCM = 0.103 (T)
IDRM = 0.005 (H)
IDCMD = 0.130 (T)
IDRMD = 0.013 (T)

d. 180-deg, 1/rev modified pattern (35), 90-percent fan speed surge



Screen

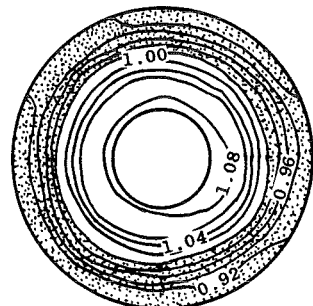
DIST1 = 23.2
IDCM = 0.020 (H)
IDRM = 0.105 (T)



ADG

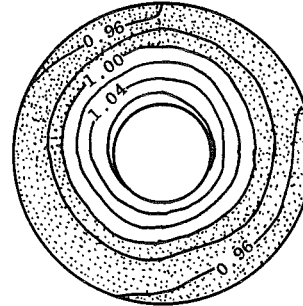
RMSE = 4.3
DIST1 = 14.3
IDCM = 0.025 (T)
IDRM = 0.042 (T)
IDCMD = 0.034 (H)
IDRMD = 0.056 (T)

e. Tip radial pattern (5), 90-percent fan speed surge



Screen

DIST1 = 16.2
IDCM = 0.009 (H)
IDRM = 0.075 (T)

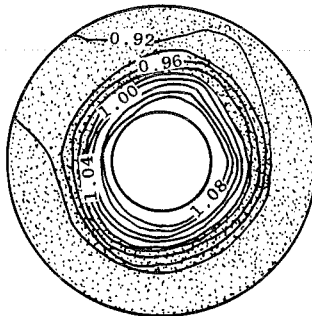


ADG

RMSE = 2.6
DIST1 = 10.9
IDCM = 0.011 (T)
IDRM = 0.037 (T)

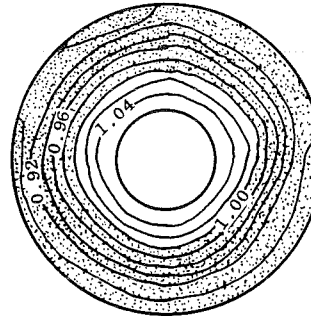
f. Tip radial pattern (6), 75-percent fan speed surge
Figure 24. Continued.

View Looking Upstream



DIST1 = 17.6
IDCM = 0.008 (T)
IDRM = 0.81 (T)

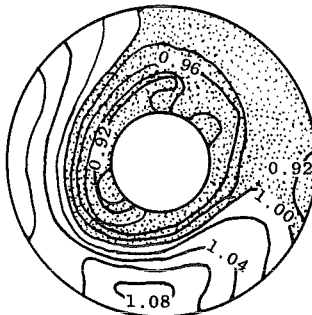
Screen



RMSE = 1.8
DIST1 = 16.2
IDCM = 0.016 (H)
IDRM = 0.081 (T)
IDCMD = 0.018 (H)
IDRMD = 0.106 (T)

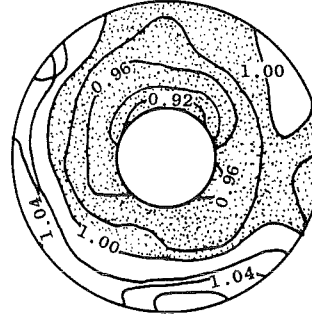
ADG

g. Tip radial pattern (7), 100-percent fan speed surge



DIST1 = 20.7
IDCM = 0.065 (T)
IDRM = 0.072 (H)

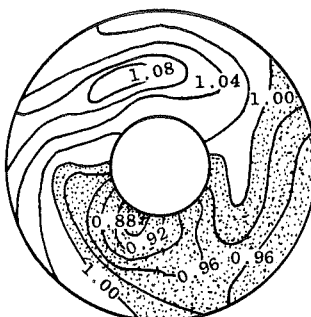
Screen



RMSE = 2.7
DIST1 = 16.3
IDCM = 0.058 (T)
IDRM = 0.050 (H)

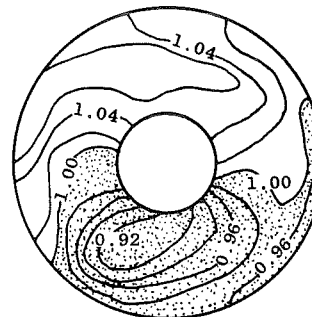
ADG

h. Composite pattern (14), sea-level-static with crosswind



DIST1 = 21.8
IDCM = 0.110 (H)
IDRM = 0.024 (H)

Screen



RMSE = 2.5
DIST1 = 16.9
IDCM = 0.076 (H)
IDRM = 0.019 (H)

ADG

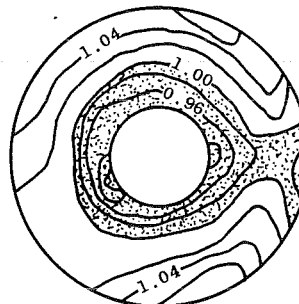
i. Composite pattern (15), PWT full-scale, sea-level-static
Figure 24. Continued.

View Looking Upstream



Screen

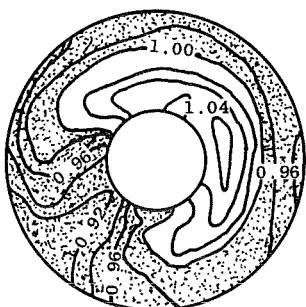
DIST1 = 22.1
IDCM = 0.071 (H)
IDRM = 0.074 (H)



ADG

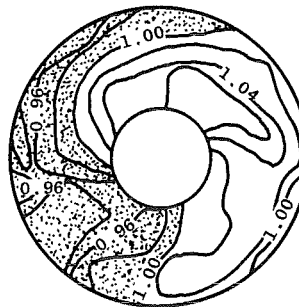
RMSE = 3.0
DIST1 = 15.6
IDCM = 0.048 (T)
IDRM = 0.059 (H)

j. Composite pattern (16), PWT full-scale, sea-level-static



Screen

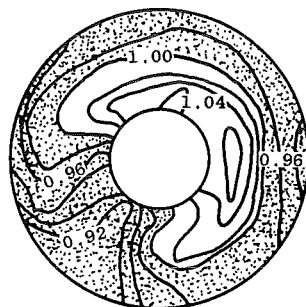
DIST1 = 16.2
IDCM = 0.104 (H)
IDRM = 0.044 (T)



ADG

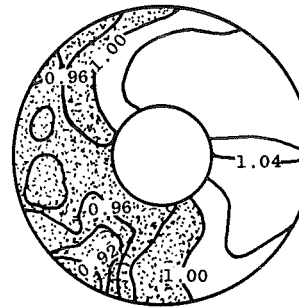
RMSE = 2.5
DIST1 = 15.9
IDCM = 0.076 (T)
IDRM = 0.015 (T)
IDCMD = 0.034 (H)
IDRMD = 0.023 (T)

k. Composite pattern (30), 100-percent fan speed surge



Screen

DIST1 = 16.2
IDCM = 0.104 (H)
IDRM = 0.044 (T)



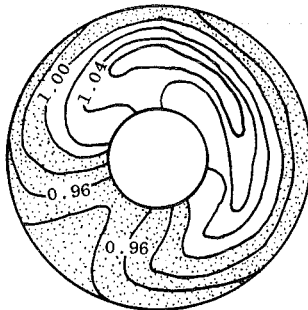
ADG

RMSE = 2.5
DIST1 = 13.3
IDCM = 0.034 (T)
IDRM = 0.010 (T)
IDCMD = 0.088 (T)
IDRMD = 0.011 (T)

l. Composite pattern (31), core surge

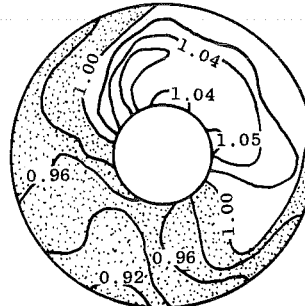
Figure 24. Continued.

View Looking Upstream



Screen

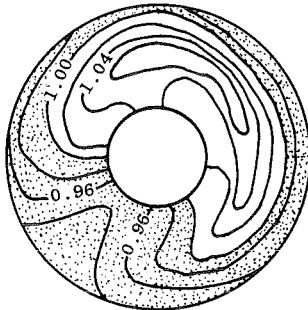
DIST1 = 13.5
IDCM = 0.084 (H)
IDRM = 0.043 (T)



ADG

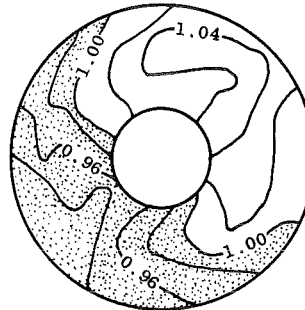
RMSE = 2.3
DIST1 = 15.3
IDCM = 0.070 (H)
IDRM = 0.024 (T)
IDCMD = 0.089 (H)
IDRMD = 0.042 (T)

m. Composite pattern (32), 100-percent fan speed surge



Screen

DIST1 = 13.5
IDCM = 0.084 (H)
IDRM = 0.043 (T)



ADG

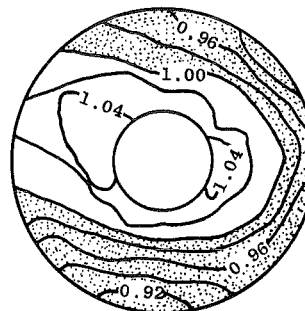
RMSE = 2.2
DIST1 = 12.7
IDCM = 0.061 (H)
IDRM = 0.016 (T)
IDCMD = 0.070 (H)
IDRMD = 0.022 (T)

n. Composite pattern (33), core surge



Screen

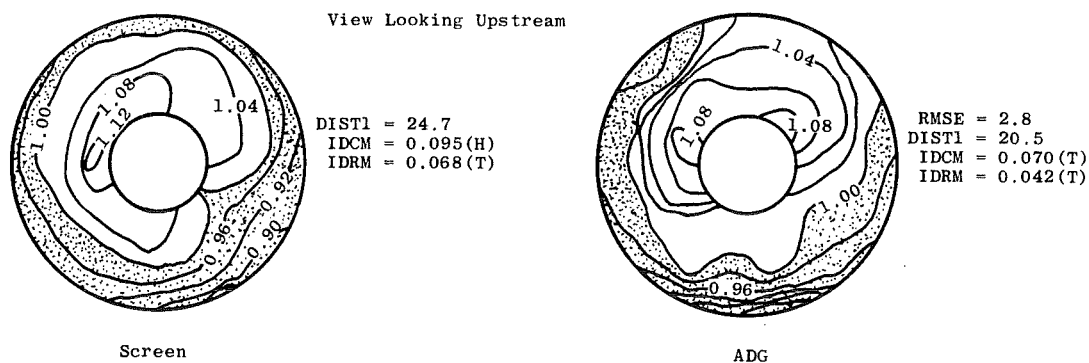
DIST1 = 24.7
IDCM = 0.084 (T)
IDRM = 0.091 (T)



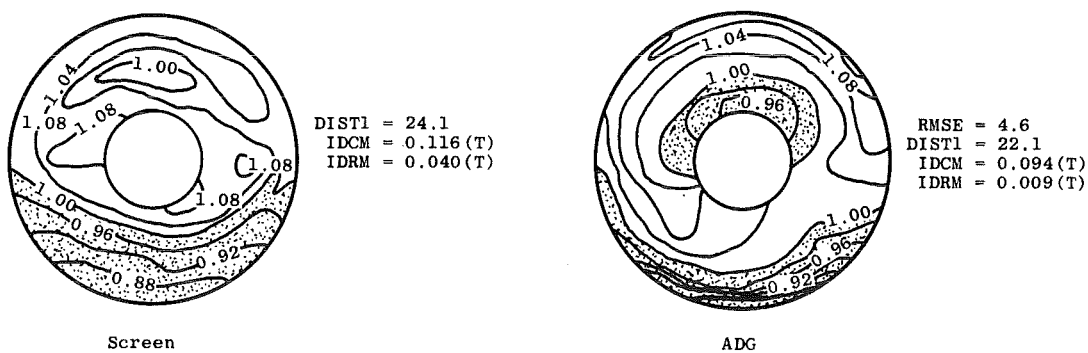
ADG

RMSE = 5.1
DIST1 = 16.8
IDCM = 0.050 (T)
IDRM = 0.042 (T)
IDCMD = 0.085 (T)
IDRMD = 0.063 (T)

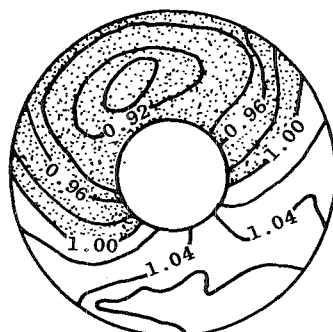
o. Composite pattern (11), simulated supersonic
Figure 24. Continued.



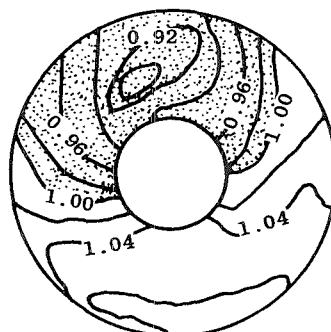
p. Composite pattern (9), simulated subsonic



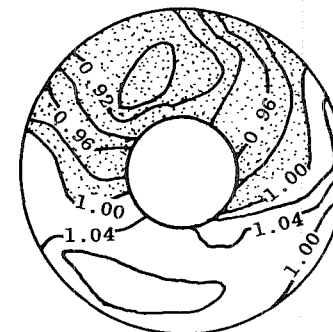
q. Composite pattern (34), modified simulated subsonic
Figure 24. Concluded.



RMSE = 2.3
DIST1 = 17.6
P1 = 8 psi
RNI = 0.6

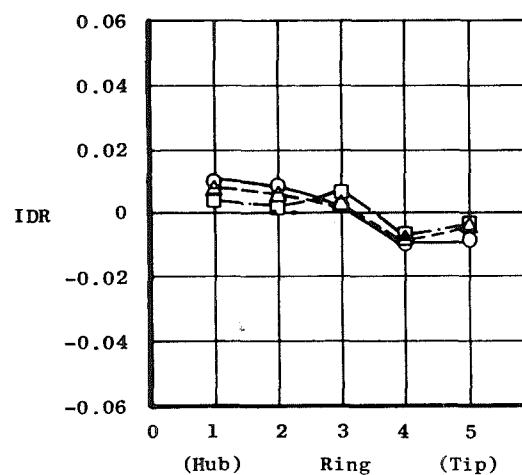
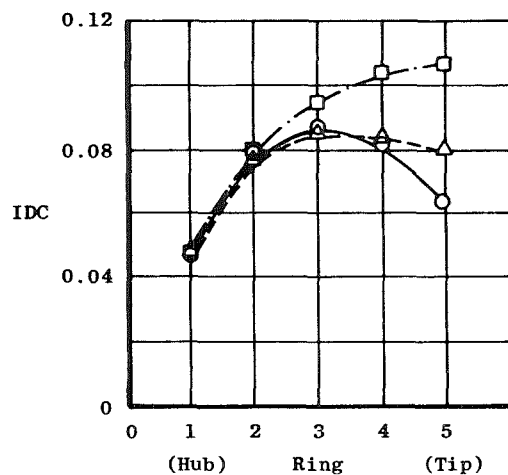


RMSE = 2.5
DIST1 = 18.6
P1 = 4 psi
RNI = 0.3

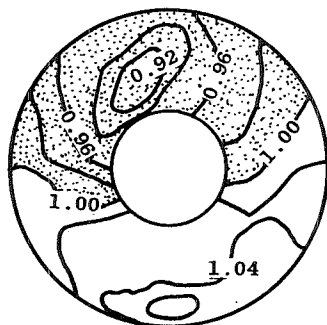


RMSE = 2.4
DIST1 = 19.2
P1 = 2 psi
RNI = 0.15

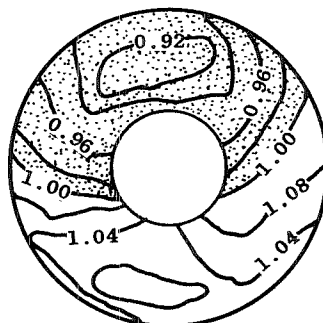
○ 8 psi
△ 4 psi
□ 2 psi



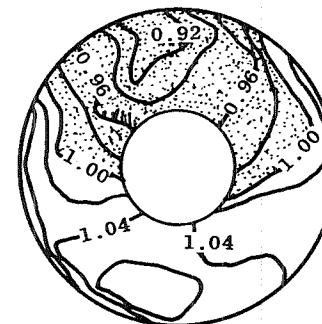
a. F101 specification pattern (26) at 100-percent fan speed surge
Figure 25. Reynolds number effect on patterns.



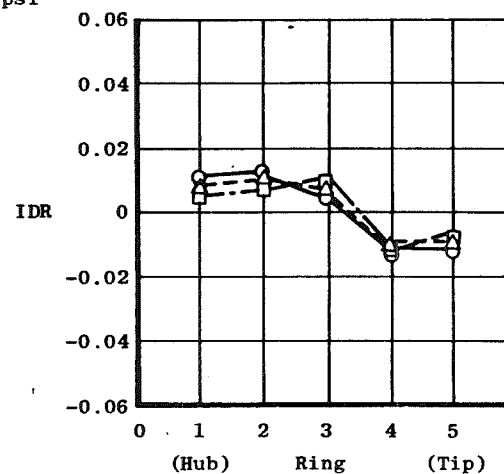
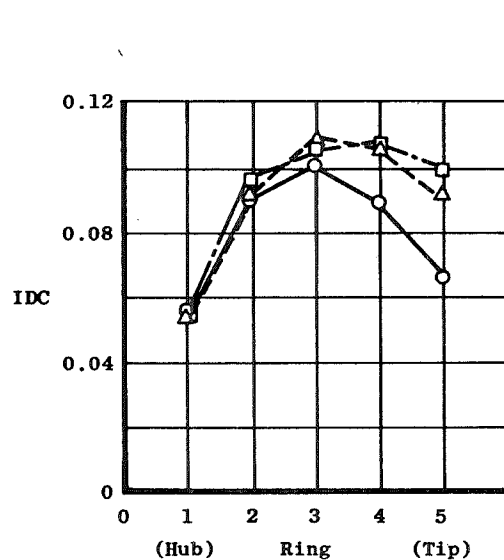
RMSE = 2.0
DIST1 = 14.7
P1 = 8 psi
RNI = 0.6



RMSE = 2.0
DIST1 = 16.1
P1 = 4 psi
RNI = 0.3



RMSE = 2.4
DIST1 = 17.0
P1 = 4 psi
RNI = 0.15



b. F101 specification pattern (27) at core surge
Figure 25. Concluded.

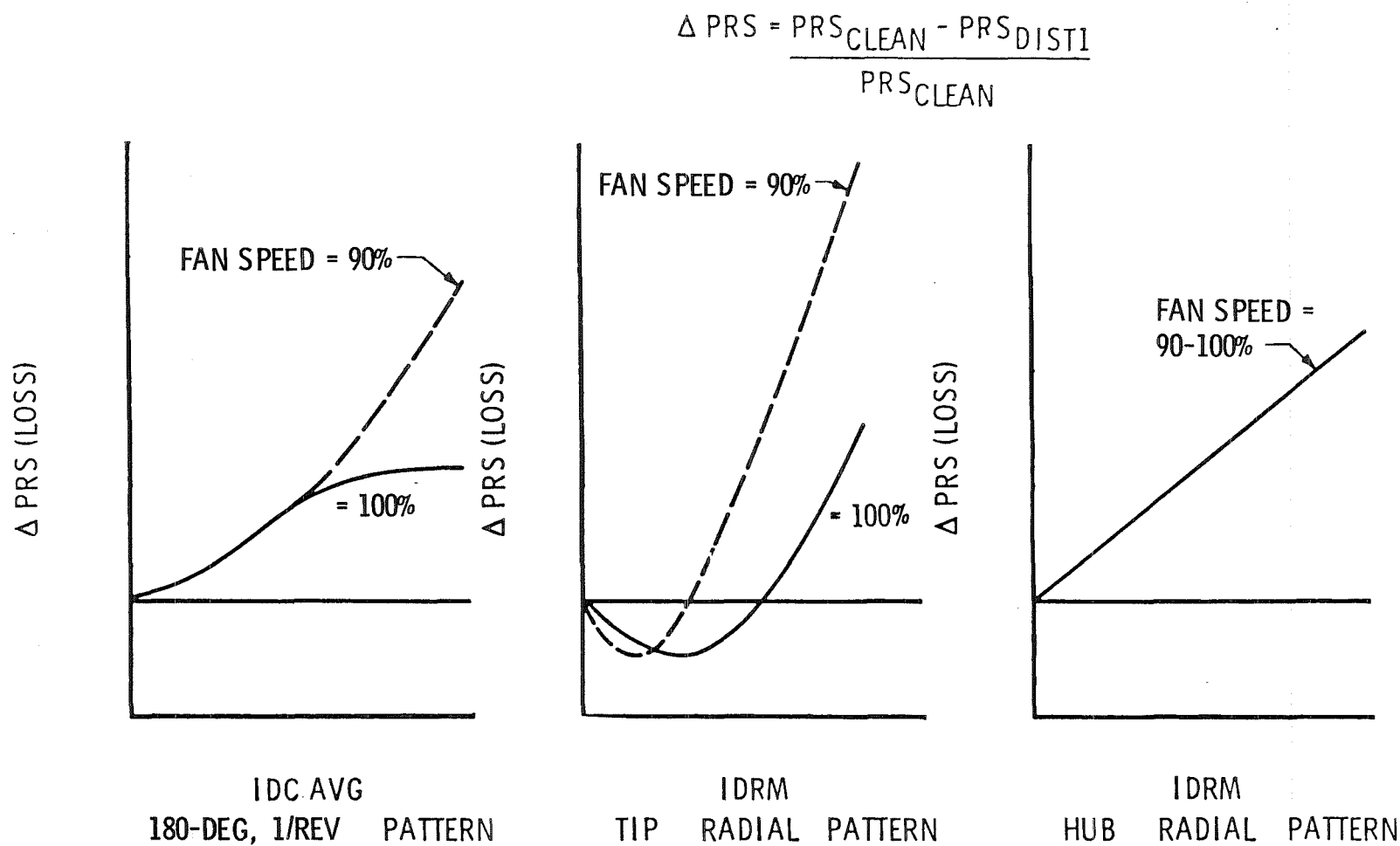
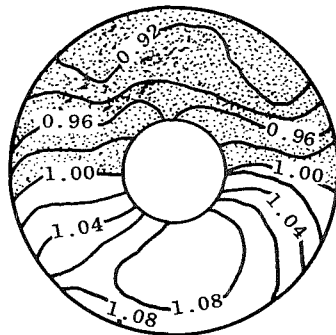
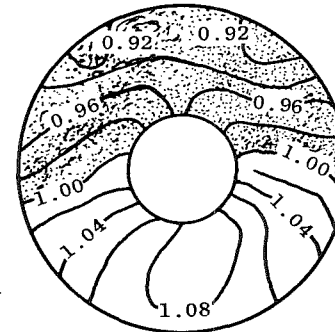


Figure 26. General Electric distortion sensitivity curves for the F101 fan.



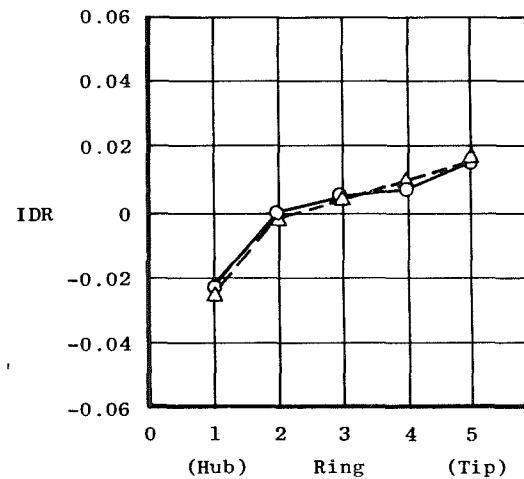
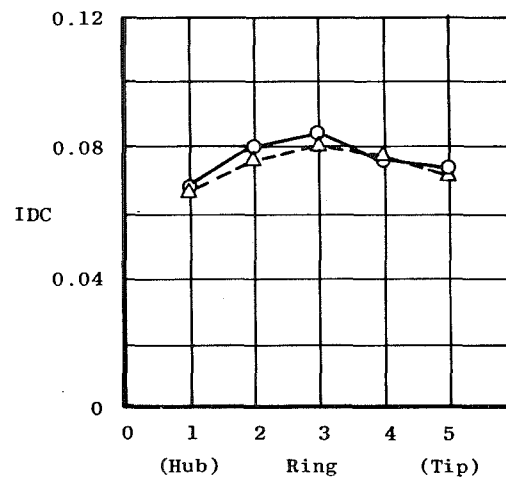
WIR = 298 lb/sec
DIST1 = 17.5



WIR = 271 lb/sec
DIST1 = 16.8

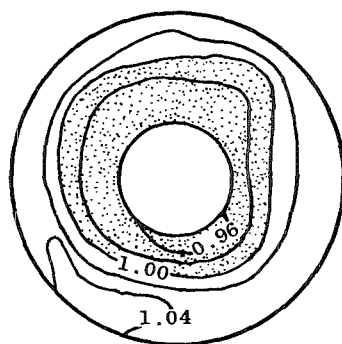
○ WIR = 308

△ WIR = 286

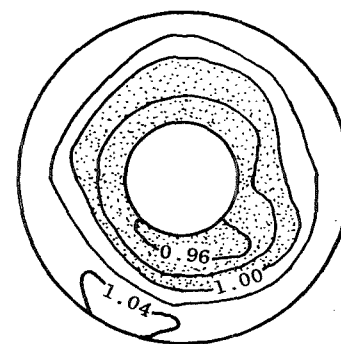


a. 180-deg, 1/rev pattern (screen 106)

Figure 27. Pattern stability during airflow change.



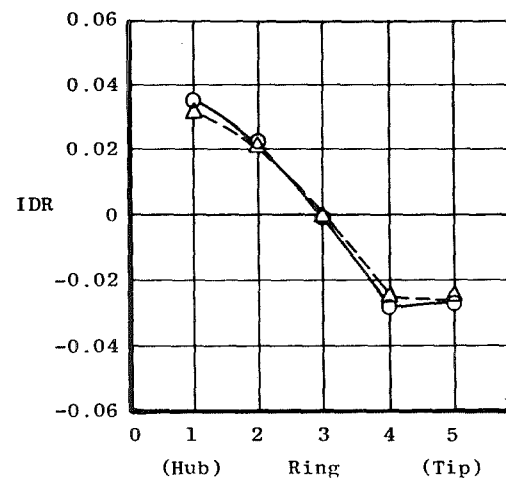
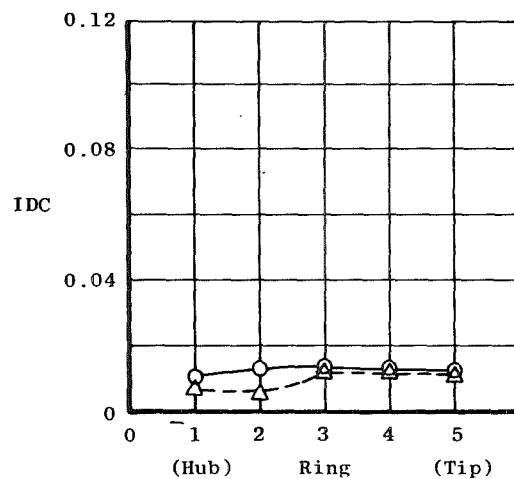
WIR = 308 lb/sec
DIST1 = 9.1



WIR = 286 lb/sec
DIST1 = 8.1

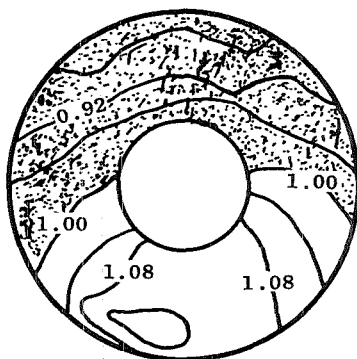
○ WIR = 298

△ WIR = 271

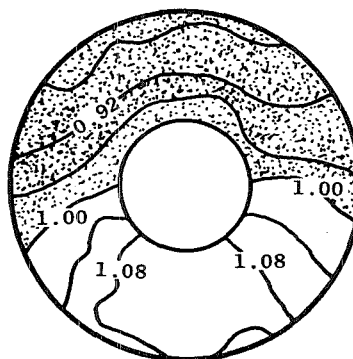


b. 50-percent hub radial pattern (screen 141)

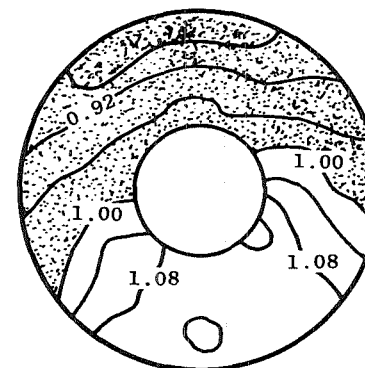
Figure 27. Concluded.



AC06 - 1039
 RMSE = 2.9
 DIST1 = 26.3
 IDCM = 0.108(T)
 IDRM = 0.028(T)



AC06 - 1046
 RMSE = 3.1
 DIST1 = 26.0
 IDCM = 0.110(T)
 IDRM = 0.026(T)



AC11 - 1010
 RMSE = 2.7
 DIST1 = 26.5
 IDCM = 0.111(T)
 IDRM = 0.022(T)

Figure 28. Pattern repeatability.

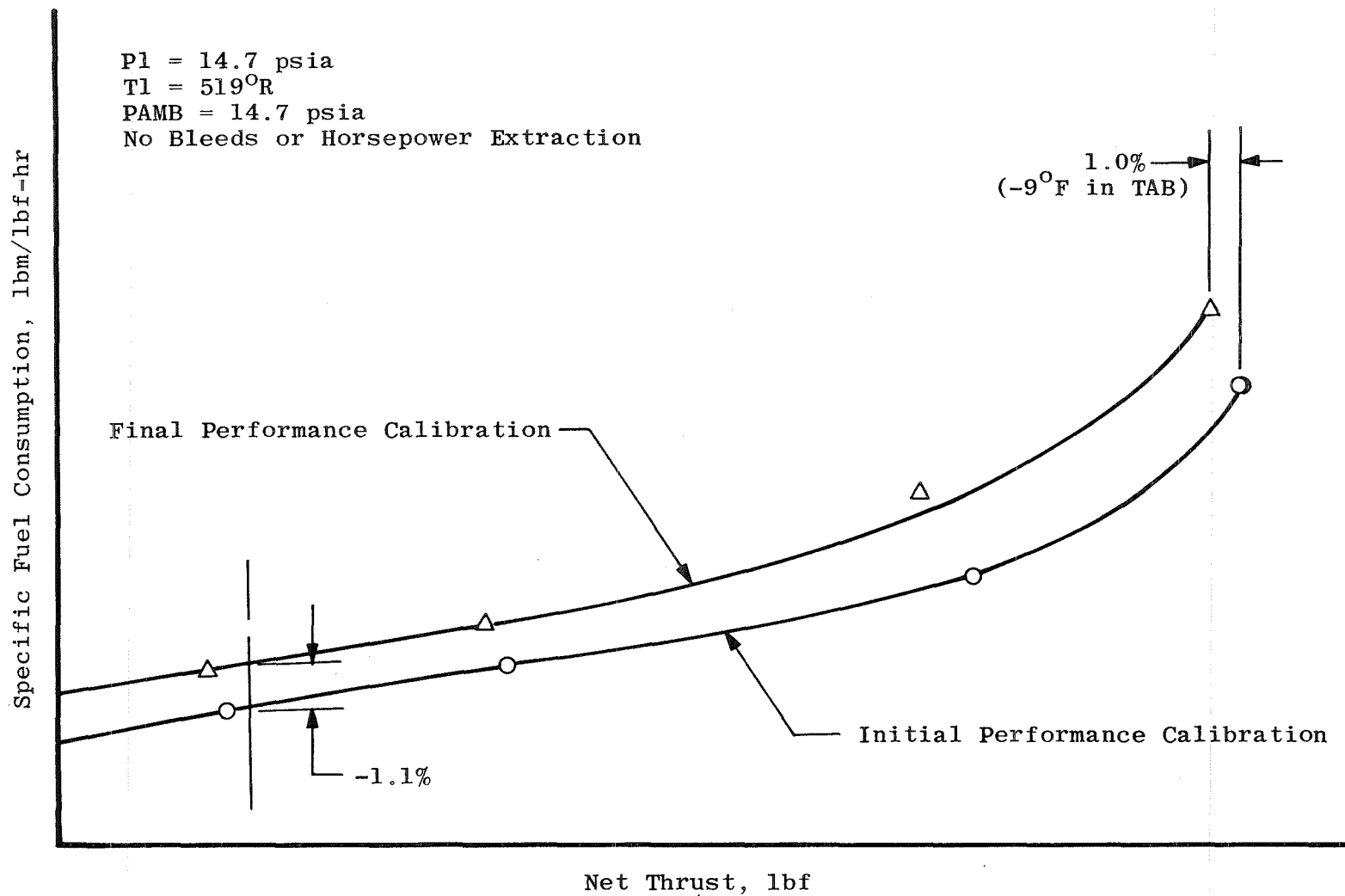


Figure 29. Engine performance deterioration.

Table 1. Posttest Estimates of Data Uncertainties
a. Parameter Measurement Uncertainty for Steady-State Data

Parameter Designation	Time Averaged over 60 sec							Range	Type of Measuring Device	Type of Recording Device	Method of System Calibration
	Precision Index (S)			Bias (B)		Uncertainty $\pm(B + t_{95}S)$					
	Percent of Reading	Unit of Measurement	Degree of Freedom	Percent of Reading	Unit of Measurement	Percent of Reading	Unit of Measurement				
Venturi Inlet Total Pressure, Station 00, psia	0.03	---	>30	0.06	---	0.12	---	14 to 25	Bonded Strain-Gage-Type Transducers	Automatic Multiple Pressure Scanning onto Sequential Sampling, Millivolt-to-Digital Converter, and Magnetic Tape Storage Data Acquisition	In-Place Application of Multiple Pressure Levels Measured with a Working Standard Pressure Calibrator Calibrated in the Standards Laboratory
	0.04	---	>30	0.08	---	0.16	---	10 to 14			
	0.08	---	>30	0.15	---	0.31	---	5 to 10			
Test Cell Ambient Pressure, psia	0.03	---	>30	0.06	---	0.12	---	14 to 20			
	0.04	---	>30	0.08	---	0.16	---	10 to 14			
	0.08	---	>30	0.15	---	0.31	---	5 to 10			
Engine Front Frame Total Pressure, Station 1.0, psia	0.02	---	>30	0.06	---	0.10	---	14 to 25			
	0.03	---	>30	0.08	---	0.14	---	10 to 14			
	0.04	---	>30	0.15	---	0.23	---	5 to 10			
Engine Inlet Lab Seal Static Pressure, Station 101, psia	0.02	---	>30	0.06	---	0.10	---	14 to 20			
	0.03	---	>30	0.08	---	0.14	---	10 to 14			
	0.06	---	>30	0.15	---	0.27	---	5 to 10			
Fan Discharge Total Pressure, Station 14, psia	0.02	---	>30	0.06	---	0.10	---	25 to 50			
	0.03	---	>30	0.08	---	0.14	---	14 to 25			
	0.07	---	>30	0.15	---	0.29	---	5 to 14			

Table 1. Continued
a. Concluded

Parameter Designation	Time Averaged over 60 sec							Range	Type of Measuring Device	Type of Recording Device	Method of System Calibration
	Precision Index (S)			Bias (B)		Uncertainty $\pm(B + t_{95}S)$					
	Percent of Reading	Unit of Measurement	Degree of Freedom	Percent of Reading	Unit of Measurement	Percent of Reading	Unit of Measurement				
Compressor Inlet Total Pressure, Station 25, psia	0.02	—	>30	0.06	—	0.10	—	25 to 50	Bonded Strain-Gage-Type Transducers	Automatic Multiple Pressure Scanning onto Sequential Sampling, Millivolt-to-Digital Converter, and Magnetic Tape Storage Data Acquisition	In-Place Application of Multiple Pressure Levels Measured with a Working Standard Pressure Calibrator Calibrated in the Standards Laboratory
	0.03	—	>30	0.08	—	0.14	—	14 to 25			
	0.07	—	>30	0.15	—	0.29	—	5 to 14			
Venturi Inlet Total Temperature, Station 00, °R	—	0.44°R	>30	—	1.86°R	—	2.74°R	490 to 960°R	Chromel-Alumel Temperature Transducers	Sequential Sampling, Millivolt-to-Digital Converter, and Magnetic Tape Storage Data Acquisition System	Millivolt Substitution on NBS Temperature versus Millivolt Table
Engine Inlet Total Temperature, Station 1, °R	—	0.44°R	>30	—	1.86°R	—	2.74°R	490 to 960°R			
Scale Force, FS, lbf	—	7 lbf	>30	—	11 lbf	—	25 lbf	<5K lbf	Bonded Strain-Gage-Type Force Transducers		In-Place Application of Multiple Force Levels Measured with Force Transducers Calibrated in the Standards Laboratory
	—	8 lbf	>30	—	14 lbf	—	30 lbf	5K to 10K			
	—	8 lbf	>30	—	15 lbf	—	31 lbf	10K to 15K			
	—	3 lbf	>30	—	25 lbf	—	43 lbf	>15K lbf			
Fuel Flow	0.08	—	>30	0.25	—	0.41	—	2K to 80K lb/hr	Turbine-Type Flowmeter		Laboratory Calibration
Airflow	0.17	—	>30	0.12	—	0.46	—	30 to 300 lb/sec	Choked Venturis		—

*REFERENCE: 14

NOTES: These uncertainties are for a plane average measurement at the indicated station.

Table 1. Continued
b. Parameter Measurement Uncertainty for Time-Averaged Transient Data

Parameter Designation	Time Averaged over 3 to 5 sec							Range	Type of Measuring Device	Type of Recording Device	Method of System Calibration
	Precision Index (S)			Bias (B)		Uncertainty $\pm(B + t_{95}S)$					
	Percent of Reading	Unit of Measurement	Degree of Freedom	Percent of Reading	Unit of Measurement	Percent of Reading	Unit of Measurement				
Engine Fuel Flow	---	13.5 lb/hr	30	---	16 lb/hr	---	43 lb/hr	300 to 1,500 lb/hr	Turbine-Type Flowmeter	Digital Data Acquisition System	Laboratory Volumetric Calibration Device
WFME	---										
Fuel Temperature Measurement TFF	---	2°F	30	---	1°F	---	5°F	-20 to 240°F	Close-Coupled Temperature Transducer		Resistance Calibration
Engine Inlet 40-Probe Average Total Pressure PY1, psia	---	0.027		---	0.013	---	0.067	2.0 to 50 psi	Close-Coupled Strain-Gage Transducers, Time Averaged		
Fan Discharge-24-Probe Average Total Pressure PY14, psia	---	0.027		---	0.013	---	0.067	2.0 to 50 psi			
Cell Pressure Single Measurement P013, psia	---	0.035	30	---	0.013	---	0.083	2.0 to 20 psi			

Table 1. Continued
b. Concluded

Parameter Designation	Time Averaged over 3 to 5 sec							Range	Type of Measuring Device	Type of Recording Device	Method of System Calibration
	Precision Index (S)			Bias (B)		Uncertainty $\pm(B + t_{95}S)$					
	Percent of Reading	Unit of Measurement	Degree of Freedom	Percent of Reading	Unit of Measurement	Percent of Reading	Unit of Measurement				
Station 1 8-Probe Total-Temperature Measurement T1	—	0.44°R	>30	—	1.86°R	—	2.74°R	490 to 960°R	150° Reference C/A Type Thermocouple	Digital Data Acquisition System, 3-sec Average of 100 Samples per sec,Digital Sampling	Resistance Calibration
Engine Fan Speed NF	0.10	—	>30	0.10	—	0.30	—		Magnetic Pickup		Frequency Substitution
Test Cell Single Tap Ambient Pressure PO, psia	0.87	—	>30	0.26	—	2.00	—	5 to 15 psia	Bonded Strain-Gage Transducer		Resistance Calibration
Engine Inlet 40-Probe Average Total Pressure PY1, psia	0.40	—	>30	0.26	—	1.06	—	5 to 25 psia			
Fan Discharge 24-Probe Average Total Pressure PY14, psia	0.40	—	>30	0.26	—	1.06	—	5 to 25 psia			

Table 1. Continued
c. Parameter Measurement Uncertainty for Transient Data

Parameter Designation	0.01-sec Data - No Average							Range	Type of Measuring Device	Type of Recording Device	Method of System Calibration
	Precision Index (S)			Bias (B)		Uncertainty $\pm(B + t_{95}S)$					
	Percent of Reading	Unit of Measurement	Degree of Freedom	Percent of Reading	Unit of Measurement	Percent of Reading	Unit of Measurement				
Engine Fuel Flow, lb/hr WFME	0.74	—	>30	1.66	—	2.14	—		Turbine-Type Flowmeter	Digital Data Acquisition, System Processed at 100 Samples per sec	Laboratory Volumn Calibration Device
Engine Core Speed, rpm NC	—	8.8	>30	—	5.0	—	22.6	5,000 to 13,000 rpm	Magnetic Pickup		Frequency Substitution
Compressor Discharge Static, psia PS3C	0.50	—	30	0.23	—	1.23	—	50 to 500 psia	Strain-Gage Transducer		Resistance Calibration
Engine Fuel Temperature, TFF °R	—	16.2	>30	—	0.9	—	19.1	460 to 750°R	150° Reference C/C Type Thermocouple		
WF/PS3C	0.89	—		0.70	—	2.29	—		Calculation		

d. Calculated Parameter Uncertainty for Steady-State Data

Parameter Designation	Time Interval of 60 sec							Range
	Precision Index (S)			Bias (B)		Uncertainty $\pm(B + t_{95}S)$		
	Percent of Reading	Unit of Measurement	Degree of Freedom	Percent of Reading	Unit of Measurement	Percent of Reading	Unit of Measurement	
Maximum - Minimum Pressure Distortion DIST1	---	0.3	>30	---	0.3	---	0.9	5- to 20-percent Distortion
Circumferential Distortion IDC	---	0.3	>30	---	0.3	---	0.9	5- to 20-percent Distortion
Radial Distortion IDR	---	0.3	>30	---	0.3	---	0.9	5- to 20-percent Distortion

Table 1. Concluded
e. Calculated Parameter Uncertainty for Time-Averaged Transient Data

Parameter Designation	Time Averaged over 3 to 5 sec							Range
	Precision Index (S)			Bias (B)		Uncertainty $\pm(B + t_{95}S)$		
	Percent of Reading	Unit of Measure-ment	Degree of Freedom	Percent of Reading	Unit of Measure-ment	Percent of Reading	Unit of Measure-ment	
Orifice Flow WSA	1.1	—	>30	2.2	—	5.3	—	1.0 to 6.0 lb/sec
Primary Flow WYIP	1.36	—	>30	0.71	—	3.4	—	Pressure Range
	0.34	—	>30	0.31	—	1.0	—	2.0 to 8.0 psia
Corrected Primary Flow WYIR	1.82	—	>30	0.96	—	4.6	—	8.0 to 30 psia
	0.48	—	>30	0.44	—	1.4	—	2.0 to 8.0 psia
Pressure Ratio PY1/PY14	1.91	—	>30	0.93	—	4.74	—	8.0 to 30 psia
	0.48	—	>30	0.24	—	1.20	—	2.0 to 8.0 psia

e. Concluded

Parameter Designation	Time Averaged over 3 to 5 sec							Range
	Precision Index (S)			Bias (B)		Uncertainty $\pm(B + t_{95}S)$		
	Percent of Reading	Unit of Measurement	Degree of Freedom	Percent of Reading	Unit of Measurement	Percent of Reading	Unit of Measurement	
Pressure Distortion DIST1	—	1.0	>30	—	0.4	—	2.4	5 to 20 percent
Circumferential Distortion Describer IDC	—	1.0	>30	—	0.4	—	2.4	5 to 20 percent
Radial Distortion Describer IDR	—	1.0	>30	—	0.4	—	2.4	5 to 20 percent

Table 2. Test Summary

Airjet Pattern Selection		Test Condition					Distortion Pattern Condition						
Number	Description	Engine Inlet Pressure, psia	Engine Inlet Temperature, °R	Ambient Pressure, psia	Engine Airflow Rate, lb/sec	Stall F-Fan C-Compressor	PRMS	RMSE, percent	IDC	IDR	DISTL, percent	Time to Set Pattern, sec	Airjet Airflow Rate, lb/sec
1	1/rev Screen No. 106	8	480	5	353	F	—	2.7	0.111(T)	0.022(T)	27	130	53
7	1/rev Screen No. 121	↓	↓	↓	353	F	0.87	1.8	0.061(H)	0.097(T)	16	135	43
23	1/rev Screen No. 106	↓	↓	↓	306	C	1.01	2.1	0.135(H)	0.041(T)	23	170	34
2	1/rev Screen No. 106	↓	522	↓	310	F	1.72	1.5	0.074(T)	0.015(T)	18	130	19
A	Manual Minimum Steady State, Maximum Dynamic	↓	↓	↓	↓	↓	—	2.1	0.008(T)	0.032(H)	7	Man	33
A	Manual Minimum Steady State, Maximum Dynamic	↓	↓	↓	↓	F	—	1.8	0.013(H)	0.019(H)	7	Man	45
—	Clean Surge Margin Demonstration	↓	↓	↓	↓	↓	—	N/A	0.010(T)	0.007(T)	3	N/A	0
37	Modified 1/rev Screen No. 303.4	↓	↓	↓	↓	↓	—	4.4	0.093(T)	0.021(T)	22	195	43
4	50% Extent Hub Radial Screen No. 141	14.2	↓	12.8	308	↓	0.78	1.2	0.026(T)	0.040(H)	10	165	24
3	50% Extent Hub Radial Screen No. 141	14.2	↓	12.8	344	↓	0.80	2.4	0.026(T)	0.059(H)	14	165	44
31	Special GE Screen No. 4	5.5	519	2.0	320	F	0.97	2.5	0.077(T)	0.015(T)	16	200	16
31	Special GE Screen No. 4	5.5	519	2.0	300	C	0.72	—	0.085(T)	0.010(T)	14	60	0
11	Simulated Supersonic Screen No. 353CD	8	517	5	280	F	1.86	5.1	0.063(T)	0.041(T)	17	230	34
32	Special GE Screen No. 2	5.1	479	3.4	340	F	0.98	2.3	0.072(H)	0.025(T)	16	150	12
32	Special GE Screen No. 2	5.1	479	3.4	—	C	—	2.2	0.060(H)	0.017(T)	13	105	—
14	Flight Test - SLS Subsonic Crosswind	8	476	5	342	↓	1.15	2.7	0.058(T)	0.050(H)	16	180	28
15	PWT FS (P/P237509) - SLS	↓	↓	↓	340	↓	1.18	2.5	0.076(H)	0.019(H)	16	210	28
16	PWT FS (P/P220801)	↓	↓	↓	340	↓	1.04	3.0	0.048(T)	0.059(H)	16	215	28
4	50% Extent Hub Radial Screen No. 141	↓	514	↓	285	F	0.92	1.4	0.011(T)	0.031(H)	9	230	14
5	50% Extent Tip Radial Screen No. 123C	↓	520	↓	277	F	1.33	4.3	0.025(T)	0.042(T)	14	120	26
35	Modified 1/rev Screen No. 303.4 New Program	↓	↓	↓	288	↓	1.11	7.8	0.0677(T)	0.0148(H)	19	210	34
35	Modified 1/rev Screen No. 303.4 New Program	↓	↓	↓	213	F	1.06	6.3	0.103(T)	0.005(H)	10	110	27
6	50% Extent Tip Radial Screen No. 123C	↓	684	↓	224	F	—	2.6	0.0105(T)	0.0366(T)	13	155	37

Table 2. Continued

Airjet Pattern Selection		Test Condition						Distortion Pattern Condition					
Number	Description	Engine Inlet Pressure, psia	Engine Inlet Temperature, °R	Ambient Pressure, psia	Engine Airflow Rate, lb/sec	Stall F=Fan C=Compressor	PRMS	RMSE, percent	IDC	IDR	DIST1, percent	Time to Set Pattern, sec	Airjet Airflow Rate, lb/sec
26	Simulated SLS Screen No. 354.7M	8	477	5	404		—	2.6	0.0931(T)	0	19	155	29
26		↓	↓	↓	408	F	0.88	2.3	0.0782(T)	0.0104(H)	17	90	17
27		↓	↓	↓	375	C	0.87	2.0	0.0734(T)	0.0099(H)	15	95	13
26		4	480	2	339	F	0.95	2.5	0.0962(T)	0.0062(H)	18	90	10
27		4	480	2	316	C	0.90	2.0	0.0947(T)	0.0073(H)	17	85	9
26		2	470	1.1	334	F	1.13	2.4	0.1008(T)	0.0061(H)	19	65	5
27		2	470	1.1	300	C	1.12	2.4	0.1044(T)	0.0041(H)	17	70	4
34	Simulated Subsonic Manual Screen No. 356.1	4	478	2	337		1.33	5.0	0.0937(T)	0.0086(T)	18	120	18
34	Simulated Subsonic Manual Screen No. 356.1	4	478	2	335		—	5.5	0.0972(T)	0.0037(T)	19	135	15
5	50% Extent Tip Screen No. 123C	8	518	5	284		1.61	4.0	0.0277(T)	0.0540(T)	16	165	40
28	Modified 1/rev Screen No. 303.4	↓	↓	↓	283		1.25	6.0	0.1174(T)	0.0097(T)	26	185	50
11	Simulated Supersonic Screen No. 353CD	↓	↓	↓	318		1.67	4.5	0.0490(T)	0.0465(T)	18	190	59
4	50% Extent Hub Radial Screen No. 141	↓	↓	↓	314		0.93	1.2	0.0318(T)	0.0368(H)	9	135	35
31	Special GE Screen No. 4	↓	↓	↓	380		1.03	2.3	0.0840(T)	0.0211(T)	16	115	43
32	Special GE Screen No. 2	↓	↓	↓	342		0.86	2.2	0.0616(H)	0.0177(T)	14	150	20
10	Simulated Subsonic Manual Screen No. 356.1	4.5	520	2	336		2.27	6.8	0.0773(T)	0.0129(H)	16	205	38
26	Simulated SLS Screen No. 354.7M	4	↓	↓	330		1.52	3.0	0.0680(H)	0.0314(H)	17	220	37
26	Simulated (Reset Airjet Valve Timers)	↓	↓	↓	341		1.22	2.4	0.0734(H)	0.0221(H)	18	225	23
26	Simulated (Modified Timer in Logic)	↓	↓	↓	341		1.17	3.1	0.0997(T)	0.0068(T)	20	135	17
27	Simulated (Modified Timer in Logic)	↓	↓	↓	338		1.10	2.1	0.0981(T)	0.0062(H)	17	120	9
27	Simulated (Modified Timer in Logic)	2.45	↓	1.33	320		—	2.3	—	—	18	230	13
1	1/rev Screen No. 106	8	516	5	343		0.94	2.9	0.1078(T)	0.0280(T)	26	160	45
1	1/rev (Reset ADG Valve Timer)	8	↓	↓	342		0.85	3.1	0.1200(T)	0.0259(T)	26	215	42
2	1/rev Screen No. 106	7.9	↓	↓	270		0.88	1.6	0.0693(T)	0.0122(T)	17	180	26
1	1/rev Screen No. 106	7.8	↓	↓	340		1.08	3.2	0.1083(H)	0.0254(T)	26	170	46

Table 2. Continued

Airjet Pattern Selection		Test Condition					Distortion Pattern Condition						
Number	Description	Engine Inlet Pressure, psia	Engine Inlet Temperature, °R	Ambient Pressure, psia	Engine Airflow Rate, lb/sec	Stall F=Fan C=Compressor	PRMS	RMSE, percent	IDC	IDR	Distl, percent	Time to Set Pattern, sec	Airjet Airflow Rate, lb/sec
3	50% Extent Hub Radial Screen No. 141	8	480	5	342	F	9.0	2.4	0.0218(T)	0.0611(H)	15	95	48
25	↓	↓	480	↓	317	C	1.07	2.0	0.0405(T)	0.0492(H)	13	150	36
4	↓	↓	520	↓	268	F	0.74	1.0	0.015(T)	0.037(H)	10	75	16
3	↓	↓	↓	↓	337	↓	1.24	2.5	0.0270(T)	0.0632(H)	15	145	46
5	↓	4	↓	2	320	↓	1.70	2.6	0.0201(H)	0.0647(H)	16	200	45
1	1/rev Screen No. 106	4	↓	2	320	↓	1.65	3.3	0.1244(T)	0.0287(T)	27	145	35
27	Simulated SLS Screen No. 354.7M	8	480	5	304	C	1.20	1.7	0.0743(T)	0.0230(H)	16	190	27
26	Simulated SLS Screen No. 354.7M	↓	↓	↓	332	F	1.18	2.3	0.0806(T)	0.0233(H)	18	145	30
4	50% Extent Hub Radial Screen No. 141	↓	↓	↓	300	↓	0.76	1.0	0.0145(T)	0.0410(H)	10	85	13
3	↓	↓	↓	↓	345	↓	1.08	2.5	0.0198(T)	0.0625(H)	14	135	33
↓	↓	↓	↓	↓	346	↓	1.07	2.5	0.0192(T)	0.0633(H)	14	120	32
↓	↓	↓	↓	↓	346	↓	1.06	—	0.0206(T)	0.0608(H)	14	—	32
↓	↓	↓	↓	↓	336	↓	1.21	—	0.0190(T)	0.0617(H)	15	—	42
1	1/rev Screen No. 106	↓	↓	↓	340	↓	0.89	2.7	0.1072(T)	0.0217(T)	25	160	40
↓	↓	↓	↓	↓	351	↓	—	—	0.068(T)	0.028(T)	20	—	—
↓	↓	↓	520	↓	349	↓	0.65	—	0.0824(T)	0.0221(T)	19	—	21
7	50% Extent Tip Radial Screen No. 121	↓	↓	↓	347	↓	0.65	—	0.0779(T)	0.0195(T)	18	—	22
3	50% Extent Hub Radial Screen No. 141	↓	↓	↓	342	↓	1.42	—	0.0092(H)	0.0807(T)	17	—	37
23	1/rev Screen No. 106	↓	↓	↓	344	↓	1.04	—	0.0356(T)	0.0628(H)	16	—	34
25	50% Extent Hub Radial Screen No. 141	↓	522	↓	344	↓	0.76	—	0.0932(T)	0.0240(T)	23	—	38
26	Simulated SLS Screen No. 354.7M	↓	↓	↓	346	↓	1.00	—	0.0286(T)	0.0576(H)	14	—	24
27	Simulated SLS Screen No. 354.7M	↓	↓	↓	344	↓	1.11	—	0.1118(T)	0.0075(H)	21	—	28
27	Simulated SLS Screen No. 354.7M	↓	↓	↓	344	↓	1.24	—	0.0814(H)	0.0144(H)	18	—	23
27	Simulated SLS Screen No. 354.7M	↓	↓	↓	345	↓	1.08	—	0.0852(T)	0.0053(H)	17	—	19
10	Simulated Subsonic Manual Screen No. 356.1	↓	↓	↓	342	↓	1.35	—	0.1019(T)	0.0211(T)	22	—	33

Table 2. Continued

Airjet Pattern Selection		Test Condition					Distortion Pattern Condition						
Number	Description	Engine Inlet Pressure, psia	Engine Inlet Temperature, °R	Ambient Pressure, psia	Engine Airflow Rate, lb/sec	Stall F=Fan C=Compressor	PRMS	RMSE, percent	IDC	IDR	DIST1, percent	Time to Set Pattern, sec	Airjet Airflow Rate, lb/sec
9	Screen No. 351.1	8	522	5	341		0.97	---	0.0704(H)	0.0425(T)	21	---	24
14	SLS Crosswind Subsonic - Flight Test	↓	↓	↓	346		1.26	---	0.0493(T)	0.0528(H)	16	---	28
26	Simulated SLS Screen No. 354.7M	↓	↓	↓	345		1.39	---	0.0744(H)	0.0209(H)	16	---	31
NA	Posttest Performance Power Hook Calibration	14.0	520	14	---		NA	NA	NA	NA	NA	NA	0
354.7M	Screen Installed	8	478	5	344	F	0.50	---	0.0902(H)	0.0288(H)	21.6	---	0
354.7M	↓	↓	↓	↓	322	C	0.47	---	0.0792(H)	0.0246(H)	20.0	---	0
141		↓	↓	↓	346	F	0.69	---	0.0110(T)	0.0718(H)	16.9	---	0
141		↓	↓	↓	320	C	0.61	---	0.0070(H)	0.0601(H)	14.0	---	0
141		↓	↓	↓	277	F	0.53	---	0.005(T, H)	0.041(H)	9.8	---	0
NA	Pretest Performance Power Hook Calibration	14.3	515	14.3	---		NA	NA	NA	NA	NA	NA	0
NA	Engine Factory Break-In Green Run	14.3	520	14.3	---		NA	NA	NA	NA	NA	NA	0
141	Screen Installed	8.11	505	5.0	171				0.006(T)	0.013(T)	3.8		0
↓	↓	8.05	500	↓	172								0
		8.35	483		354								0
		8.35	483		354				0.011(T)	0.075(T)	16.9		0
		8.03	480		354				0.011(T)	0.076(T)	17.1		0
		8.14	↓		347								0
		8.14	↓		329								0
		8.14	↓		329				0.008(T)	0.061(T)	14.3		0
		8.14	↓	↓	329								0
		8.03	477	5.01	356				0.011(T)	0.077(T)	17.2		0
		8.03	477	5.01	351								0
		8.02	477	5.0	356	F			0.011(T)	0.077(T)	17.2		0
		8.01	478	↓									0
		7.66	479	↓	332								0

Table 2. Continued

Airjet Pattern Selection		Test Condition					Distortion Pattern Condition						
Number	Description	Engine Inlet Pressure, psia	Engine Inlet Temperature, °R	Ambient Pressure, psia	Engine Airflow Rate, lb/sec	Stall F-Fan C-Compressor	PRMS	RMSE, percent	IDC	IDR	DISTl, percent	Time to Set Pattern, sec	Airjet Airflow Rate, lb/sec
141	Screen Installed	7.64	519	5.01	333	—							
		8.3		5.0	336	—							
		8.3			336	—							
		8.35			352	—							
					352	—							
			520		301	—							
			520		301	—							
		8.00	518	5.00	312	—							
		8.02	519	5.01	313	—							
		8.02			313	—			0.016(T)	0.013(H)	4.69		
		8.05			298	—							
		8.07		5.00	283	—							
		8.07		5.0	283	—			0.011(T)	0.010(H)	4.16		
2	Using ADG	7.89			271	—							
2		7.89			271	—			0.073(T)	0.015(H)	16.98		38.44
		8.06	518	6.05	349	—							
		8.06			349	—			0.019(T)	0.0146(H)	5.68		
7		7.8			331	—							
		7.8			331	—			0.012(H)	0.083(H)	19.39		42.21
8		7.93	519	6.06	329	—							
8		7.93	519		329	—			0.107(T)	0.008(T)	20.92		36.77
8		7.95	519		344	—							
9		8.15	518		320	—							
9		8.15	518		320	—			0.081(T)	0.0347(H)	17.20		13.09
10		7.91	519	6.07	343	—							

Table 2. Concluded

Airjet Pattern Selection		Test Condition					Distortion Pattern Condition						
Number	Description	Engine Inlet Pressure, psia	Engine Inlet Temperature, °R	Ambient Pressure, psia	Engine Airflow Rate, lb/sec	Stall F=Fan C=Compressor	PRMS	RMSE, percent	IDC	IDR	DISTl, percent	Time to Set Pattern, sec	Airjet Airflow Rate, lb/sec
10	Using ADG	7.91	519	6.07	343	—			0.096(T)	0.0249(H)	19.40		29.04
3	↓	7.85	518	6.05	344	—							
3		7.85	518	6.05	344	—			0.026(T)	0.067(T)	17.97		33.88
None		8.01	520	6.08	239	—							
		14.57	↓	13.51	350	—							
		14.68	↓	13.48	335	—							
		14.61	521	13.47	313	—							
		14.63	520	13.46	301	—							
		14.60	520	13.49	293	—							
None		8.07	483	4.99	350	—							
None		8.06	480	5.0	349	—			0.019(T)	0.014(H)	5.73		
1		7.83	481	5.03	351	—							
1		7.83	481		351	F			0.011(T)	0.031(H)	25.847		39.89
None		8.02	480		354	—							
		8.02	↓		354	—			0.019(T)	0.0145(H)	5.70		
		8.03	↓		344	—							
		8.07	479		329	—							
		8.07	479		329	—			0.017(T)	0.013(H)	5.17		
23		7.9	480	5.02	324	—			0.110(T)	0.025(H)	25.346		36.78
23		7.9	480	5.02	324	C							
None		8.0	520	5.04	310	—							
None		8.0	↓	5.04	↓	—			—	—	—		
2		8.2	↓	5.0		—			0.082(H)	0.016(H)	18.74		24.79
2		8.2	↓	5.0	↓	F							

Table 3. Chronological Test Summary

<u>Test</u>	<u>Date</u>	<u>Comments and Accomplishments</u>
	3/18/77	F101-GE-100(S/N 470006/10) engine arrived at AEDC
CK01	4/18/77	Airjet rake structural check
	4/20/77	Engine installation in Test Cell J-2 initiated
CK02	4/22/77	Dec-10 data acquisition checkout
CK03	4/27/77	End-to-end instrumentation and data acquisition checkout
CK04	4/29/77	End-to-end instrumentation and data acquisition checkout
CK05	5/2/77	Engine systems checked at windmill and idle conditions
CK06	5/4/77	Engine systems checked at idle and intermediate conditions
CK07	5/6/77	Installed screen 106 - conducted fan and compressor surge investigation (2 intentional stalls)
CK08	5/10/77	Cancelled because of computer problems
CK09	5/12/77	Cancelled because of fuel contamination
CK10	5/17/77	Airjet system checkout, simulated 1 pattern
AA01	5/18/77	Simulated screen No. 106 distortion pattern with airjet - conducted fan and core surge investigation (3 intentional stalls)
AA02	5/19/77	Simulated screen and flight distortion patterns with airjet
CK11	9/12/77	End-to-end instrumentation and data acquisition checkout
CK12	9/14/77	Engine systems check at idle and intermediate conditions
BA01	9/16/77	Installed screen No. 141 - conducted fan surge investigation (1 intentional stall)

Table 3. Continued

<u>Test</u>	<u>Date</u>	<u>Comments and Accomplishments</u>
	2/28/78	F101-GE-100 (S/N470006/11) engine arrived at AEDC
	3/8/78	Engine installation in Test Cell J-2 initiated
CK01	3/23/78	Engine systems checked at windmill and idle conditions
CK02	3/28/78	False P3 orifice limited engine maximum speed - orifice removed and standard fuel pulse system reinstalled engine factory break-in cycle initiated - engine oil consumption excessive
AA01	3/30/78	Dual test period - completed factory break-in and performance power hook calibration airoff - installed distortion screen No. 141 - conducted fan and compressor surge investigation (3 intentional stalls) stators opened 5 deg for core stall - engine oil consumption excessive
<u>Modified Engine Gear Box By Adding 1-in. Vent Line (Previously Assumed - To Be Internally Vented)</u>		
<u>Removed Screen No. 141 and Installed Screen No. 354.7M</u>		
AB02	4/4/78	Conducted compressor surge investigation (1 intentional stall)
AB03	4/7/78	Conducted fan surge investigation (1 intentional stall)
<u>Removed Screen No. 354.7M and Installed Airjet Distortion Generator Hardware</u>		
CK03	4/13/78	Checked out airjet high-pressure airflow and temperature control system - checked out airjet computer control pattern setting capability - operation demonstrated by setting 10 programmed patterns
AC04	4/20/78	Simulated screen No. 354.7M distortion pattern with airjet - conducted fan (ADG Pattern No. 26) and compressor (ADG No. 27) surge investigation (2 intentional stalls)

Table 3. Concluded

<u>Test</u>	<u>Date</u>	<u>Comments and Accomplishments</u>
AC05	4/27/78	Simulated screen No. 141 distortion pattern with airjet - conducted fan (ADG Nos. 3 and 4) and compressor (ADG No. 25) surge investigation (3 intentional stalls)
AC06	5/4/78	Attempted matching large gradient distortion patterns with airjet - setting errors larger than anticipated - optimized ADG control variables and techniques for remaining test requirements
AC07	5/11/78	Simulated screen No. 354.7M distortion pattern with airjet (ADG Nos. 26 and 27) for Reynolds Number effect on surge investigation (6 intentional stalls)
AC08	5/17/78	Simulated screen Nos. 141, 123c, and 303.4 distortion patterns with airjet (ADG Nos. 4, 5, and 35, respectively) - conducted fan surge investigation (3 intentional stalls)
AC09	5/22/78	Simulated screen Nos. 353CD, 4, and 2 distortion patterns with airjet (ADG Nos. 11, 31 and 32, respectively) - conducted fan compressor (Nos. 2 and 4 only) surge investigation (5 intentional stalls)
AC10	5/26/78	Computer systems damaged by electrical storms - posttest performance power hook calibration conducted at sea-level conditions
AC11	5/31/78	Simulated screen No. 106 and 121 distortion patterns with airjet (ADG 2, 23, 1, and 7) conducted fan and compressor (No. 106 only) surge investigation (4 intentional stalls) - manually set a minimum steady state - maximum dynamic distortion pattern for fan stall verified fan clean surge margin
AC11	5/31/78	At completion of air period, preserved engine fuel systems with oil and treated inlet guide fans with oil

Table 4. Pattern Matches during Baseline Testing

Pattern	Screen	Fan Speed, percent	DIST1, percent			RMSE, Percent	
			Screen	ADG			
180-deg, 1/rev							
1	106	100	26.9	26.2 ⁽¹⁾	26.9	2.5 ⁽¹⁾	2.7
23	106	95	23.6	23.4 ⁽¹⁾	22.8	2.5 ⁽¹⁾	2.1
2	106	90	16.3	17.9 ⁽¹⁾	16.8	2.5 ⁽¹⁾	1.5
50-percent Hub Radial							
3	141	100	16.8	15.1		2.4	
25	141	94	14.0	13.1		2.0	
4	141	90	9.8	10.2		1.1	
F101 Spec							
26	354.7M	100	23.4	17.5		2.3	
27	354.7M	93	20.0	15.5		1.7	

(1) May 1977 Results

Table 5. Pattern Matches (Other Than Baseline)

Pattern	Screen	Fan Speed, percent	RMSE, percent	DIST1, percent		$(\Delta P_{RMS}/P_F) \times 100$	
				Desired	ADG		
180-deg, 1/rev							
1	106	100	2.7	26.9	26.9	1.1% (1.7% Max.)	
23	106	94	2.1	23.6	22.8	1.1 (1.8)	
2	106	90	1.5	16.3	16.8	0.6 (1.0)	
35	303.4	90	6.3	32.3	22.1	1.3 (2.0)	
50-percent Tip Radial							
7	121	100	1.8	17.6	16.2	1.7 (2.3)	
5	123C	90	4.3	23.2	14.3	1.5 (2.1)	
6	123C	75	2.6	16.2	10.9	-	
F101 Spec							
11	353CD	90	5.1	24.7	16.8	1.8 (2.5 Max.)	
9	351.1	100	2.8	24.7	20.5	1.0 (1.6)	
34	356.1	100	4.6	24.1	22.1	1.3 (2.1)	
B-1 Flt Test							
14	SLS-C/W	100	2.7	20.7	16.3	1.3 (2.0)	
Inlet Model							
15	PWT-SLS	100	2.5	21.8	16.9	1.2 (1.9)	
16	PWT-SLS	100	3.0	22.1	15.6	1.0 (1.6)	
Special (Composite Patterns)							
30	GE#4	97	2.5	16.2	15.9	1.2 (1.8)	
31	GE#4	93	2.5	16.2	13.3	1.1 (2.1)	
32	GE#2	100	2.3	13.5	15.3	0.9 (1.4)	
33	GE#2	95	2.2	13.5	12.7	0.8 (1.1)	

Table 6. Engine Stability Comparison for Baseline Tests

Pattern	Screen	Airflow at Surge (ADG), lb/sec	Type Surge	Surge Pressure Ratio ⁽¹⁾ Comparison
180-deg, 1/rev				
1	106	348	Fan	+1.0% ⁽²⁾
23	106	330	Core	0 ⁽²⁾
50-percent Hub Radial				
3	141	342	Fan	+2.3
4	141	286	Fan	+1.0
25	141	320	Core	-1.4
F101 Spec				
26	354.7M	343	Fan	+0.4
27	354.7M	320	Core	+0.6

(1) $(PR_{S_{ADG}} - PR_{S_{SCR}}) \times 100 / PR_{S_{SCR}}$

(2) May 1977 Results

Table 7. Engine Stability Comparison (Other Than Baseline)

Pattern	Screen	Airflow at Surge (ADG), lb/sec	Type Surge	RMSE, percent	Comparison of Surge Pressure Ratio $\left(\frac{PRS_{ADJ} - PRS_{DES}}{PRS_{DES}} \right)$, percent
180-deg, 1/rev					
1	106	345	Fan	2.7	-1.6
2	106	271	Fan	1.5	+2.6
23	106	314	Core	2.1	-0.9
35	303.4	276	Fan	6.3	+6.3
50-percent Tip Radial					
7	121	331	Fan	1.8	-2.3
5	123C	277	Fan	4.3	+15.9
F101 Spec					
11	353CD	276	Fan	5.1	+13.8

Table 8. Surge Pressure Ratio Comparison after Correction to Desired Distortion Level

Pattern	Screen	Fan Speed, percent	$\left(\frac{PRS - PRS_{SCR}}{PRS_{SCR}} \times 100 \right)$ MEAS, percent	$\left(\frac{PRS - PRS_{SCR}}{PRS_{SCR}} \times 100 \right)^{(1)}$ MEAS-CORR(SS), percent	$\left(\frac{PRS - PRS_{SCR}}{PRS_{SCR}} \times 100 \right)^{(1)}$ MEAS-CORR(DYN), percent
3	141	100	2.3	0.7	0.7
4	141	90	1.0	0.2	0.2
1	106	100	-1.6	-1.9	-1.8
2	106	90	2.6	2.6	3.9
7	121	100	-2.3	-2.3	2.6
5	123C	90	15.9	-2.0	2.0
35	303.4	90	6.3	-3.2	1.8

⁽¹⁾ General Electric Distortion Sensitivity Curves Used for Corrections

APPENDIX A METHODS OF CALCULATION

The general methods and equations used to compute parameters presented in this report are given below. Where applicable, the arithmetic average of the pressure and temperature was used. The enthalpy, specific heat, and entropy properties were extensively developed from data in Refs. 4 and 5. Where applicable, the equilibrium composition of the gas was determined from Gibbs free energy properties from Ref. 5. Corrections to the ideal gas properties for van de Waal effects were made where applicable by computing virial coefficients from Ref. 6.

AIRFLOW

All measured airflows were calculated from the equation:

$$W = \frac{CT \cdot CF \cdot A \cdot PS \sqrt{(H - HS) \cdot G \cdot J \cdot 2}}{R \cdot TS}$$

where $H = f(T,P)$, $TS = f(T,P,PS)$, $CT = f(T,P,PS)$, and $CF = 1.0$ for all locations except venturi where the $CF = f(T,P)$.

ALTITUDE

Flight altitude was calculated from equations which represent the geopotential tables from Ref. 3.

$$ALT = f(PAMB)$$

FLIGHT VELOCITY AND MACH NUMBER

The flight velocity and Mach number were calculated using an isentropic relationship with P_1 , T_1 , and $PAMB$.

$$\text{Flight velocity, } V_{\infty} = \sqrt{2 \cdot G \cdot J (H - HS)}$$

$$\text{Sonic velocity, } a = \sqrt{G \cdot \gamma \cdot R \cdot TS}$$

where

$$H = f(T_1, P_1)$$

$$TS = f(T_1, P_1, PAMB)$$

$$HS = f(TS, PAMB)$$

$$\gamma = f(TS, PAMB)$$

$$\text{Mach Number, } M = V/a$$

INLET PATTERN ERROR

The inlet pattern error RMSE was calculated using the following equation

$$RMSE = \sqrt{\frac{\sum_{i=1}^N \left[\frac{P_{\text{measured}}}{P_{\text{desired}}} - 1 \right]^2}{N}} \times 100, \text{ percent}$$

where N = number of total-pressure probes.

INLET TOTAL-PRESSURE DISTORTION

The distortion at the engine inlet (DIST1) was defined as follows:

$$DIST1 = \frac{P_{1_{\text{max}}} - P_{1_{\text{min}}}}{P_{1_{\text{face}}}} \times 100, \text{ percent}$$

RADIAL DISTORTION

Radial total-pressure pattern distortion (IDR) was defined as follows:

$$IDR = \frac{P_{\text{face}} - P_{\text{ring}_{\text{avg}}}}{P_{\text{face}}}$$

CIRCUMFERENTIAL DISTORTION

Circumferential total-pressure pattern distortion (IDC) is defined as follows:

$$IDC = \frac{P_{\text{ring}_{\text{avg}}} - P_{\text{ring}_{\text{min}}}}{P_{\text{face}}}$$

RMS OF TIME-VARIANT TOTAL PRESSURE

Root mean square (RMS) values for each total pressure were determined by an electronic analog wave analyzer. Mathematically, RMS is defined for a function $p(t)$ as

$$RMS = \left[\frac{1}{T} \int_0^T (p(t))^2 dt \right]^{1/2}$$

where T is the time span of the data and $p(t)$ is the instantaneous value of the time variant total pressure. The RMS values used in this report are normalized by the face-averaged total pressure. The face-averaged value of RMS (PRMS) is defined as:

$$PRMS = \frac{1}{N} \sum_{i=1}^N RMS_i = \frac{1}{N T^{1/2}} \sum_{i=1}^N \left[\int_0^T (p(t)_i)^2 dt \right]^{1/2}$$

The PRMS values presented in this report have been normalized by the face-averaged pressure (PF) as follows:

$$\frac{\text{PRMS}}{\text{PF}} = \frac{\sum_{i=1}^N \text{RMS}_i}{N \sum_{i=1}^N P_i}$$

POWER SPECTRAL DENSITY FUNCTION

The power spectral density (PSD) function was computed by an electronic analog wave analyzer and presented graphically as a function of frequency. The PSD function of a stationary signal is mathematically defined as

$$\text{PSD} = \lim_{T \rightarrow \infty} \lim_{\Delta f \rightarrow 0} \frac{1}{(\Delta f)T} \int_0^T Y^2(t, f, \Delta f) dt$$

where T is the averaging time of the data, f is the bandwidth of the electrical filter used, and $Y(t, f, \Delta f)$ is the instantaneous value of the data waveform at time t within the bandwidth Δf . The square root of the total area under the PSD curve is equal to the total root-mean-square (RMS) value of the signal. The PSD function indicates the magnitude, the energy distribution with frequency, and the existence of any discrete frequency components of the total input signal. The PSD functions presented in this report were normalized by the steady-state total pressure as follows:

$$\frac{\text{PSD}}{(P)^2} = \frac{(\Delta P/P)^2}{\text{Hz}}$$